Engineered Neural Stem Cells for Targeted Glioblastoma Therapy: Strategies for Cell Recognition and Response and Cytotoxicity

Hannah Verge

A thesis submitted to the University of Ottawa
in partial fulfillment of the requirements for the
Master's degree in Microbiology and Immunology

Department of Biochemistry, Immunology and Microbiology
Faculty of Medicine, University of Ottawa

Abstract

Glioblastoma (GBM) remains the most aggressive primary brain malignancy, with median survival of 12–15 months despite maximal treatment. Its resistance to conventional therapy is driven by intratumoral heterogeneity, diffuse invasion, an immunosuppressive tumor microenvironment, and the blood-brain barrier, which restricts delivery of systemic biologics. Engineered neural stem cells (NSCs) offer a promising solution to these challenges owing to their intrinsic tumor tropism, which enables localized and sustained therapeutic delivery directly within the GBM microenvironment. This study describes the engineering of peripheral blood-induced NSCs (PBiNSCs) derived from adult blood through OCT4-free epigenetic reprogramming as a dual-strategy therapeutic platform for GBM. In the first strategy, PBiNSCs were engineered with a SyNthetic Intramembrane Proteolysis Receptor (SNIPR) system to couple tumor antigen recognition to inducible expression of light-chain leader PTEN-Long (lclPTENL), a secretable isoform of the tumor suppressor PTEN. This represents the first demonstration of SNIPR functionality in PBiNSCs, establishing them as a new cellular vehicle for synthetic receptor platforms. Initial validation using an anti-CD19 SNIPR confirmed antigen-dependent, dose-responsive activation in both bead-based and cell-based co-culture systems. The SNIPR was subsequently retargeted toward two GBM-associated antigens: IL13Rα2, using a mutant IL13(E13Y) ligand domain, and EGFRvIII, using the tumor-specific MR1 single-chain variable fragment. The MR1-EGFRvIII SNIPR demonstrated highly selective activation, with 74–81% BFP-positive cells in EGFRvIII-expressing primary GBM co-cultures compared to near-background levels in wild-type controls, an effect maintained in a 3D onco-neurosphere model. By contrast, the IL13(E13Y)-based SNIPR exhibited high sensitivity activation, attributed to residual IL13Rα2 cross-reactivity and the ultra-high affinity of the protein-based binding domain. SNIPR-driven lclPTENL expression was confirmed in CD19 co-culture conditions, and conditioned media from PBiNSCs constitutively expressing lclPTENL induced a statistically significant increase in p16 expression in primary GBM cells, demonstrating downstream biological activity and validating the therapeutic rationale for PTEN restoration. In the second strategy, PBiNSCs were engineered to constitutively secrete a bispecific Fc fusion protein simultaneously targeting CD47 a ubiquitous "don't eat me" signal overexpressed on GBM cells and either IL13Rα2 or EGFRvIII. The construct employs knob-into-hole Fc engineering and a

P2A/furin co-expression strategy to produce a stable heterodimeric bispecific from a single transcript. Both the IL13/SIRPα and MR1/SIRPα variants were successfully expressed and secreted by engineered PBiNSCs, and binding to primary GBM cell lines was confirmed by Western blot. A novel antigen-affinity purification strategy using biotinylated EGFRvIII as a capture ligand enabled selective isolation of functionally intact bispecific protein. Collectively, these findings establish a proof-of-concept for a modular, cell-based delivery platform that combines the tumor-tropic properties of PBiNSCs with SNIPR-controlled therapeutic gene expression and innate immune checkpoint blockade, addressing multiple mechanisms of GBM treatment resistance simultaneously.

Acknowledgements

First and foremost, I would like to thank my supervisor, Dr. Ian Lorimer for their mentorship, guidance, and constant support throughout my graduate studies. Their encouragement, scientific insight, and patience challenged me to grow both personally and professionally, and I am incredibly grateful for the opportunity to learn from them.

I would also like to thank my lab mates and colleagues for creating such a supportive and enjoyable research environment. Whether through scientific discussions, troubleshooting experiments, or simply making long days in the lab more enjoyable, your support meant more than you know.

To my family and friends, thank you for your endless encouragement, patience, and belief in me throughout this journey. Your support carried me through the difficult moments and helped me celebrate the successes along the way.

Table of Figures

Abbreviations

ADCC – Antibody dependent cellular cytotoxicity

ADCP – Antibody dependent cellular phagocytosis

BBB – Blood-brain barrier

BFP – Blue fluorescent protein

bsAbs – Bi-specific antibodies

CAR – Chimeric antigen receptor

CDC – Complement dependent cytotoxicity

EGFR - Epidermal growth factor receptor

EGFRvIII - Epidermal growth factor receptor variant III

FcRn – Neonatal Fc receptor

FcγR – Fc gamma receptor

GBM – Glioblastoma

GFP – Green fluorescent protein

GSC – Glioma stem-like cells

HIF – Hypoxia-inducible factor

HNF1α – Hepatocyte nuclear factor 1-alpha

IgG – Immunoglobulin G

IL13 – Interleukin 13

IL13Ra2 – Interleukin 13 receptor alpha 2

iNSCs – Induced neural stem cells

lclPTENL - Light-chain leader phosphatase and Tensin homolog -long

mAbs – Monoclonal antibodies

NRR – Negative regulatory region

NSC – Neural stem cells

PBiNSCs – Peripheral blood induced neural stem cells

PriGO – Primary glioblastoma

PTEN – Phosphatase and Tensin homolog

PTEN-L - Phosphatase and Tensin homolog–long

scFv – Single chain variable fragment

SIRPα – Signal regulatory protein-α

SNIPR – Synthetic intramembrane proteolysis receptor

synNotch – Synthetic notch

TAM – Tumor-associated macrophages

TCR – T-cell receptor

TIL – Tumor infiltrating lymphocytes

TME – Tumor microenvironment

1. Introduction

1.1. Glioblastoma

1.1.1. Clinical Overview

Glioblastoma (GBM) is the most common and aggressive primary malignant brain tumor in adults and represents a major unmet clinical challenge in neuro-oncology. In Canada, GBM affects approximately 4 per 100,000 individuals annually, with incidence increasing with age and peaking between the sixth and eighth decades of life[1]. Standard of care treatment consists of a combination of radiation therapy, temozolomide administration and maximal safe surgical rection which provides a median survival of 12-15 months with inevitable recurrence[2]. According to the World Health Organization (WHO) Classification of Tumours of the Central Nervous System (CNS), updated in 2021 and further refined in 2024, GBM is defined as a diffuse astrocytic tumor that is isocitrate dehydrogenase (IDH)–wildtype and classified as WHO grade 4, irrespective of histological appearance when specific molecular criteria are met[3]. These criteria include telomerase reverse transcriptase (TERT) promoter mutation, epidermal growth factor receptor (EGFR) amplification, or combined whole chromosome 7 gain and chromosome 10 loss (+7/−10)[3]. In cases where these molecular features are absent, diagnosis relies on histopathological findings, including the presence of microvascular proliferation or necrosis. This molecularly integrated definition reflects a paradigm shift away from purely histopathological classification toward a biologically driven framework that more accurately predicts clinical behavior and prognosis.

1.2. Biological Barriers to Effective Glioblastoma Therapy

Despite well-defined diagnostic criteria and standardized treatment protocols, GBM remains one of the most treatment-refractory human malignancies. The current standard-of-care regimen consists of maximal safe surgical resection followed by concurrent radiotherapy and temozolomide chemotherapy, and subsequent adjuvant temozolomide administration. This regimen, established by the landmark Stupp protocol, extends median survival by only a few months compared to radiotherapy alone and has not substantially changed long-term survival outcomes[4,5]. Numerous efforts to intensify or augment this regimen, including dose-dense temozolomide schedules, alternative alkylating agents, and combination chemotherapy, have failed to produce meaningful

survival benefits, underscoring the profound and multifactorial resistance of GBM to conventional cytotoxic therapies.[4,6,7]

1.2.1. Inter-and Intratumoral Heterogeneity

GBM arises from glial-lineage cells, which undergo malignant transformation following the accumulation of genetic, epigenetic, and chromosomal alterations[8]. These alterations disrupt core cellular processes including cell cycle regulation, DNA damage response, apoptosis, and metabolic homeostasis[9]. Canonical molecular alterations in GBM include loss of heterozygosity on 10q, amplification or mutation of EGFR, loss of tumor suppressors such as PTEN and TP53, dysregulation of the PI3K/AKT/mTOR and RAS/MAPK signaling pathways, and inactivation of cell cycle regulators including CDKN2A/B[10–14]. At the transcriptional level, GBM exhibits substantial molecular heterogeneity and can be broadly categorized into three major molecular subtypes: classical, mesenchymal, proneural, based on gene expression profiling[3]. The classical subtype is characterized by high-level EGFR amplification or mutation, frequent chromosome 7 gain and chromosome 10 loss, and relative preservation of TP53 function. Tumors of this subtype demonstrate strong activation of proliferative signaling pathways and are associated with high mitotic activity. In contrast, the mesenchymal subtype is defined by alterations in NF1, enrichment of inflammatory and immune-related gene signatures, and increased expression of mesenchymal markers such as CHI3L1 and MET. This subtype is often associated with enhanced invasiveness, resistance to therapy, and a more aggressive clinical course. The proneural subtype is characterized by alterations in PDGFRA, TP53 mutations, and gene expression patterns associated with neural development and oligodendrocyte precursor cells. Although initially linked to younger patient age and slightly improved prognosis, proneural tumors frequently undergo subtype switching at recurrence, often adopting a mesenchymal phenotype, which may contribute to therapeutic resistance.

1.2.2. Invasion and Diffuse Growth

One of the defining biological features of GBM is its highly infiltrative growth pattern. GBM cells migrate extensively along white matter tracts, blood vessel walls, and the subpial surface, leading to diffuse invasion of surrounding brain parenchyma. Tumor cells co-opt routes

surrounding blood vessels, exploiting the oxygen and nutrient supply and even disrupting the blood brain barrier as they disseminate along vessel walls, with studies showing the majority of glioma cells contacting blood vessels early in invasion[15,16]. White matter tracts composed of myelinated axons, such as the corpus callosum and internal capsule provide other pathways that enable cells to spread widely across hemispheres[17]. This invasive behavior precludes complete surgical resection, as tumor cells extend well beyond radiographically apparent margins. These infiltrative tumor cells often reside in eloquent brain regions responsible for language, motor, and sensory function, placing strict limits on surgical aggressiveness[18]. Even with advanced intraoperative techniques such as fluorescence-guided surgery and awake craniotomy, microscopic residual disease persists, providing the substrate for inevitable local recurrence.

1.2.3. Radiation and Chemotherapy Resistance

Resistance to radiotherapy further constrains therapeutic efficacy. GBM cells exhibit constitutive activation of DNA damage response pathways, including ATM, ATR, and DNA-dependent protein kinase, enabling efficient repair of radiation-induced double-strand breaks[19,20]. Glioma stem-like cells (GSCs) are particularly resistant, as they preferentially activate homologous recombination and non-homologous end-joining repair mechanisms and display prolonged cell cycle arrest that allows survival following genotoxic stress. Hypoxia within the tumor microenvironment exacerbates radioresistance by reducing oxygen-dependent free radical formation and inducing hypoxia-inducible factor (HIF) signaling, which promotes stemness, angiogenesis, and metabolic adaptation[21–23]. Clinical attempts to overcome radioresistance, such as radiation dose escalation or hypoxia-targeting agents, have largely failed due to unacceptable toxicity or lack of efficacy[24]. Chemotherapy resistance represents a central and persistent challenge in GBM management. Temozolomide induces cytotoxic DNA lesions through alkylation at the O6 position of guanine; however, its clinical effectiveness is strongly dependent on epigenetic silencing of the MGMT gene[25,26]. Tumors with unmethylated MGMT promoters exhibit rapid repair of temozolomide-induced damage and derive minimal benefit from chemotherapy[27]. Importantly, even patients with MGMT-methylated tumors frequently develop acquired resistance through activation of alternative DNA repair pathways, loss of mismatch repair function, and increased tolerance to DNA damage. Multiple clinical trials evaluating alternative chemotherapeutic agents, including lomustine, procarbazine, and combination regimens such as

PCV, have failed to significantly improve outcomes in the recurrent or newly diagnosed setting[28,29].

1.2.4. The Blood-Brain Barrier

The blood–brain barrier (BBB) poses a major pharmacological obstacle by restricting delivery of many systemic agents to the tumor and infiltrative margins[30]. Tight junctions between brain capillary endothelial cells eliminate paracellular transport and severely restrict passive diffusion, such that molecules can only enter the brain via lipid-mediated diffusion or specific carrier- or receptor-mediated transport systems[31]. As a result, approximately 98% of small-molecule drugs and nearly all large biologics including antibodies and protein therapeutics fail to adequately penetrate the BBB, limiting the efficacy of many systemic cancer therapies[32]. Although the BBB is disrupted within the tumor core, it often remains intact in regions of microscopic invasion where residual disease persists keeping these cells protected[33]. Active efflux transporters, abnormal tumor vasculature, and elevated interstitial pressure further reduce effective intratumoral drug concentrations with only 20% of the smallest therapeutic agents reaching the tumor at therapeutic levels[34,35]. These limitations have contributed to the failure of numerous systemically administered agents that demonstrate potent anti-glioma activity in preclinical models but lack clinical efficacy. Among clinically established approaches, the use of an Ommaya reservoir provides a direct method to bypass of the BBB by enabling repeated intracerebroventricular (IVC) administration of therapeutics[36]. The Ommaya reservoir is a surgically implanted catheter-reservoir system placed into the cerebral ventricles, allowing drugs to be delivered directly into the cerebrospinal fluid, where they can diffuse throughout the central nervous system and reach infiltrative tumor regions[37]. This method has been widely used in the treatment of leptomeningeal metastases and central nervous system lymphomas, where intrathecal or intraventricular administration of agents such as methotrexate has demonstrated improved drug distribution compared to systemic delivery[38,39]. These clinical applications provide proof-of-concept that bypassing the BBB can achieve therapeutically relevant drug concentrations within the CNS[40]. However, limitations including invasiveness, risk of infection, and uneven drug distribution within solid tumor masses highlight that, while the BBB is not insurmountable, effective and broadly applicable delivery strategies for GBM remain an ongoing challenge[41,42].

1.2.5. Tumor Microenvironment

The GBM tumor microenvironment (TME) is a profoundly immunosuppressive milieu that contributes to therapeutic resistance and disease progression[43,44]. A hallmark of GBM is chronic hypoxia, driven by aberrant vasculature and rapid metabolic demand, which promotes angiogenesis and tumor cell survival but also coordinates the spatial distribution of immunosuppressive myeloid populations[45,46]. Myeloid cells, principally tumor-associated macrophages (TAMs) and resident microglia, constitute a dominant fraction of the immune infiltrate in GBM; studies estimate that TAMs can comprise 30–50 % of all tumor cells, with both microglia and bone marrow-derived macrophages contributing substantially to this pool[47–49]. In addition to hypoxia-driven recruitment, these myeloid populations are actively drawn to regions of tumor cell turnover, where apoptotic and necrotic cells release "find-me" and "eat me" signals that promote phagocytic clearance[50–52]. This process, while essential for tissue homeostasis, contributes to an immunosuppressive environment, as engulfment of apoptotic cells is associated with the release of anti-inflammatory mediators and suppression of pro-inflammatory signalling[53–55]. Within the TME, macrophages and microglia often adopt immunosuppressive phenotypes that inhibit effective anti-tumor immunity[56–58]. These cells secrete high levels of transforming growth factor-β (TGF-β) and interleukin-10 (IL-10)**,** cytokines that suppress cytotoxic T-cell functions, promote regulatory T-cell development, and dampen antigen presentation, thereby enforcing immune tolerance and protection of tumor cells from immune attack[59,60]. Concurrently, GBM exhibits low levels of effector T-cell infiltration, with both CD4+ and CD8+ T lymphocytes present at relatively low percentages compared to the dominant myeloid compartment, and those T cells that are present frequently express exhaustion markers such as PD-1, further limiting anti-tumor immune responses.[61] Together, the combination of hypoxia-driven immune organization, recruitment of myeloid cells to apoptotic tumor regions, sustained production of immunosuppressive cytokines paucity of functional T-cell effectors defines a "cold" TME that hinders effective immunosurveillance and contributes to GBM's resistance to immunotherapies[62].

1.3. Cell-Based Therapies for Cancer

1.3.1. Conceptual Framework of Cell-Based Therapies

Cell-based therapies have redefined the oncology landscape by using living cells as programmable agents. Unlike conventional small molecules or monoclonal antibodies, engineered cells can sense environmental cues, integrate signals, migrate toward disease sites, and execute context-dependent effector functions conceptualize living cells as programmable therapeutics rather than passive drug carriers. The most well-established examples are chimeric antigen receptor (CAR) T-cell therapies, in which a patient's own T cells are engineered to express synthetic receptors that direct cytotoxic activity against defined tumor antigens[63–65]. CAR-T therapies targeting CD19 such as Tisagenlecleucel have achieved remarkable outcomes in hematologic malignancies, such as relapsed or refractory large B-cell lymphoma, with durable complete remission rates in over half of treated patients and regulatory approvals in multiple countries establishing engineered cellular therapy as a clinically viable oncologic modality[66]. Similarly, adoptive cell therapy using ex vivo–expanded tumor-infiltrating lymphocytes (TILs), pioneered by Steven A. Rosenberg, demonstrated durable tumor regression in metastatic melanoma, further validating that transferred immune cells can mediate meaningful anti-tumor activity in humans[67]. However, translating these successes into solid tumors, including GBM, has proven challenging due to factors such as antigen heterogeneity, immunosuppressive tumor microenvironments, and poor infiltration of effector cells, all of which limit CAR-T persistence and efficacy outside of blood cancers. Alternative cell-based platforms such as CAR-NK cells and T-cell receptor (TCR) engineered cells are under investigation to overcome some of these barriers by offering broader antigen targeting or reduced graft-versus-host risk, though they face many of the same impediments within solid tumors[68–72].

In the context of GBM specifically, early clinical and preclinical studies illustrate both the promise and the limits of current cell therapies. First-generation CAR-T approaches targeting antigens like EGFRvIII or IL13Rα2 have induced measurable tumor shrinkage in subsets of recurrent GBM patients, but responses are typically transient and limited by antigen escape and the hostile immunosuppressive microenvironment characteristic of GBM[73,74]. To address these challenges, next-generation strategies are being developed that include bi- or tri-specific CAR constructs designed to recognize multiple GBM antigens simultaneously, reducing the likelihood of immune escape, and approaches that deliver cells regionally (e.g., intracavitary or intraventricular infusion) to improve local tumor access[75,76]. Early "off-the-shelf" allogeneic CAR-

T products have also shown safety and signs of clinical activity in phase I GBM studies, demonstrating transient tumor reduction and necrosis in a majority of treated patients, a milestone in personalized cell therapy translation for brain tumors[77].

Mechanistically, these strategies offer advantages over static biologics. Living cells can proliferate in vivo, enabling local amplification of therapeutic effect at the tumor site; they can persist over time, adapt to antigen exposure, and exert serial cytotoxic activity, properties not achievable with fixed-dose antibodies or chemotherapeutics[66,78–80]. Moreover, cellular therapies can be genetically engineered to incorporate synthetic circuits, combinatorial antigen recognition, cytokine secretion, or resistance to inhibitory signals, expanding their functional versatility[81,82]. However, while hematologic malignancies have demonstrated the curative potential of this approach, extending these benefits to solid tumors, including GBM, requires overcoming barriers such as antigen heterogeneity, immunosuppressive signaling, and impaired trafficking within the tumor microenvironment[66,78,83,84]. These challenges have driven exploration of next-generation cellular platforms capable not only of antigen-specific killing but also of reshaping the local tumor milieu[81,83]. Among these, stem cell–based therapies have emerged as a promising platform due not only to their regenerative capacity but also to their ability to function as programmable delivery vehicles. Increasing evidence supports the use of neural stem cells (NSCs), mesenchymal stem cells (MSCs), induced pluripotent stem cells (iPSCs), and hematopoietic stem cells (HSCs) in therapeutic development, with NSCs and MSCs being the most extensively investigated in oncologic applications[85–87].

1.3.2. Neural Stem Cells as Therapeutic for GBM

A defining characteristic supporting the use of stem cells as therapeutic delivery systems is their intrinsic tumor-tropic behavior. NSCs have been shown to migrate toward tumor sites in response to chemokines, inflammatory mediators, hypoxia-related signals, and growth factors produced within the tumor microenvironment[88–90]. They demonstrate the ability to home to tumor tissue and sites of inflammation, where they can localize within or around neoplastic lesions[91]. This migratory capacity provides a biological mechanism for overcoming limitations of conventional therapeutics, including poor tumor penetration and nonspecific systemic distribution[92]. As a result, neural stem cells can serve as vehicles to transport therapeutic payloads

directly to tumor tissue, potentially enhancing local efficacy while reducing systemic toxicity. Beyond tumor homing, neural stem cells are highly amenable to genetic modification, enabling them to express therapeutic transgenes or carry biologically active agents. NSCs have been engineered to deliver enzyme–prodrug systems, immunomodulatory cytokines, apoptosis-inducing ligands, and oncolytic viruses in preclinical models[92–96]. For example, NSCs have been modified to express suicide genes that convert non-toxic prodrugs into cytotoxic compounds at the tumor site, thereby achieving localized chemotherapeutic activation[96,97]. These strategies illustrate the dual function of neural stem cells: they act both as migratory carriers and as active therapeutic mediators once they reach the tumor microenvironment.

Clinical translation further supports the rationale for stem cell–based delivery systems. Early-phase clinical investigations of stem cell–mediated enzyme/prodrug therapy in malignant brain tumors have demonstrated feasibility and tolerability, without evidence of malignant transformation attributable to the administered stem cells[98,99]. The safety profile of NSCs is further supported by their relatively low immunogenicity and immunomodulatory properties, which reduce the risk of acute immune rejection following administration [100]. Literature emphasizes that while concerns remain regarding long-term efficacy and safety, stem cell therapies evaluated to date have not demonstrated uncontrolled malignant transformation when properly characterized and administered under controlled conditions[101]. Nevertheless, safety remains a central consideration in the development of stem cell–based therapeutics. Potential risks include aberrant differentiation, uncontrolled proliferation, or unintended interactions within the tumor microenvironment. The literature therefore highlights the importance of stringent cell characterization, genetic stability testing, and incorporation of safety mechanisms such as suicide switches or irradiation protocols prior to clinical application[102]. These safeguards are critical to establishing stem cells as reliable and controllable therapeutic platforms rather than biologically unpredictable agents. Collectively, current evidence supports stem cells as adaptable and biologically rational delivery vehicles in cancer therapy[103]. Their inherent tumor tropism, capacity for precise genetic engineering, and emerging clinical safety data justify continued investigation into stem cell–mediated therapeutic systems. When combined with advances in gene editing, synthetic biology, and targeted molecular therapies, stem cells represent a modular and potentially

transformative platform capable of enhancing specificity, reducing systemic toxicity, and improving therapeutic index in oncology.

1.3.3. Generating Human Neural Stem Cells by Epigenetic Reprogramming

The development of iPSCs showed that OCT4-driven reprogramming can return somatic cells to a pluripotent state, enabling patient-specific disease modeling and regenerative research[104–107]. However, differentiating iPSCs into defined cell types is often slow and technically complex[104,108]. Direct lineage conversion using neural transcription factors can generate induced neurons (iNs), but these cells are postmitotic, inefficiently produced, and frequently retain age-related molecular signatures, limiting their therapeutic scalability[109–112]. Attempts to generate induced neural precursor cells (iNPCs) addressed some of these issues, yet many early methods relied on OCT4, raising concerns about transient pluripotency and genomic instability[113–119]. Moreover, producing expandable, adult-derived neural stem cells (NSCs) with robust self-renewal and multipotency has remained difficult[113,114,118,120]. Sheng et al. established an OCT4-free approach to directly generate induced NSCs (iNSCs) from adult peripheral blood cells, avoiding invasive tissue collection[121]. Using non-integrating vectors, Sheng et al. produced stable, clonally self-renewing, tripotent cells that respond to lineage cues. Notably, these iNSCs show marked reduction of age-associated epigenetic and transcriptional signatures, supporting their potential for translational applications in disease modeling and cell-based therapy[121]. These properties make OCT4-free induced neural stem cells (iNSCs) particularly attractive for GBM therapy. First, their derivation from adult peripheral blood cells provides a minimally invasive, readily accessible, and clinically scalable cell source, an important consideration for autologous or personalized treatment strategies. Second, their demonstrated genomic stability, long-term self-renewal, and clonogenicity enable the generation of well-characterized, quality-controlled cell batches suitable for repeated dosing or large-scale manufacturing. Unlike induced neurons, their proliferative capacity allows expansion without loss of stemness, while their responsiveness to lineage cues preserves functional plasticity. Importantly, the erasure of age-associated DNA methylation and transcriptional signatures may enhance therapeutic consistency and performance, reducing variability linked to donor age[121]. Together, these features position iNSCs as a robust and translationally viable platform for targeted delivery of cytotoxic agents, oncolytic constructs, or immune-modulatory therapies in GBM.

1.4. Cell Engineering Tools

1.4.1. Viral Transduction for Protein Expression

The earliest generation of engineered cellular therapies relied on constitutive gene expression systems, in which therapeutic transgenes are placed under strong viral promoters to drive continuous expression following genomic integration. Adeno-associated virus (AAV) vectors represent a non-pathogenic gene delivery platform with a strong clinical safety record and predominantly episomal persistence, reducing integration-associated oncogenic risk[122]. AAV vectors demonstrate relatively low immunogenicity and stable transgene expression in vivo; however, their limited packaging capacity (~4.7 kb) constrains the complexity of synthetic gene circuits that can be delivered[123–126]. Retroviral and lentiviral vectors became foundational tools for stable genetic modification because of their ability to integrate into host chromosomal DNA and enable durable transgene expression across cell divisions[127]. Lentiviral vectors in particular demonstrated improved safety profiles compared with earlier γ-retroviral systems due to self-inactivating (SIN) designs that reduce promoter activity within long terminal repeats, thereby lowering the risk of proto-oncogene activation[128–130]. Lentivirus is typically produced by transient transfection of packaging cells with a multi-plasmid system consisting of a transfer plasmid containing the gene of interest flanked by long terminal repeats (LTRs), packaging plasmids encoding viral structural proteins, and an envelope plasmid, often encoding the vesicular stomatitis virus glycoprotein (VSV-G), which broadens viral tropism. Replication-defective viral particles that contain the RNA genome encoding the transgene are reverse transcribed into DNA and integrated into the host genome by viral integrase, enabling stable and long-term expression of the transgene in dividing and non-dividing cells.

1.4.2. Engineered Synthetic Receptors for Target Recognition

Collectively, these early engineering tools enabled the first wave of gene-modified cell therapies but were fundamentally static expression systems. They lacked the ability to dynamically sense extracellular cues and convert contextual antigen recognition into regulated transcriptional programs, a limitation that became particularly apparent in solid tumors characterized by antigen heterogeneity and spatial complexity. An early and influential approach to inducible cellular signaling was the Tango system, which was developed to convert transient receptor activation into

a stable, amplifiable transcriptional output. In this system, a transcription factor (tTA) was tethered to the cytoplasmic tail of a membrane receptor via a specific protease cleavage site, while a second fusion protein combined a protease with a signaling adaptor; ligand-induced recruitment of this protease resulted in cleavage and release of the transcription factor into the nucleus, where it activated a reporter gene in a ligand-dependent manner[131]. The Tango assay proved versatile across multiple receptor classes, including G protein-coupled receptors, receptor tyrosine kinases, and steroid hormone receptors, but its reliance on multi-component fusion proteins and exogenously introduced proteases limited its direct applicability as a therapeutic switch[131]. Building on the rationale of converting extracellular cues into regulated gene expression, more recent strategies such as Modular Extracellular Sensor Architecture (MESA) have been developed[132]. MESA constructs place engineered sensor components at the cell surface and couple ligand binding to release of transcriptional regulators via defined proteolytic events, offering a plug-and-play architecture that can be tuned for diverse inputs; however, like Tango, MESA systems still face challenges including basal activation and the need for careful calibration of protease activity and signal amplification to achieve both sensitivity and specificity in complex tissue environments[132].

1.4.3. SynNotch Receptors

Synthetic Notch (synNotch) receptors represent a mechanistically distinct class of engineered receptors that couple extracellular antigen recognition to customizable transcriptional outputs. These receptors are derived from the endogenous Notch signaling pathway, which operates through ligand-induced conformational changes that expose a proteolytic cleavage site within the negative regulatory region (NRR), enabling sequential cleavage by ADAM metalloproteases and γ-secretase[133]. This intramembrane proteolysis releases the Notch intracellular domain, which translocates to the nucleus to regulate transcription[134]. SynNotch receptors retain the core regulatory and transmembrane architecture of Notch but replace the native ligand-binding domain with a customizable extracellular recognition module, such as a single-chain variable fragment (scFv) targeting a tumor-associated antigen[135,136]. Unlike CARs, which directly couple antigen binding to intracellular activation motifs (e.g., CD3ζ, CD28, 4-1BB), synNotch receptors function as signal-to-gene converters, decoupling antigen detection from effector function. A major goal of synthetic biology has been to program cell behavior predictively by engineering modular transcriptional circuits. However, while intracellular gene networks

became increasingly sophisticated, there remained no broadly customizable way to link user-defined extracellular inputs to specific intracellular decisions without relying on endogenous receptor pathways. Early receptor engineering approaches such as CARs successfully redirected antigen recognition but retained native T-cell activation as the output. SynNotch receptors advanced this concept by introducing modular control over both input and transcriptional output.

1.4.4. SyNthetic Intramembrane Proteolysis Receptors (SNIPRs)

SyNthetic Intramembrane Proteolysis Receptors (SNIPRs) build upon the proteolysis-activated transcriptional framework of synNotch while introducing refinements to receptor architecture, modularity, and translational suitability. Like synNotch receptors, SNIPRs rely on ligand-dependent intramembrane proteolysis to release a transcriptional effector domain[133,136,137]. However, SNIPRs incorporate optimized extracellular, juxtamembrane, and transmembrane regions to improve signal fidelity and reduce ligand-independent background cleavage[138]. One of the primary design advantages of SNIPRs is enhanced modularity, enabling interchangeable extracellular recognition domains and transcriptional outputs while maintaining predictable activation kinetics[138]. This modular design allows engineering of receptors responsive to tumor-associated antigens and supports integration into complex synthetic circuits. Additionally, SNIPR constructs have been optimized using humanized components to reduce immunogenic potential, an important consideration for clinical translation[139]. Functionally, SNIPRs enable precise tumor-specific activation logic. For instance, engagement of tumor antigen A can induce transcription of a CAR targeting antigen B or trigger expression of cytokines, immune modulators, or checkpoint inhibitors, effectively implementing transcriptionally controlled AND-gate logic[138,140]. This separation of antigen sensing from effector execution allows engineered cells to discriminate complex antigen combinations characteristic of heterogeneous tumors such as GBM[140]. By requiring multiple contextual signals, SNIPR systems reduce unintended activation in normal tissues expressing only a single antigen, thereby improving therapeutic specificity while preserving potent antitumor activity.

1.5. Antibody Based Immunotherapy

Therapeutic antibodies represent one of the most transformative advances in modern oncology. Since the approval of rituximab in 1997, monoclonal antibody–based therapies have reshaped the treatment landscape across hematologic and solid malignancies[141,142]. Antibody engineering has progressed from murine hybridoma-derived IgG molecules to humanized, fully human, bispecific, and Fc-optimized formats, significantly expanding both mechanistic scope and clinical efficacy[143–147]. Antibody-based therapeutics function through a combination of antigen-specific targeting and immune effector engagement. Structurally, conventional immunoglobulin G (IgG) antibodies consist of two antigen-binding Fab regions and an Fc domain capable of interacting with Fc gamma receptors (FcγRs) and complement proteins; however, many therapeutic antibodies are specifically engineered or selected to minimize FcγR engagement in order to reduce unwanted immune activation[148]. This modular architecture enables both direct tumor targeting and immune-mediated cytotoxicity[148–151].

1.5.1. Monoclonal and Bispecific Antibodies

The development of monoclonal antibodies (mAbs) originated with hybridoma technology, enabling production of antigen-specific murine antibodies[141]. Early clinical applications were limited by immunogenicity, leading to the development of chimeric, humanized, and fully human antibodies that retained target specificity while minimizing anti-drug immune responses[144,147,152,153]. In oncology, monoclonal antibodies function through several distinct but overlapping mechanisms: direct inhibition of oncogenic signaling pathways, induction of receptor internalization and degradation, complement-dependent cytotoxicity (CDC), and Fc-mediated immune effector functions such as antibody-dependent cellular cytotoxicity (ADCC) and antibody-dependent cellular phagocytosis (ADCP)[150,154,155]. Engagement of FcγRIIIa (CD16) on natural killer (NK) cells promotes cytotoxic granule release, whereas binding to FcγRI and FcγRIIa on macrophages enhances phagocytosis and inflammatory cytokine production, thereby linking tumor antigen recognition to innate immune activation[149–151]. Clinical successes have validated this strategy. Antibodies targeting CD20, HER2, and EGFR have demonstrated durable survival benefits in lymphoma and solid tumors, while immune checkpoint inhibitors targeting PD-1 and PD-L1 have redefined treatment paradigms across multiple malignancies[156–159]. Notably, in GBM the anti-VEGF monoclonal antibody bevacizumab has shown the ability to reduce tumor-associated edema and improve progression-free survival by inhibiting angiogenesis, although

these benefits do not consistently translate into improved overall survival. Monoclonal antibodies exhibit important limitations. Their efficacy often depends on sufficient and homogeneous antigen expression as tumor antigen heterogeneity permits immune escape through antigen loss variants[160–162]. Moreover, Fc-dependent effector function requires adequate immune cell infiltration and functional competence within the tumor microenvironment (TME), which is frequently immunosuppressive in solid tumors[160]. Resistance mechanisms including compensatory signaling activation and modulation of Fcγ receptor interactions can further attenuate long-term therapeutic responses[163,164]. To overcome some of these constraints, bispecific antibodies (bsAbs) were developed to simultaneously engage two distinct targets. These constructs may bind either two tumor-associated antigens or bridge tumor cells to immune effector cells, most notably through CD3 engagement on T cells[165–168]. Bispecific T-cell engagers facilitate formation of an artificial immune synapse, lowering the activation threshold for cytotoxic T lymphocytes and enabling MHC-independent tumor cell killing[169,170]. This approach has demonstrated significant efficacy in hematologic malignancies, but are still showing challenges in GBM. Early-phase clinical trials, in the form of CD3-engaging T-cell engagers that redirect cytotoxic T cells towards tumor-associated antigens such as EGFRvIII have demonstrated safety but limited efficacy. However, bispecific antibodies remain dependent on systemic immune cell recruitment and can induce cytokine release syndrome due to potent T-cell activation[171]. Although monoclonal and bispecific antibodies have transformed modern oncology, their mechanisms largely rely on extracellular antigen recognition and recruitment of endogenous immune effector pathways.

1.5.2. Fc-fusion proteins

Fc-fusion proteins represent an evolution of antibody-derived therapeutics that preserve Fc-mediated immune engagement while expanding structural and functional versatility. These proteins function by genetically coupling an active targeting or receptor domain to the Fc region of an immunoglobulin, most commonly human IgG1, thereby harnessing both specific tumor engagement and innate immune effector mechanisms[172,173]. This architecture provides several pharmacological and immunological advantages that make Fc-fusion constructs attractive therapeutic platforms, including applications in oncology. Structurally, Fc-fusion proteins form dimers through the IgG hinge region, allowing two of the same or different fused ligands to be presented simultaneously, thereby increasing binding avidity and functionality[174]. The Fc domain

also interacts with the neonatal Fc receptor (FcRn), which protects IgG from lysosomal degradation and recycles it back into circulation, substantially prolonging the plasma half-life of Fc-fusion therapeutics[175,176]. As a result, these molecules typically remain in circulation for approximately one to two weeks, significantly longer than most recombinant proteins. In addition to improving pharmacokinetics, the Fc domain enables interactions with Fcγ receptors (FcγRs) expressed on immune cells, including natural killer (NK) cells, macrophages, and dendritic cells, which can promote immune-mediated effector responses such as antibody-dependent cellular cytotoxicity (ADCC)[173,177]. This mechanism is well established in antibody-based cancer therapies such as rituximab and trastuzumab, where FcγRIIIa engagement on NK cells contributes to tumor cell killing[178]. Fc-fusion proteins can therefore be engineered to either enhance or minimize these effector interactions depending on therapeutic goals. For example, modifications within the Fc domain, such as amino-acid substitutions or altered glycosylation patterns can increase affinity for FcγRIIIa and thereby enhance immune-mediated tumor destruction[179]. Many Fc-fusion therapeutics instead function by modulating receptor–ligand interactions. The tumor necrosis factor (TNF) inhibitor etanercept, for instance, consists of the extracellular domain of the TNF receptor fused to IgG1 Fc and acts as a soluble decoy receptor that neutralizes TNF-α[180]. Similarly, other Fc-fusion constructs such as aflibercept and abatacept function by intercepting ligands or costimulatory molecules to regulate signaling pathways involved in inflammation or immune activation[181,182]. Beyond functional activity, the Fc domain also improves the biochemical properties of fusion proteins by enhancing solubility, structural stability, and manufacturability[172,174]. Together, these features extended half-life, immune effector engagement, increased ligand avidity, and improved manufacturability have established Fc-fusion proteins as a versatile and increasingly important class of biologics for therapeutic development, including emerging strategies in cancer immunotherapy.

1.6. Glioblastoma Therapeutic Targets

1.6.1. Interleukin-13 Receptor Alpha 2

Interleukin-13 receptor alpha 2 (IL13Rα2) is a well-characterized tumor-associated antigen and an important therapeutic target in GBM[183,184]. IL13Rα2 is highly overexpressed in many GBM tumors while demonstrating minimal expression in normal brain tissue, making it an attractive target for tumor-selective immunotherapies[183,185]. Although initially described as a decoy receptor

that binds IL-13 with high affinity, subsequent studies have shown that IL13Rα2 can actively contribute to tumor progression by promoting glioma cell invasion, migration, and survival[186–189]. Importantly, IL13Rα2 is expressed in a substantial proportion of GBM tumors and has also been detected on glioma stem-like cells, which are thought to contribute to tumor recurrence and treatment resistance[190,191]. These characteristics have led to the development of multiple IL13Rα2-targeted therapeutic strategies, including IL-13–based cytotoxins, monoclonal antibodies, peptide and dendritic cell vaccines, and CAR T-cell therapies designed to recognize IL13Rα2-expressing tumor cells[192]. Clinical evidence supporting IL13Rα2 as a therapeutic target was demonstrated in a notable case study reported in the *New England Journal of Medicine*, in which a patient with recurrent multifocal GBM received CAR T cells engineered to target IL13Rα2[193]. The patient was treated with multiple intracranial infusions of IL13Rα2-specific CAR T cells over a period of approximately 220 days, delivered first into the resected tumor cavity and later into the ventricular system to allow broader distribution within the central nervous system[193–196]. Following treatment, imaging revealed regression of all intracranial and spinal tumors, accompanied by increased immune cell and cytokine levels in the cerebrospinal fluid, indicating robust immune activation[193]. The patient experienced a complete clinical response that lasted approximately 7.5 months without grade ≥3 toxicities, demonstrating the feasibility and potential efficacy of targeting IL13Rα2 in GBM[193]. However, the disease ultimately recurred, and analysis of recurrent lesions showed reduced IL13Rα2 expression, highlighting the challenge of antigen heterogeneity and immune escape in targeted immunotherapies for GBM.

1.6.2. Epidermal Growth Factor Receptor Variant III

Epidermal growth factor receptor variant III (EGFRvIII) is one of the most well-characterized tumor-specific mutations in GBM and represents an important molecular target for immunotherapy[194–201]. EGFRvIII arises from a genomic rearrangement in the EGFR gene that deletes exons 2–7, resulting in an in-frame fusion of exon 1 to 8 and producing a truncated receptor lacking a portion of the extracellular ligand-binding domain and generating a novel epitope[202,203]. This mutation results in a constitutively active receptor that signals independently of ligand binding, driving oncogenic pathways that promote tumor cell proliferation, invasion, angiogenesis, and resistance to apoptosis[200,204–207]. EGFRvIII is present in approximately 25–33% of GBM tumors and is typically absent from normal tissues, making it an attractive tumor-specific antigen

for targeted therapies[208]. The mutant receptor preferentially activates downstream signaling pathways such as PI3K/Akt, which contribute to tumor growth and resistance to radiation and chemotherapy[205,209,210]. Because of its tumor-restricted expression and role in GBM progression, numerous therapeutic strategies have been developed to target EGFRvIII. These include monoclonal antibodies, peptide vaccines, chimeric antigen receptor (CAR) T-cell therapies, and bispecific T-cell engager molecules designed to selectively recognize and eliminate EGFRvIII-expressing tumor cells[211–214]. Preclinical and clinical studies have demonstrated that targeting EGFRvIII can induce tumor-specific immune responses and inhibit tumor growth in experimental models[24,215,216]. However, therapeutic responses have been limited by challenges such as intratumoral heterogeneity and the loss or downregulation of EGFRvIII expression following targeted treatment[217]. Despite these limitations, EGFRvIII remains a promising target for precision immunotherapy approaches in GBM, particularly when incorporated into combination strategies aimed at overcoming antigen escape and tumor heterogeneity.

1.7. Cytotoxic Therapeutic Strategies

1.7.1. Phosphatase and Tensin Homolog Restoration in Glioblastoma

Loss or mutation of the tumor suppressor phosphatase and Tensin homolog (PTEN) is a frequent molecular alteration in GBM and contributes significantly to tumor progression through dysregulation of the phosphoinositide 3-kinase (PI3K)/AKT signaling pathway[218–220]. PTEN functions as a lipid phosphatase that antagonizes PI3K signaling by dephosphorylating phosphatidylinositol-3,4,5-trisphosphate (PIP3), thereby preventing activation of AKT and downstream pathways that promote cell survival, proliferation, and metabolic activity[218]. Consequently, PTEN loss leads to constitutive activation of PI3K–AKT signaling, which is commonly observed in GBM and contributes to aggressive tumor growth and resistance to therapy[221]. Because of its central role in regulating oncogenic signaling, restoration of PTEN expression has been investigated as a potential therapeutic strategy for GBM. Experimental studies have demonstrated that reintroduction of wild-type PTEN into PTEN-deficient glioma cells can significantly suppress tumor cell growth. For example, adenoviral-mediated delivery of PTEN into endometrial and colorectal cell lines resulted in a marked inhibition of proliferation and induction of apoptosis, accompanied by reduced AKT phosphorylation and suppression of downstream survival signaling[222,223]. In another experimental approach, PTEN gene transfer into glioma cells

produced substantial cell-cycle effects, including accumulation of tumor cells in the G0/G1 phase and decreased progression through the S phase, ultimately leading to inhibition of tumor cell expansion[224]. Importantly, these effects translated into measurable antitumor efficacy in vivo[224]. In xenograft models of GBM, restoration of PTEN expression significantly suppressed tumor growth and reduced tumor volume compared with control-treated tumors, demonstrating that reactivation of PTEN signaling can impair glioma progression in living systems[224]. More recent gene-therapy strategies have continued to explore PTEN restoration approaches using viral vectors designed to enhance delivery and expression in tumor cells[225,226]. In these studies, PTEN gene delivery was shown to inhibit glioma cell proliferation, reduce migratory capacity, and induce apoptosis, highlighting the continued therapeutic interest in restoring PTEN function in PTEN-deficient GBM[227]. A particularly promising strategy for restoring PTEN activity in GBM involves the use of PTEN-L, a translational isoform of PTEN that contains an additional N-terminal extension enabling secretion and intercellular transfer of the protein[228]. PTEN-L is generated from an alternative upstream start codon, adding 173 amino acids that include a polyarginine motif facilitating uptake into neighboring cells, allowing PTEN activity to be restored in PTEN-deficient cells through extracellular delivery mechanisms[229]. Building on this concept, engineered variants of PTEN-L have been developed to improve secretion and intercellular transfer efficiency. One such construct, light-chain leader PTEN-L (lclPTENL), replaces the native PTEN-L leader sequence with a human IgG light-chain leader peptide to enhance secretion through the classical secretory pathway[228]. In GBM models, cells engineered to express lclPTENL efficiently secreted the protein into the extracellular environment, where it was subsequently taken up by neighboring PTEN-deficient tumor cells and restored catalytic PTEN activity, resulting in reduced AKT phosphorylation and suppression of tumor cell proliferation[229]. Importantly, neural stem cells engineered to express lclPTENL were able to transfer catalytically active PTEN to adjacent GBM cells and significantly inhibit tumor cell motility and proliferation in coculture experiments, demonstrating the feasibility of cell-mediated delivery of functional PTEN activity to tumor cells [228]. These findings suggest that NSC-mediated delivery of lclPTENL represents a promising strategy for restoring tumor suppressor signaling within the GBM microenvironment, providing a mechanistic foundation for therapeutic approaches that combine stem-cell tumor tropism with intracellular tumor suppressor restoration[228].

1.7.2. CD47 Anti-Cancer Therapy

The CD47–SIRPα signaling axis has emerged as an important innate immune checkpoint in cancer immunotherapy, functioning primarily to regulate macrophage-mediated phagocytosis. CD47 is a ubiquitously expressed transmembrane protein belonging to the immunoglobulin superfamily that serves as a marker of "self" on healthy cells[230–233]. When CD47 binds to signal regulatory protein-α (SIRPα), a receptor expressed on macrophages and other myeloid cells, inhibitory signaling is initiated that suppresses phagocytosis of the interacting cell[234,235]. This interaction therefore functions as a critical "don't eat me" signal, preventing immune-mediated clearance of healthy host tissues under normal physiological conditions[230–232,236]. Mechanistically, engagement of CD47 with the extracellular Ig-like domain of SIRPα triggers phosphorylation of immunoreceptor tyrosine-based inhibitory motifs (ITIMs) within the cytoplasmic domain of SIRPα[236]. These phosphorylated motifs recruit the phosphatases SHP-1 and SHP-2, which suppress cytoskeletal rearrangements necessary for phagocytic synapse formation in macrophages[237–239]. As a result, accumulation of myosin II at the phagocytic interface is inhibited, effectively blocking engulfment of the target cell[240]. Macrophage-mediated clearance of cells is therefore determined by a balance between activating "eat me" signals and inhibitory signals such as CD47, and disruption of this balance is a key mechanism by which tumor cells evade immune surveillance . Many cancers exploit this pathway by overexpressing CD47, thereby amplifying inhibitory signaling and preventing immune-mediated elimination[241]. Elevated CD47 expression has been documented across numerous malignancies and is frequently associated with poor clinical outcomes due to enhanced immune evasion and tumor progression[241]. In GBM, CD47 is highly expressed on tumor cells and particularly enriched on GBM stem-like cells, which are believed to contribute to tumor initiation, recurrence, and therapeutic resistance[242]. Increased CD47 expression in glioma has been correlated with tumor grade and unfavorable prognosis, supporting its role as a key immune evasion mechanism within the GBM microenvironment[242–244]. Preclinical studies targeting this pathway have demonstrated that blockade of CD47 can restore macrophage phagocytic activity against tumor cells. In GBM models, treatment with anti-CD47 antibodies increases macrophage-mediated engulfment of glioma cells and glioma stem cells, leading to inhibition of tumor growth and improved survival in experimental models[242]. Additionally, CD47 blockade has been shown to promote a shift toward pro-inflammatory macrophage phenotypes

within the tumor microenvironment, further enhancing antitumor immune responses[245]. These findings highlight the therapeutic potential of targeting innate immune checkpoints to overcome tumor immune evasion. Based on these promising preclinical results, several CD47-targeting therapeutics have entered clinical development. These include monoclonal antibodies such as Hu5F9-G4, as well as engineered fusion proteins such as SIRPα-Fc constructs (e.g., TTI-621) that act as decoy receptors to block CD47 signaling while simultaneously engaging Fc receptors on macrophages to promote phagocytosis[246–248]. Early-phase clinical trials are underway reporting the safety and tolerability and their encouraging antitumor activity in hematologic malignancies and solid tumors[249]. However, these approaches also reveal important challenges that have limited the clinical application of systemic CD47 blockade. One of the primary obstacles to systemic CD47-targeting therapies is on-target toxicity in normal tissues, particularly anemia[248,250]. Because CD47 is broadly expressed on healthy cells, including erythrocytes and platelets, systemic administration of CD47-blocking antibodies can trigger macrophage-mediated clearance of red blood cells, leading to hemolytic anemia and thrombocytopenia[251,252]. These toxicities arise because inhibition of the CD47–SIRPα interaction removes a protective signal that normally prevents macrophages from engulfing circulating blood cells. As a result, many therapeutic strategies require dose-priming regimens or antibody engineering approaches to mitigate hematologic toxicity[246,253]. Beyond toxicity concerns, systemic CD47 blockade also faces challenges related to tumor specificity and therapeutic index. Because CD47 is expressed on nearly all cells, systemically delivered antibodies must achieve sufficient concentrations at the tumor site without inducing widespread immune activation in normal tissues. This limitation is particularly relevant in GBM, where the blood–brain barrier further restricts drug delivery and contributes to heterogeneous antibody penetration within the tumor microenvironment. These challenges have motivated the development of alternative delivery strategies aimed at localizing CD47 blockade within the tumor microenvironment[254].

1.8. Study Rationale and Objectives

GBM remains one of the most aggressive and treatment-resistant primary brain tumors, characterized by diffuse invasion, marked intratumoral heterogeneity, and the presence of the blood–brain barrier (BBB), all of which limit the efficacy of conventional and targeted therapies. Although antibody-based immunotherapies, including monoclonal and bispecific constructs, have

demonstrated clinical success in other cancers, their application in GBM has been constrained by poor tumor penetration, limited persistence within the tumor microenvironment, and off-target toxicities. Targeting GBM-associated antigens such as CD47 and IL13Rα2 and EGFRvIII presents a promising strategy to improve tumor specificity and overcome immune evasion; however, effective and controlled delivery of these biologics remains a significant challenge.

Engineered neural stem cells (NSCs) offer a unique solution to these limitations due to their intrinsic tumor-tropic properties, allowing them to migrate toward and infiltrate GBM lesions. Leveraging NSCs as cellular delivery vehicles enables localized and sustained production of therapeutic agents directly within the tumor microenvironment. In this project, PBiNSCs are engineered with a SNIPR system to provide antigen-dependent recognition and response to control of therapeutic expression. SNIPRs are designed to recognize specific tumor-associated antigens such as IL13Ra2 and EGFRvIII and, upon engagement, activate intracellular transcriptional programs that drive expression of a therapeutic payload such as lclPTENL. This inducible system introduces an additional layer of spatial and molecular specificity, ensuring that therapeutic protein production is preferentially activated in the presence of tumor cells, thereby reducing off-target effects and improving safety.

The therapeutic payload investigated in this study is a bispecific Fc fusion protein targeting CD47 and IL13Rα2. Fc fusion proteins offer several advantages, including enhanced stability, dimerization, and prolonged half-life, while bi-specificity enables simultaneous targeting of multiple tumor-associated pathways. This cytotoxic payload can further potentiate anti-tumor immunity through FcγR engagement, promoting the recruitment and activation of immune effector cells such as macrophages and T cells. Concurrently, blockade of CD47 signaling relieves the inhibitory “don’t eat me” signal that suppresses phagocytosis, thereby enabling more effective immune recognition and clearance of tumor cells within the GBM microenvironment.

The rationale of this study is therefore: (1) to investigate SNIPR-based and NSC-mediated systems as a strategy for tumor-specific, inducible therapeutic activation, and (2) to evaluate a GBM bispecific Fc fusion protein designed to block CD47 signaling while promoting Fcγ receptor–mediated immune responses in GBM.

2. Results

2.1. SyNthetic Intramembrane Proteolysis Receptor for Glioblastoma Recognition and Response

2.1.1. SyNthetic Intramembrane Proteolysis Receptor Design

The SNIPR-based system is engineered as a modular, ligand-inducible signaling platform that couples extracellular antigen recognition to customizable transcriptional outputs[138]. The receptor design is adapted from the core regulatory mechanism of the Notch signaling pathway, in which ligand binding induces conformational changes that expose a proteolytic cleavage site within the transmembrane domain. Structurally, the SNIPR consists of an extracellular antigen recognition domain, typically a single-chain variable fragment (scFv) specific to a target antigen such as CD19, fused to a Notch-derived regulatory core containing a negative regulatory region (NRR), transmembrane domain, and juxtamembrane cleavage sites (Figure 1A). Upon antigen engagement, mechanical forces generated through receptor–ligand interaction relieve autoinhibition of the NRR, enabling sequential proteolytic cleavage events that release the intracellular transcription factor domain (Figure 1C). In this system, the intracellular domain is replaced with a chosen orthogonal transcription factor, HNF1A, which is not endogenously expressed in PBiNSCs, as confirmed by RNA sequencing analysis (GSE117720), which showed read counts between 0–1, thereby ensuring tight control over downstream transcriptional activation[121]. Complementing the receptor, the SNIPR response element is designed as a synthetic, transcription factor–responsive expression cassette that translates receptor activation into gene expression (Figure 1B). This construct consists of tandem repeats of transcription factor binding motifs specific to the released intracellular domain (e.g., HNF1A response elements) positioned upstream of a minimal promoter with low basal activity. This configuration minimizes background expression while enabling strong inducible transcription upon activation. Downstream of this promoter, an inducible gene, initially a fluorescent reporter such as BFP is expressed, while a separate constitutive promoter drives expression of a fluorescent marker (mCitrine) to label transduced cells and allow normalization of activation efficiency. The modular architecture of this response element enables straightforward substitution of the reporter gene with alternative payloads, such as therapeutic proteins, without altering upstream regulatory components. Assembly of both the SNIPR receptor and response element plasmids is achieved through standard

molecular cloning strategies, including restriction enzyme digestion and recombination-based methods allowing flexible exchange of extracellular recognition domains, intracellular transcription factors, and inducible output genes to tailor the system for specific applications.

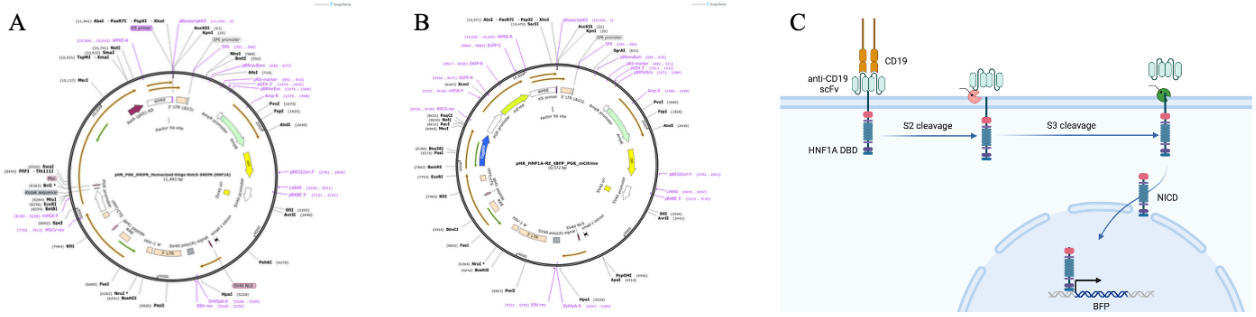

Figure 1: Plasmid maps illustrating the lentiviral constructs used for SNIPR-based engineering (A) SNIPR receptor construct (pHR_PGK_SNIPR_Humanized Hinge Notch SNIPR (HNF1A) was a gift from Kole Roybal (Addgene plasmid #188384 ; http://n2t.net/addgene:188384 ; RRID:Addgene:188384)), encoding an antigen-recognition extracellular domain fused to a synthetic Notch receptor core consisting of a Notch1 transmembrane domain and Notch2 juxtamembrane domain, coupled to an inducible transcription factor (HNF1A DNA-binding domain fused to p65 activation domain), and (B) complementary SNIPR construct (pHR_HNF1A-RE_tBFP_PGK_mCitrine was a gift from Kole Roybal (Addgene plasmid #188387 ; http://n2t.net/?addgene:188387 RRID:Addgene:188387)) used for expression of the corresponding signaling or reporter components. Both constructs are driven by constitutive promoters within a lentiviral backbone, enabling stable integration and expression in target cells. (C) Schematic representation of the SNIPR mechanism: upon binding of the extracellular domain to a tumor-associated antigen, the receptor undergoes conformational activation and proteolytic cleavage within the Notch core. This releases the intracellular transcriptional domain, which translocates to the nucleus and induces expression of downstream target genes. This system enables tightly controlled, antigen-dependent activation of therapeutic gene expression.

2.1.2. Functional Validation of the Anti-CD19 SNIPR System in PBiNSCs

2.1.2.1. Streptavidin bead-based antigen presentation approach of activation

To evaluate antigen-dependent activation of the engineered receptor, SNIPR functionality was assessed using a streptavidin bead-based stimulation system presenting CD19. PBiNSCs transduced with increasing lentiviral volumes (100–500 µL) of CD19 SNIPR inducible BFP were exposed to CD19-conjugated streptavidin beads to enable receptor engagement under controlled

conditions. Fluorescence imaging was used to assess activation, with constitutive mCitrine expression identifying transduced cells and inducible BFP expression serving as a readout of SNIPR activation (Figure 2A). Images were acquired under consistent exposure settings and quantified using Fiji (ImageJ) by normalizing total BFP signal to total mCitrine signal to account for differences in transduction efficiency. Quantitative analysis revealed a clear lentiviral volume–dependent increase in SNIPR activation in the CD19-positive condition, with activation rising from approximately 0.1% at 100 µL, to 0.4% at 200 µL, 1.8% at 300 µL, 4.5% at 400 µL, and reaching 4.7% at 500 µL (Figure 2B). In contrast, CD19-negative control conditions exhibited minimal activation across all viral inputs, remaining low at approximately 0.2–0.3% at 100–300 µL, with only a modest increase to 0.6% at 400 µL and 0.3% at 500 µL. This demonstrates a clear separation between antigen-presenting and control conditions, particularly at higher lentiviral inputs. Across lentiviral volumes, increasing viral input correlated with enhanced SNIPR activation in CD19-positive conditions, suggesting that higher receptor expression improves sensitivity to ligand engagement. However, a slight increase in basal activation was also observed at higher viral inputs in control conditions, indicating that elevated receptor expression may contribute to low-level ligand-independent signaling. Collectively, these findings demonstrate that the SNIPR system exhibits antigen-dependent activation in response to CD19, with activation increasing in a dose-dependent manner while maintaining low background in the absence of ligand.

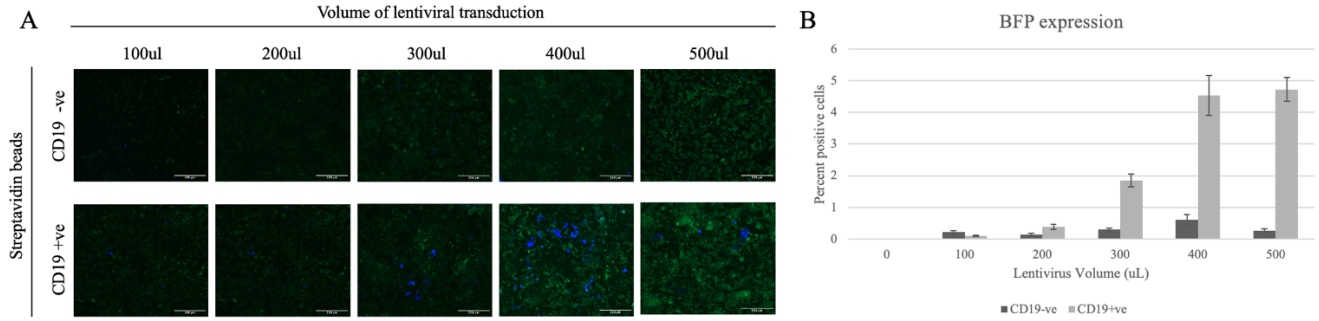

Figure 2: Streptavidin bead-based activation of CD19 SNIPR inducible BFP in PBiNSCs. PBiNSCs transduced with increasing lentiviral volumes (100–500 µL) of CD19 SNIPR and BFP reporter constructs were co-cultured for 72 hours with streptavidin-coated beads conjugated to biotinylated CD19 antigen to induce receptor activation. As a negative control, cells were cultured with streptavidin-coated beads lacking CD19. Following incubation, cells were fixed on coverslips and imaged at 10× magnification using a Zeiss Axio Imager M2 fluorescence microscope. Constitutive mCitrine expression identifies PBiNSCs successfully transduced with SNIPR response element, while SNIPR activation is indicated by induction of BFP expression. Scale bar = 200 µm. (B) Quantification of SNIPR

activation, represented as the percentage of BFP-positive cells per condition. Cells were analyzed using Fiji (ImageJ), and the proportion of activated (BFP^+) cells was calculated relative to the total $mCitrine^+$ population. Error bars represent the standard error of the mean (SEM) across 8 image fields.

2.1.2.2. Cell-based approach of SNIPR activation

To evaluate SNIPR activation in a physiologically relevant context, receptor functionality was assessed using a cell-based co-culture system with CD19-expressing target cells. CD19 SNIPR inducible BFP expressing PBiNSCs were co-cultured with CD19-positive Raji cells, enabling assessment of receptor activation in response to native ligand presentation, or CD19-negative THP-1 cells as a negative control. Fluorescence imaging was used to quantify activation, with constitutive mCitrine expression identifying transduced cells and inducible BFP expression serving as a readout of SNIPR activation (Figure 3A). BFP signal was normalized to mCitrine expression to account for differences in transduction efficiency. Quantitative analysis revealed a lentiviral volume–dependent increase in SNIPR activation in the CD19-positive co-culture condition, with activation rising from approximately 4% at 100 µL, to 38% at 200 µL**,** 43% at 300 µL, and peaking at 53% at 400 µL, before decreasing to 28% at 500 µL (Figure 3B). In contrast, THP-1 control co-cultures exhibited lower levels of activation across all conditions, increasing from approximately 0.22% at 100 µL to 8% at 200 µL and 300 µL, 12% at 400 µL, and 25% at 500 µL. This demonstrates a clear separation between CD19-positive and CD19-negative conditions at intermediate viral inputs, with reduced specificity observed at the highest lentiviral volume. Across lentiviral inputs, increasing viral transduction volumes was associated with increased SNIPR activation in both conditions however, maximal antigen-specific activation was observed at 400 µL, suggesting an optimal balance between receptor expression and specificity. The decline in activation at 500 µL in CD19-positive cells, coupled with increased basal activation in control cells, may reflect receptor overexpression leading to reduced signaling efficiency or increased ligand-independent activation. Collectively, these findings demonstrate robust and antigen-dependent activation of the SNIPR system in a cell-based model, with significantly greater activation compared to bead-based stimulation and an optimal functional window at intermediate receptor expression levels.

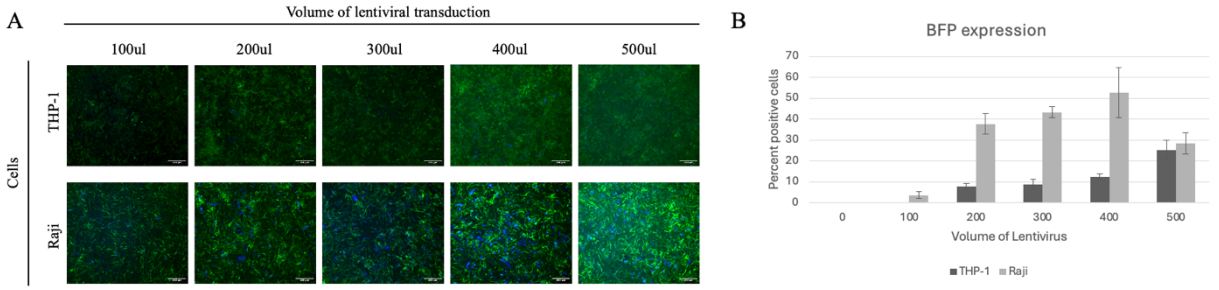

Figure 3: Cell-based activation of CD19 SNIPR inducible BFP in PBiNSCs. (A) PBiNSCs transduced with increasing lentiviral volumes (100–500 µL) of CD19 SNIPR and BFP reporter constructs were co-cultured for 72 hours with CD19+ve cells (Raji cells). As a negative control, cells were cultured with CD19-ve cells (THP-1) cells. Following incubation, cells were fixed on coverslips and imaged at 10× magnification using a Zeiss Axio Imager M2 fluorescence microscope. Constitutive mCitrine expression identifies PBiNSCs successfully transduced with SNIPR response element, while SNIPR activation is indicated by induction of BFP expression. Scale bar = 200 µm. (B) Quantification of SNIPR activation, represented as the percentage of BFP-positive cells per condition. Cells were analyzed using Fiji (ImageJ), and the proportion of activated (BFP^+) cells was calculated relative to the total $mCitrine^+$ population. Error bars represent the standard error of the mean (SEM) across 8 image fields.

2.1.3. Construction and Validation of the SNIPR-lclPTENL Therapeutic Plasmid

Following confirmation of CD19 SNIPR activation, the next objective was to engineer the SNIPR system to express lclPTENL as a therapeutic payload upon receptor activation. lclPTENL is an optimized form of the secreted PTEN-Long isoform of PTEN, a tumor suppressor frequently lost or functionally inactivated in many cancers[228]. Expression of lclPTENL has been shown to restore PTEN signaling in recipient cells through its ability to enter neighboring cells and antagonize oncogenic PI3K/AKT signaling pathways[228]. To generate a SNIPR-responsive therapeutic construct, the lclPTENL coding sequence was inserted into the SNIPR response element in place of the BFP reporter gene. Additionally, a variation of the Woodchuck Hepatitis Virus Posttranscriptional Regulatory Element (WPRE) was added to the end of the lclPTENL sequence[255]. This regulatory element creates a tertiary structure when its translated that helps to enhance the expression of transgenes in viral vectors. Insertion of the lclPTENL sequence into the SNIPR target plasmid was performed using HiFi DNA assembly at a 2:1 insert-to-backbone ratio. This cloning strategy utilizes a mixture of exonuclease, polymerase, and ligase activities to generate complementary single-stranded overhangs, allowing seamless annealing and ligation of the insert into the vector backbone. The assembled plasmids were subsequently transformed into competent *E. coli* for amplification, followed by plasmid purification. Correct assembly of the

SNIPR inducible lclPTENL constructs was verified by restriction digest analysis using restriction digest which produced DNA fragments corresponding to the expected sizes of approximately 7.9 kb for the plasmid backbone and 2.0 kb for the inserted lclPTENL sequence**,** confirming successful cloning of the therapeutic payload.

2.1.4. CD19 SNIPR-Induced Expression of lclPTENL in PBiNSCs

2.1.4.1. Streptavidin bead-based approach to CD19 SNIPR inducible lclPTENL activation

To evaluate the functionality of the engineered SNIPR system for inducible expression and secretion of lclPTENL, activation was first assessed using the streptavidin bead–based system. Streptavidin-coated beads conjugated with biotinylated CD19 were co-cultured with CD19 SNIPR inducible lclPTENL expressing PBiNSCs at a 1:5 bead-to-cell ratio to provide a defined and localized source of antigen presentation. Control conditions included streptavidin beads lacking CD19 to assess ligand-independent activation. After 72 hours, co-culture supernatant was collected to assess secretion of lclPTENL. To detect secreted protein, conditioned media was subjected to immunoprecipitation to enrich for lclPTENL prior to Western blot analysis. As a positive control, immunoprecipitated samples from PBiNSCs constitutively expressing lclPTENL were run in parallel to provide a reference for maximal expression and secretion levels. Western blot analysis revealed minimal detectable lclPTENL at 65kDa in the SNIPR-activated condition, with a faint band observed at only one lentiviral input, 300uL (Figure 4). No corresponding signal was detected in the CD19-negative control, indicating that expression remained antigen-dependent. However, the signal intensity was substantially lower than that observed in the constitutive expression control, suggesting limited activation and/or secretion under these conditions. Due to the low abundance of detected protein, band intensity was insufficient for reliable quantification using Image Lab software. These findings are consistent with the modest activation levels observed in the BFP reporter system under bead-based stimulation and suggest that while the SNIPR system is capable of inducing lclPTENL expression in an antigen-dependent manner, overall protein output under these conditions is limited.

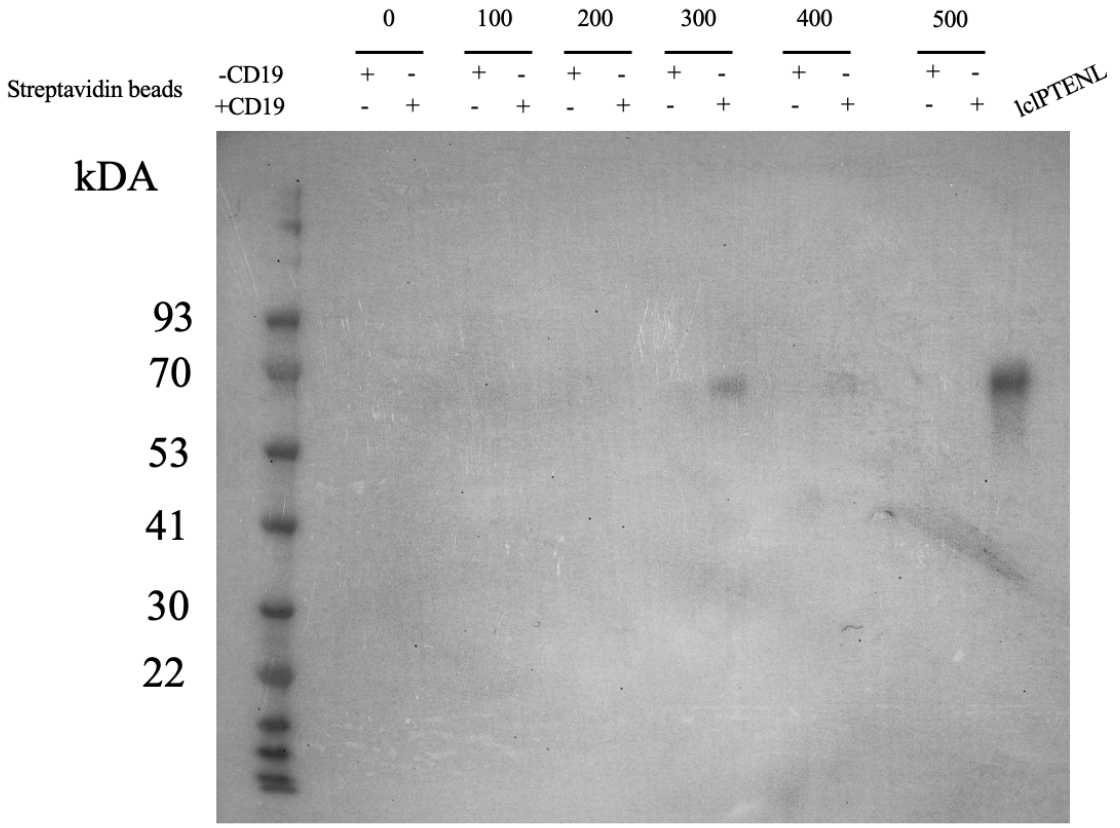

Figure 4: Streptavidin bead-based activation of CD19 SNIPR inducible lclPTENL in PBiNSC immunoprecipitation samples. Immunoprecipitation was performed on media from WT PBiNSCs transduced with increasing volumes (100ul-500ul) of CD19 SNIPR inducible lclPTENL lentivirus was co-cultured with streptavidin beads with or without biotinylated CD19 attached and was analyzed by SDS-PAGE and immunoblotting. PTEN was probed using a PTEN monoclonal antibody (clone D4.3, rabbit IgG1; 1:1000 dilution). A band at ~65 kDa is consistent with lclPTENL and a band at ~50 kDa is consistent with endogenous PTEN. Molecular weight marker (left) indicates protein size in kDa.

2.1.4.2. Cell-based approach to CD19 SNIPR inducible lclPTENL activation

Following bead-based activation, the system was further evaluated using a cell-based stimulation model to better assess SNIPR-driven expression in a physiologically relevant context. CD19 SNIPR inducible lclPTENL expressing PBiNSCs were co-cultured with CD19-positive Raji cells at a 1:1 effector-to-target ratio. This approach enabled analysis of both intracellular protein and secreted protein levels. After 72 hours, both cell lysates and cell culture supernatant were collected and prepared for Western blot analysis. Analysis of cell lysates demonstrated a lentiviral volume–dependent increase in lclPTENL expression; however, expression was observed in both

CD19-negative and CD19-positive conditions, indicating a degree of ligand-independent activation (Figure 5A) . Band intensities were quantified using Image Lab software and normalized to GAPDH as a loading control (Figure 5B). Maximal expression was observed in the 500 µL CD19-positive condition. Endogenous PTEN expression in PBiNSCs was detected at ~50 kDa, while lclPTENL was observed at the expected molecular weight of ~65 kDa, confirming successful expression of the engineered construct. Co-culture supernatant samples were subjected to immunoprecipitation prior to Western blot analysis to enrich for secreted lclPTENL. In contrast to lysate samples, a clearer distinction between CD19-negative and CD19-positive conditions was observed following immunoprecipitation, with increased lclPTENL signal detected in the presence of antigen (Figure 6A). Notably, when compared to the positive control consisting of constitutively expressed constitutive lclPTENL, the 400 µL CD19-positive condition demonstrated approximately two-fold higher levels of lclPTENL following immunoprecipitation (Figure 6B). Although some ligand-independent activation was detected across conditions, expression was consistently elevated in the CD19-positive groups, supporting antigen-dependent activation of the SNIPR system.

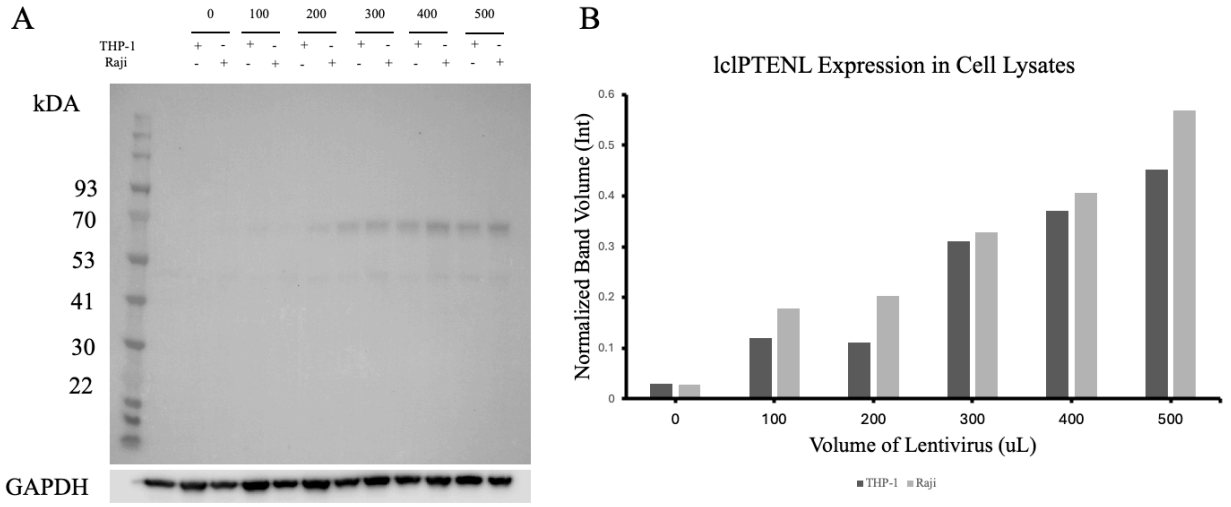

Figure 5: Cell based activation of CD19 SNIPR inducible lclPTENL in PBiNSC cell lysates. (A) Lysates from WT PBiNSCs transduced with increasing volumes (100ul-500ul) of CD19 SNIPR inducible lclPTENL lentivirus co-cultured with Raji or THP-1 cells and was analyzed by SDS-PAGE and immunoblotting. PTEN was probed using a PTEN monoclonal antibody (clone D4.3, rabbit IgG1; 1:1000 dilution). A band at ~65 kDa is consistent with lclPTENL and a band at ~50 kDa is consistent with endogenous PTEN. Molecular weight marker (left) indicates protein size in kDa. (B) Band intensities from the western blot were quantified by Image Lab analysis.

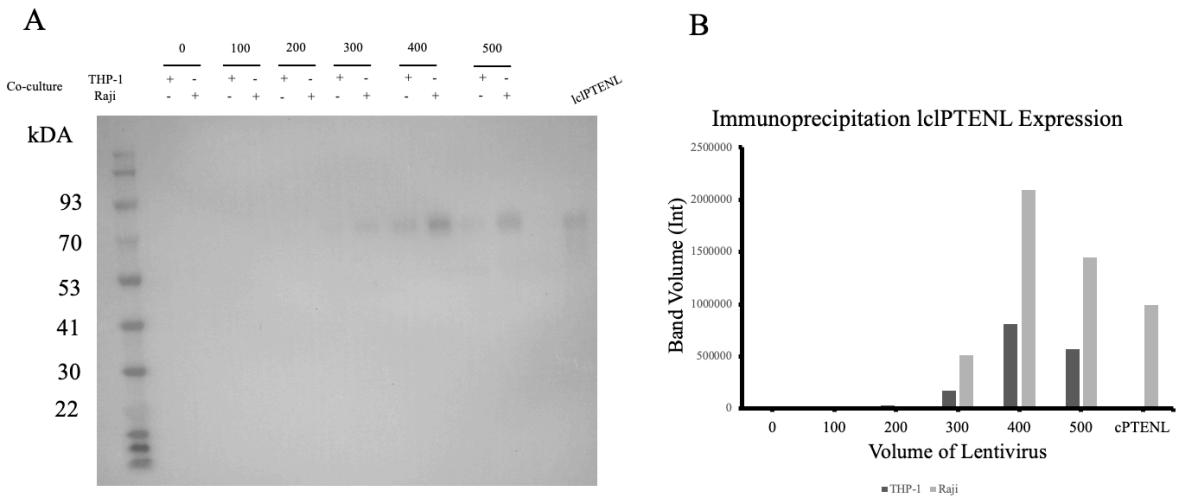

Figure 6: Cell based activation of CD19 SNIPR inducible lclPTENL in PBiNSC immunoprecipitation samples. Immunoprecipitation was performed on media from WT PBiNSCs transduced with increasing volumes (100ul-500ul) of CD19 SNIPR inducible lclPTENL lentivirus co-cultured with Raji or THP-1 cells and was analyzed by SDS-PAGE and immunoblotting. PTEN was probed using a PTEN monoclonal antibody (clone D4.3, rabbit IgG1; 1:1000 dilution). A band at ~65 kDa is consistent with lclPTENL and a band at ~50 kDa is consistent with endogenous PTEN. Molecular weight marker (left) indicates protein size in kDa. (B) Band intensities from the western blot were quantified by Image Lab analysis.

2.1.5. Biological Impact of lclPTENL on Glioblastoma Cells: Modulation of p16 Expression

To investigate the biological impact of lclPTENL uptake in GBM cells, expression of the cell cycle regulator p16 (CDKN2A) was assessed by Western blot following treatment with conditioned media from constitutively expressing lclPTENL PBiNSCs (Figure 7A). p16 is a key inhibitor of CDK4/6 that regulates G1–S cell cycle progression through the RB pathway and is frequently dysregulated in GBM[256]. To isolate the effects of lclPTENL independent of inducible systems, primary GBM cell lines (PriGO9 and PriGO17) were treated with conditioned media derived from PBiNSCs constitutively expressing lclPTENL. Following 48 hours of treatment, cell lysates were collected and analyzed by Western blot for p16 expression (Figure 7A). In PriGO9 and PriGO17 cells, p16 was detected as a band at approximately 16 kDa and quantified by Image Lab software (Figure 7B). Band intensities were normalized to GAPDH to control for loading differences. In agreement with the initial hypothesis, treatment with lclPTENL-conditioned media resulted in an increase in p16 expression in PriGO9 cells compared to WT-conditioned media,

with this increase reaching statistical significance. The selective increase in p16 expression observed in WT CDKN2A PriGO9 cells, but not WT CDKN2A PriGO17 cells, is consistent with previous findings from our lab showing decreased proliferation in only PriGO9 cells following lclPTENL treatment.

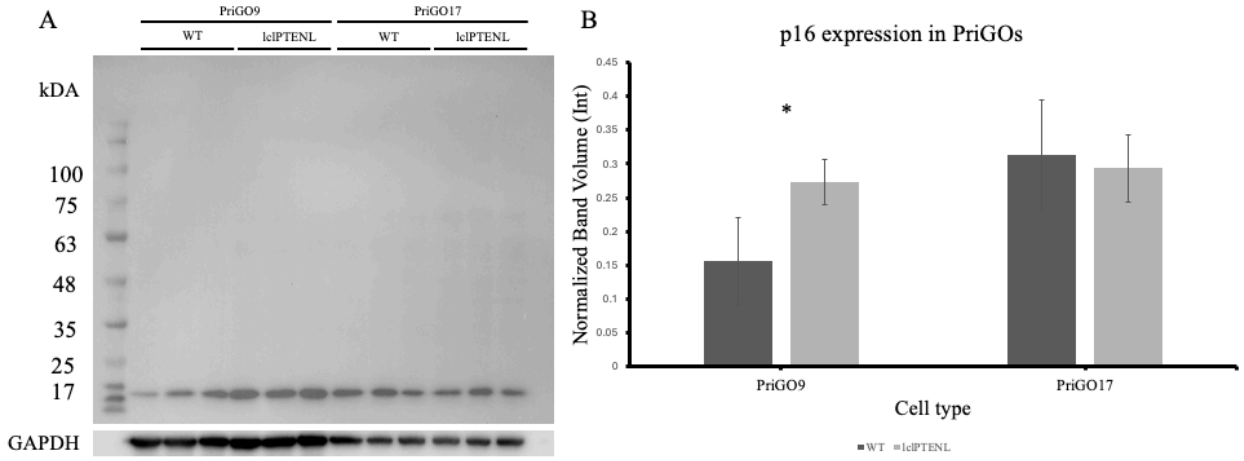

Figure 7: Impact of lclPTENL on p16 expression in PriGO cells (A) Cell lysates from PriGO9, and PriGO17 cells cultured in either WT-conditioned media or lclPTENL-conditioned media for 72h were analyzed by SDS-PAGE and immunoblotting. p16 was probed using a P16INK4a monoclonal antibody (clone 1D7D2, mouse IgG1; 1:1000 dilution). A band at ~16 kDa is consistent with p16. Molecular weight marker (left) indicates protein size in kDa. (B) Quantification of p16 protein expression in and PriGO9 and PriGO17 cells cultured in WT or lclPTENL conditioned media. Band intensities from (A) were quantified by Image Lab analysis and averages of GAPDH normalized band volumes are shown. Error bars show standard deviation of 3 replicates. * $p<0.05$

2.1.6. Engineering a Glioblastoma-Specific SNIPR Targeting IL13Rα2

2.1.6.1. Design of rIL13-SNIPR Receptor

Given that CD19 is not a GBM-specific antigen, the SNIPR receptor was re-engineered to incorporate a disease-relevant extracellular domain (ECD) capable of recognizing GBM-associated targets. The modular architecture of the SNIPR system allows for straightforward substitution of the ECD, enabling retargeting of the receptor toward different antigens without altering the intracellular signaling machinery[138]. Structurally, the ECD is a critical determinant of receptor specificity and must maintain proper ligand binding affinity, spatial orientation, and compatibility with the mechanotransduction requirements necessary for receptor activation. While the original CD19-targeting SNIPR utilizes a single-chain variable fragment (scFv), alternative

ligand-binding domains can be incorporated to expand targeting capabilities. In this study, the ECD was redesigned to target IL13Rα2, a GBM-associated antigen that is overexpressed in tumor cells relative to normal brain tissue[183,185]. To achieve this, a mutated form of interleukin-13 (rIL13) containing a E13Y substitution was used as the binding domain[183]. This engineered ligand is not an scFv, but rather a protein-based targeting moiety that has been optimized to enhance specificity for IL13Rα2 over IL13Rα1, both of which may be expressed in GBM. Importantly, IL13(E13Y)-based targeting strategies have been successfully utilized in other therapeutic platforms, including CAR-T cell therapies, supporting its suitability for targeted GBM applications[69,192]. To generate the rIL13 SNIPR construct, the CD19-binding domain was replaced with the IL13(E13Y) sequence. The rIL13 (E13Y) insert was generated via PCR amplification from a synthesized gBlock and assembled into the SNIPR backbone using HiFi DNA assembly, followed by bacterial amplification and plasmid purification.

2.1.6.2. Activation of IL13Rα2 SNIPR inducible BFP in Glioblastoma Co-culture

Following engineering of the IL13Rα2-targeting SNIPR, receptor functionality was validated using a GBM cell-based activation system to assess antigen-dependent signaling in a physiologically relevant context. IL13Rα2 SNIPR inducible BFP-expressing PBiNSCs were co-cultured with primary GBM (PriGO) cells that had been lentivirally modified to express IL13Rα2, as these cells exhibit minimal endogenous expression of the target receptor. Notably, unlike earlier experiments utilizing suspension target cells, these GBM cells are adherent, representing a different mode of ligand presentation compared to in vitro systems described in the original SNIPR study[138]. This distinction may influence the magnitude and kinetics of SNIPR activation due to differences in cell–cell contact dynamics and mechanotransduction. A 1:1 effector-to-target ratio was used, consistent with previously established SNIPR activation conditions. Cells were imaged using live-cell fluorescence microscopy to assess inducible BFP expression alongside constitutive mCitrine expression, allowing normalization of activation to transduced cell populations (Figure 8A). Upon analysis, appreciable ligand-independent activation was observed across conditions, showing 40% of cells BFP^+ in both the WT and IL13Ra2 PriGO9 conditions raising concerns regarding the specificity and tunability of the system using this specific extracellular domain (Figure 8B). This unintended activation is particularly notable in the context of existing evidence

suggesting complex binding dynamics between IL13 and IL13 receptor subunits, including potential high-affinity or off-target interactions that may contribute to baseline signaling. In contrast, in the WT PriGO8 minimal activation, ~20% was seen in IL13Rα2-negative conditions as well as IL13Rα2-positive conditions (Figure 8B).

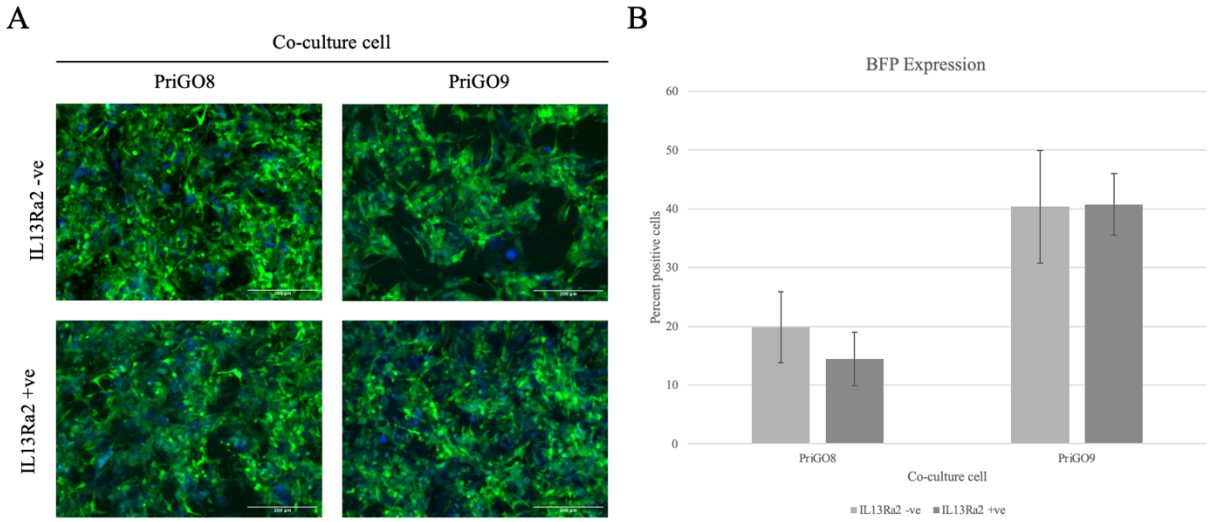

Figure 8: Cell-based activation of IL13Ra2 SNIPR inducible BFP in PBiNSCs co-cultured with PriGO8 and PriGO9 cells. (A) PBiNSCs transduced with 500uL lentivirus expressing IL13Ra2 SNIPR inducible BFP were co-cultured with WT PriGO8/9 (IL13Ra2 negative) or PriGO8/9 cells transduced with lentivirus expressing IL13Ra2. Cells were imaged on the BioTek Cytation 5 after 72h at 10X magnification. Constitutive mCitrine expression identifies PBiNSCs successfully transduced with SNIPR response element, while SNIPR activation is indicated by induction of BFP expression. Scale bar =200um was added using Fiji software. (B) Quantification of SNIPR activation, represented as the percentage of BFP-positive cells per condition. Cells were analyzed using Fiji (ImageJ), and the proportion of activated (BFP^+) cells was calculated relative to the total $mCitrine^+$ population. Error bars represent the standard error of the mean (SEM) across 6 image fields.

2.1.7. Engineering a Glioblastoma-Specific SNIPR Targeting EGFRvIII

2.1.7.1. Design of EGFRvIII-SNIPR Receptor

In another attempt to expand the targeting versatility of the SNIPR platform toward clinically relevant GBM antigens, a receptor construct specific for EGFRvIII was engineered through incorporation of an MR1-derived single-chain variable fragment (scFv) as the extracellular recognition domain. EGFRvIII is a tumor-specific, constitutively active mutant of EGFR that arises from an in-frame deletion of exons 2–7 and is frequently expressed in GBM while being absent from normal tissues, making it an attractive and highly specific therapeutic

target. The MR1 scFv, which has been previously validated for selective recognition of EGFRvIII, was selected to confer antigen specificity to the SNIPR receptor[257]. To generate this construct, the existing SNIPR receptor was modified by replacing the extracellular CD19- or IL13-based targeting domain with the MR1 scFv, while preserving the core receptor architecture required for regulated intramembrane proteolysis and downstream transcriptional activation. This modular design enables retention of the transmembrane and juxtamembrane Notch-derived domains, as well as the intracellular HNF1A transcription factor, ensuring that antigen binding remains coupled to inducible gene expression. The MR1 scFv sequence was introduced via PCR amplification and seamless cloning into the SNIPR vector using HiFi assembly, followed by bacterial amplification and plasmid purification. This strategy highlights the modularity of the SNIPR system, in which extracellular domains can be readily exchanged to retarget receptor specificity, and establishes a framework for evaluating EGFRvIII-directed activation and therapeutic payload delivery in GBM models.

2.1.7.2. Activation of MR1 SNIPR in Glioblastoma Co-culture

To determine whether the MR1 SNIPR system can selectively recognize and respond to GBM cells expressing EGFRvIII, receptor functionality was evaluated in a tumor-relevant co-culture model. This approach enables assessment of antigen-specific activation in the context of native cell surface presentation, providing a more biologically meaningful measure of SNIPR performance. MR1 SNIPR inducible BFP PBiNSCs (300ul-500ul) were co-cultured with PriGO cells engineered to express EGFRvIII, allowing for direct interrogation of receptor activation in response to tumor-associated antigen. An equivalent 1:1 effector-to-target ratio was maintained across conditions to ensure consistency. Following incubation, cells were fixed and analyzed by fluorescence imaging, with constitutive reporter expression used to identify transduced PBiNSCs and inducible BFP expression serving as a readout of SNIPR activation (Figure 9A and C). Images were acquired at 40X under consistent exposure settings and quantified using Fiji (ImageJ) by calculating total BFP signal normalized to total constitutive mCitrine reporter expression to account for differences in transduction efficiency. Quantitative analysis revealed robust SNIPR activation in EGFRvIII-expressing PriGO9 cells across all lentiviral input conditions, with a ratio of 74% of total BFP-positive cells at 300 µL**,** 72% at 400 µL**,** and 76% at 500 µL (Figure 9D). In contrast, wild-type PriGO cells exhibited minimal activation, with BFP expression remaining near

background levels at lower viral inputs and increasing only slightly at the highest condition **(**~0–1% at 300–400 µL, rising to ~2–5% at 500 µL). This indicates a clear separation between EGFRvIII-positive and wild-type conditions. In the EGFRvIII-expressing PriGO8A cell co-culture results show 81% activation at 300 µL**,** 77% at 400 µL, and 66% at 500 µL, while wild-type cells again remained low (~0% at 300–400 µL, increasing to ~5–7% at 500 µL) (Figure 9B). The slight increase in basal activation at higher viral inputs is consistent with increased receptor expression potentially lowering the activation threshold or promoting low-level ligand-independent signaling. Across lentiviral input conditions, SNIPR activation in EGFRvIII-expressing cells remained consistently high, with only modest variation between 300–500 µL, suggesting that receptor activation reaches a near-maximal threshold at lower viral inputs. Collectively, these findings demonstrate that the EGFRvIII SNIPR construct is functionally responsive in a GBM-relevant cellular context and is capable of selectively detecting EGFRvIII-expressing tumor cells, supporting its potential application in targeted therapeutic strategies.

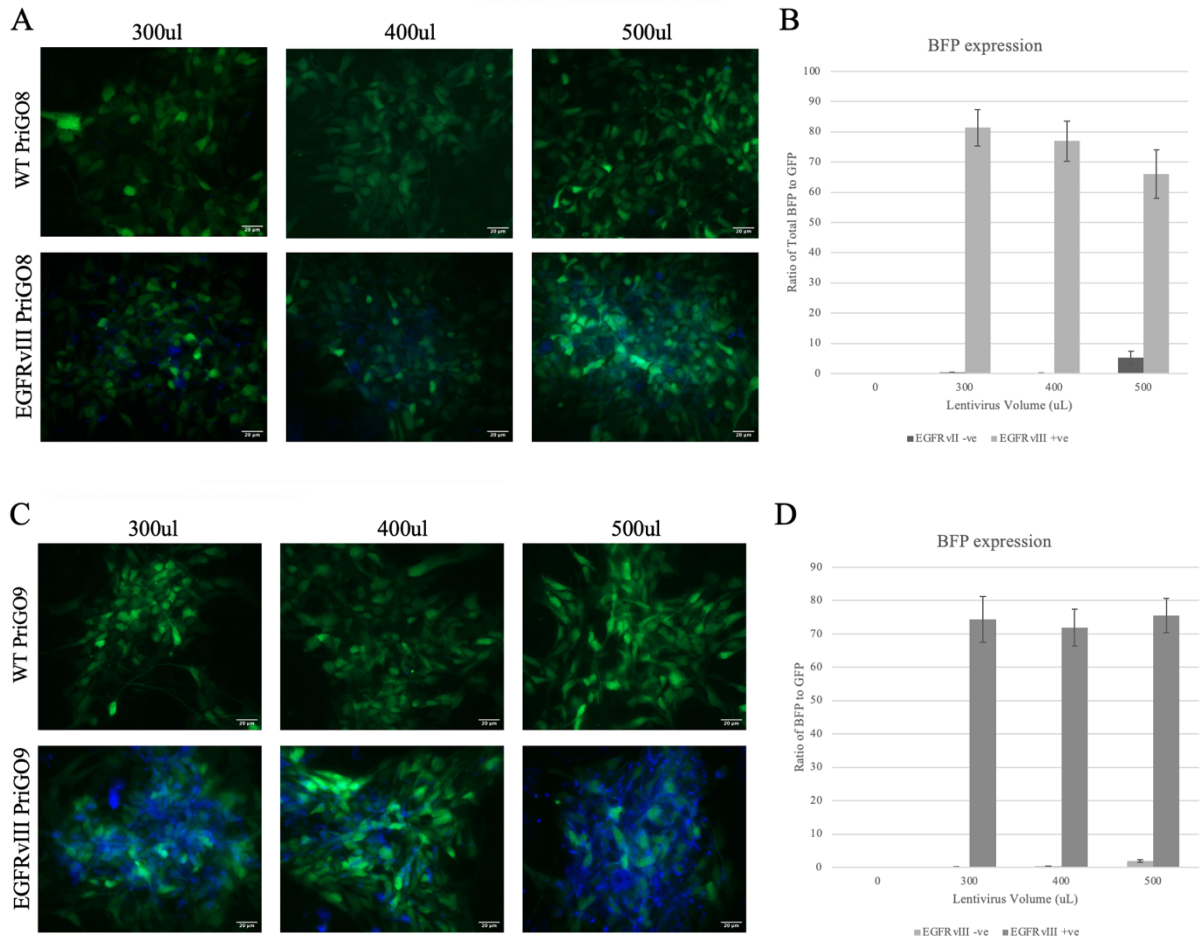

Figure 9: Cell-based activation of EGFRvIII SNIPR inducible BFP in PBiNSCs co-cultured with PriGO8 and PriGO9 cells. (A) PBiNSCs transduced with lentivirus containing EGFRvIII SNIPRs were co-cultured with WT PriGO9 (EGFRvIII negative) or PriGO9 cells transduced with lentivirus containing EGFRvIII and fixed on coverslips after 72h. Coverslips were imaged on the M2 microscope at 40X magnification. Constitutive mCitrine expression identifies PBiNSCs successfully transduced with SNIPR response element, while SNIPR activation is indicated by induction of BFP expression. Scale bar =20um was added using Fiji software. (B) Quantification of SNIPR activation, represented as the percentage of BFP-positive cells per condition. Cells were analyzed using Fiji (ImageJ), and the proportion of activated (BFP^+) cells was calculated relative to the total $mCitrine^+$ population. Error bars represent the standard error of the mean (SEM) across 6 image fields. (C) PBiNSCs transduced with lentivirus containing EGFRvIII SNIPRs were co-cultured with WT PriGO8 (EGFRvIII negative) or PriGO8 cells transduced with lentivirus containing EGFRvIII and fixed on coverslips after 72h. Coverslips were imaged on the M2 microscope at 40X magnification. Constitutive mCitrine expression identifies PBiNSCs successfully transduced with SNIPR response element, while SNIPR activation is indicated by induction of BFP expression. Scale bar =20um was added using Fiji software. (D) Quantification of SNIPR activation, represented as the percentage of BFP-positive cells per condition. Cells were analyzed using Fiji (ImageJ), and the proportion of activated (BFP^+) cells was calculated relative to the total $mCitrine^+$ population. Error bars represent the standard error of the mean (SEM) across 6 image fields.

2.1.8. Evaluating activation of EGFRvIII SNIPR inducible lclPTENL expression using bead-based approach

To evaluate the functionality of the engineered MR1 SNIPR system for inducible expression of lclPTENL, activation was assessed using a streptavidin bead–based system presenting biotinylated EGFRvIII. SNIPR-transduced PBiNSCs were initially co-cultured with EGFRvIII-conjugated beads at a 1:1 bead-to-cell ratio to provide a controlled source of antigen presentation. Following 72 hours of incubation, both cell culture supernatant and cell lysates were collected for analysis. Initial attempts to detect secreted lclPTENL via immunoprecipitation of cell culture supernatant were unsuccessful, as protein levels were below the detection threshold on western blot. As a result, subsequent analysis was performed using whole-cell lysates. Western blot analysis revealed only a very faint band corresponding to lclPTENL (~65 kDa) in the EGFRvIII-positive condition, with no detectable signal in control conditions lacking antigen (Figure 10A). Given that previous experiments using a bead-based approach to SNIPR activation demonstrated minimal differences in activation across lentiviral inputs, subsequent experiments were performed using only the highest viral condition (500 μL) to maximize receptor expression. To further enhance receptor activation, the bead-to-cell ratio was increased to 3:1 based on optimization strategies reported in the literature. Under these conditions, a detectable band corresponding to lclPTENL was observed in the EGFRvIII-positive samples (Figure 10B). Although the signal remained relatively weak, this level of expression is consistent with the modest activation typically observed using bead-based stimulation approaches. Collectively, these findings indicate that the EGFRvIII SNIPR system is capable of inducing antigen-dependent expression of lclPTENL in response to EGFRvIII engagement.

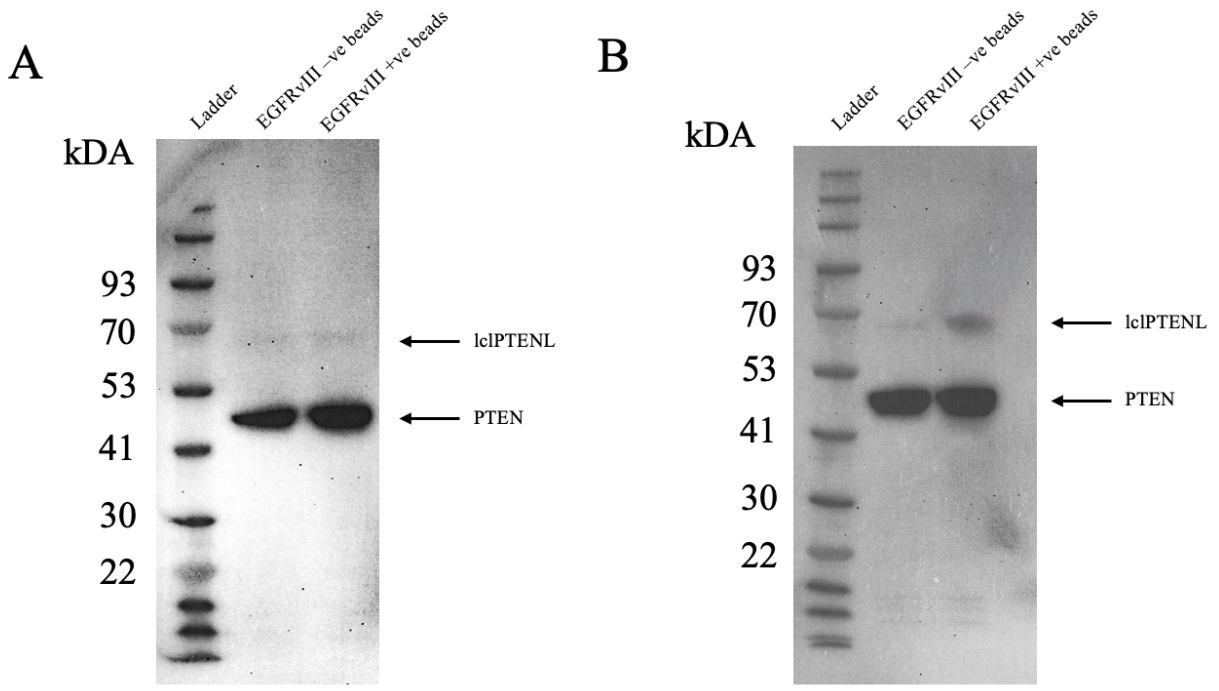

Figure 10: Bead-based activation of EGFRvIII SNIPR inducible lclPTENL in PBiNSC cell lysates. Lysates were collected from PBiNSCs transduced with 500ul of EGFRvIII SNIPR and ind. lclPTENL lentivirus co-cultured with streptavidin beads coated with biotinylated EGFRvIII at a **(A)** 1:1 bead:cell ratio **(B)** 3:1 bead:cell ratio. Samples were analyzed by SDS-PAGE and immunoblotting. PTEN was probed using a PTEN monoclonal antibody (clone D4.3, rabbit IgG; 1:1000 dilution). A band at ~65 kDa is consistent with lclPTENL and a band at ~50 kDa is consistent with endogenous PTEN. Molecular weight marker (left) indicates protein size in kDa.

2.1.9. Evaluating activation of EGFRvIII SNIPR using lclPTENL expression using cell-based approach

To determine whether a more physiologically relevant stimulation context could enhance lclPTENL expression, the EGFRvIII SNIPR system was next evaluated in a cell-based co-culture model using EGFRvIII-expressing PriGO cells. EGFRvIII SNIPR inducible lclPTENL-transduced PBiNSCs (300 µL-500 µL lentiviral volume) were co-cultured with either WT or EGFRvIII-positive PriGO cells to enable receptor activation through native cell surface ligand presentation. Following incubation, both cell culture supernatant and cell lysates were collected and analyzed by Western blot to assess lclPTENL expression Despite the robust EGFRvIII SNIPR activation observed in this system using the BFP response element, no detectable lclPTENL signal (~65 kDa)

was observed in either lysate or cell culture supernatant across all conditions, including EGFRvIII-positive co-cultures (Figure 11A and B). Control conditions similarly showed no detectable signal, confirming the absence of background expression.

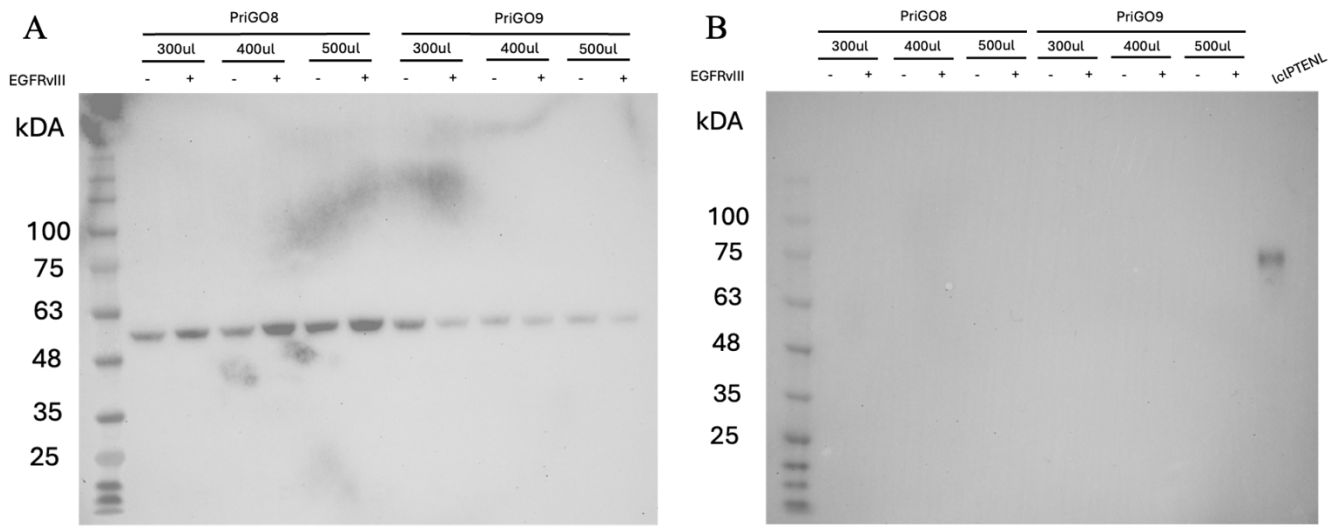

Figure 11: Cell based activation of EGFRvIII SNIPR inducible lclPTENL PBiNSCs co-cultured with PriGO8 and PriGO9 cells. (A) Lysates from WT PBiNSCs transduced with varying volumes of EGFRvIII SNIPR and inducible lclPTENL lentivirus co-cultured with WT PriGO8 or PriGO9 as a control or EGFRvIII expressing PriGO8 or PriGO9 cells was analyzed by SDS-PAGE and immunoblotting. (B) Immunoprecipitation was performed on cell culture supernatant from WT PBiNSCs transduced with increasing volumes (300uL-500uL) of EGFRvIII SNIPR and inducible lclPTENL lentivirus co-cultured with WT PriGO8 or PriGO9 as a control or EGFRvIII expressing PriGO8 or PriGO9 cells was analyzed by SDS-PAGE and immunoblotting. PTEN was probed using a PTEN monoclonal antibody (clone D4.3, rabbit IgG; 1:1000 dilution). A band at ~65 kDa is consistent with lclPTENL and a band at ~50 kDa is consistent with endogenous PTEN. Molecular weight marker (left) indicates protein size in kDa.

2.1.10. Onco-neurosphere model of EGFRvIII SNIPR activation

To more closely model the cell–cell interactions expected in vivo, a 3D onco-neurosphere co-culture system was utilized. This approach enables increased physical contact between GBM (PriGO) cells and SNIPR-expressing PBiNSCs, thereby providing a more physiologically relevant environment for assessing receptor activation. Within this model, SNIPR activation was evaluated through inducible BFP expression in response to EGFRvIII presented by PriGO cells. Onco-neurospheres were generated by co-seeding PriGO cells labeled with mCherry and EGFRvIII SNIPR inducible BFP PBiNSCs labeled with GFP at a 1:1 ratio in non-adherent 6-well plates lacking laminin or Matrigel. Cultures were maintained for 72 hours to allow for sphere formation.

At this time point, neurospheres were imaged using a BioTek live-cell imager at 10× magnification, enabling visualization of cellular organization as well as BFP expression as a readout of SNIPR activation. Fluorescence imaging revealed distinct spatial organization within the onco-neurospheres, with GFP-positive EGFRvIII SNIPR inducible BFP PBiNSCs predominantly localized to the core and mCherry-positive PriGO cells forming an outer layer (Figure 12). Consistent with previous 2D co-culture results, robust BFP expression was observed in neurospheres containing EGFRvIII-expressing PriGO cells, whereas minimal to no activation was detected in neurospheres formed with wild-type PriGOs. This demonstrates that SNIPR activation is maintained in a 3D context and remains dependent on EGFRvIII expression.

To confirm that this neurosphere architecture was preserved when the inducible BFP reporter was replaced with the therapeutic payload and check for detectable lclPTENL levels, a parallel onco-neurosphere experiment was performed using PBiNSCs transduced with the EGFRvIII SNIPR inducible lclPTENL construct. Neurospheres were generated under identical conditions: mCherry-labeled PriGO8 or PriGO9 cells and GFP-labeled EGFRvIII SNIPR ind. lclPTENL PBiNSCs were co-seeded at a 1:1 ratio in non-adherent 6-well plates and cultured for 72 hours prior to imaging. In this experiment, fluorescence imaging shows a different result in that PriGO cells formed the majority of the neurosphere while there are only a few PBiNSCs cells within the onco-neurosphere (Figure 13). This spatial organization was consistent across both WT and EGFRvIII-expressing PriGO8 and PriGO9 conditions.

When the same experiment was done using PriGO17 cells, the GBM cells and the EGFRvIII SNIRP inducible lclPTENL PBiNSCs did grow together but did not form tightly packed, round neurospheres under non-adherent conditions, consistent with their previously characterized inability to grow as suspension spheroids alone (Figure 14). Importantly, the expression of EGFRvIII did not rescue or alter the non-sphere-forming phenotype of PriGO17 cells, indicating that EGFRvIII expression alone is insufficient to confer the adhesion-independent growth properties required for neurosphere formation. A notable and unexpected observation in the PriGO17 co-culture conditions was that the EGFRvIII SNIPR inducible lclPTENL PBiNSCs, which normally require laminin or Matrigel substrate for adherent growth, displayed adherence to the culture plate surface in the presence of PriGO17 cells even in the absence of exogenous extracellular matrix coating. This substrate-independent adhesion of PBiNSCs was observed in

both EGFRvIII-positive and wild-type PriGO17 conditions and resulted in a growth pattern in which PBiNSCs appeared to grow around and in association with the non-sphere-forming PriGO17 cells, resembling the spatial organization observed in the lclPTENL neurosphere experiments with PriGO8 and PriGO9. One plausible explanation for this phenomenon is that PriGO17 cells deposit or express extracellular matrix proteins such as fibronectin, laminin, or collagen that provide a permissive substrate for PBiNSC adhesion, but this still need to be explored.

When onco-neurospheres from co-cultures with EGFRvIII SNIPR inducible lclPTENL in both EGFRvIII-positive and WT PriGO conditions were collected at the 72-hour endpoint and analyzed by Western blot for lclPTENL expression, no detectable band corresponding to lclPTENL (~65 kDa) was observed in either condition (Figure 15). This absence of detectable lclPTENL in the 3D neurosphere model is consistent with the results obtained in the 2D cell-based EGFRvIII SNIPR co-culture system.

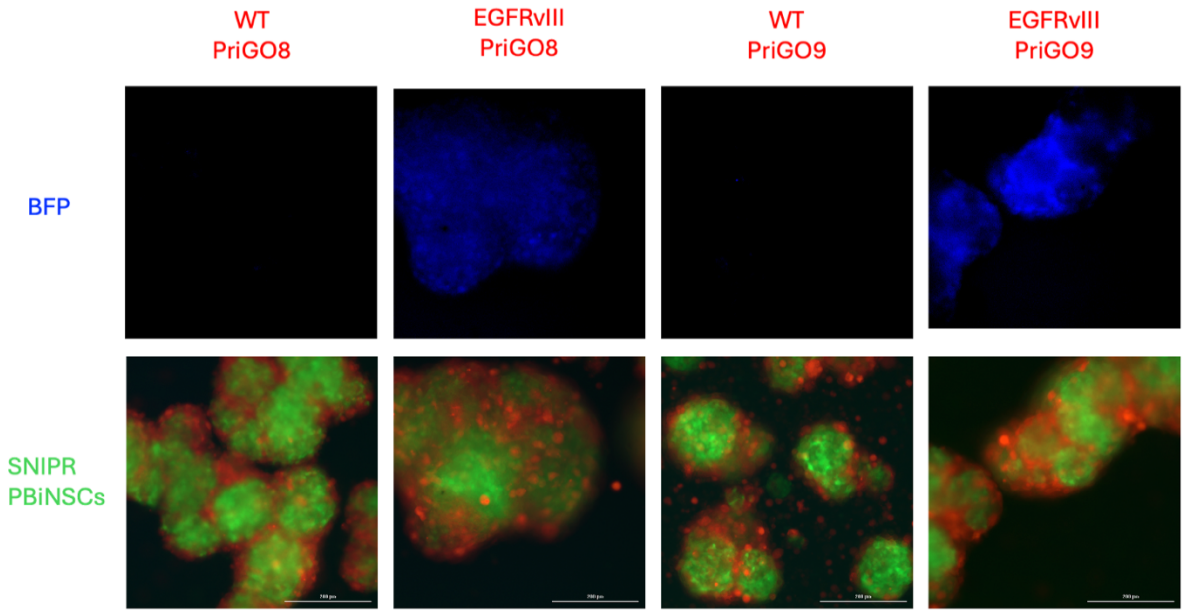

Figure 12: Onco-neurosphere model of activation of EGFRvIII SNIPR inducible BFP in PBiNSCs with PriGO8 and PriGO9s. PBiNSCs transduced with lentivirus containing EGFRvIII SNIPR ind. BFP were co-cultured with WT PriGO8/9 (EGFRvIII negative) or PriGO8/9 cells transduced with lentivirus containing EGFRvIII in non-adherent plates and left to grow for 72h. Onco-neurospheres were imaged using the BioTek Cytation 5 imager at 10X. Constitutive mCitrine plasmid present in all PBiNSCs resulting in green fluorescence and all PriGO cell lines are

labeled with mCherry. Activation of EGFRvIII SNIPR in PBiNSCs shown by blue fluorescence. Scale bar =200um is shown.

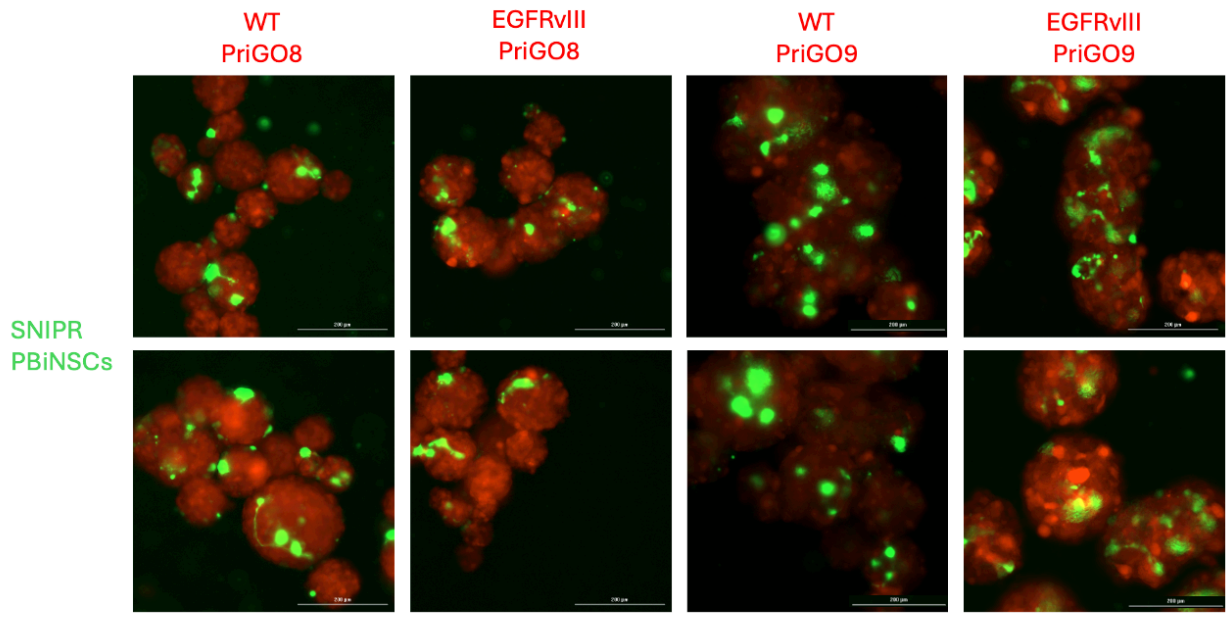

Figure 13: Onco-neurosphere model of EGFRvIII SNIPR inducible lclPTENL in PBiNSCs with PriGO8 and PriGO9s. PBiNSCs transduced with 500uL of lentivirus containing EGFRvIII SNIPR inducible lclPTENL were co-cultured with WT PriGO8/9 (EGFRvIII negative) or PriGO8/9 cells transduced with lentivirus containing EGFRvIII in non-adherent plates and left to grow for 72h. Onco-neurospheres were imaged using the BioTek Cytation 5 imager at 10X. Constitutive mCitrine plasmid present in all PBiNSCs resulting in green fluorescence and all PriGO cell lines are labeled with mCherry. Scale bar =200um is shown.

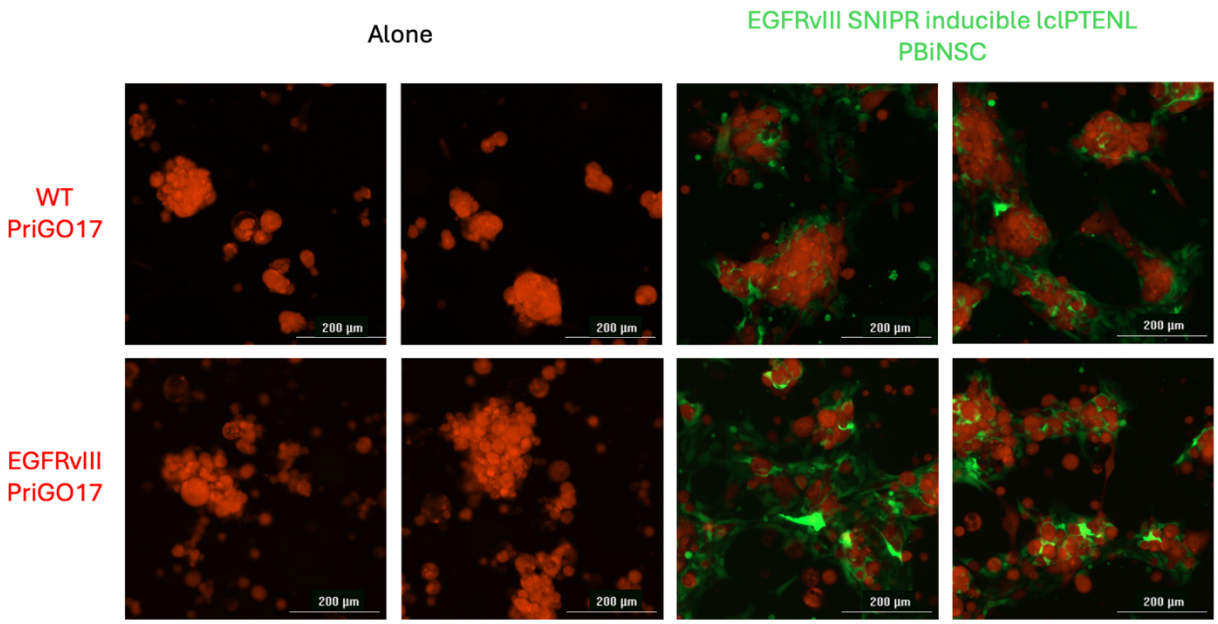

Figure 14: Co-culture of EGFRvIII SNIPR inducible PBiNSCs with PriGO17s in onco-neurosphere model. PBiNSCs transduced with lentivirus containing EGFRvIII SNIPR ind. lclPTENL were co-cultured with mCherry WT PriGO17 (EGFRvIII negative) or mCherry PriGO17s cells transduced with lentivirus containing EGFRvIII in non-adherent plates and left to grow for 72h. Onco-neurospheres were imaged using the BioTek Cytation 5 imager at 10X. Constitutive mCitrine plasmid present in all PBiNSCs resulting in green fluorescence and all PriGO cell lines are labeled with mCherry. Activation of EGFRvIII SNIPR in PBiNSCs shown by blue fluorescence. Scale bar =200um is shown.

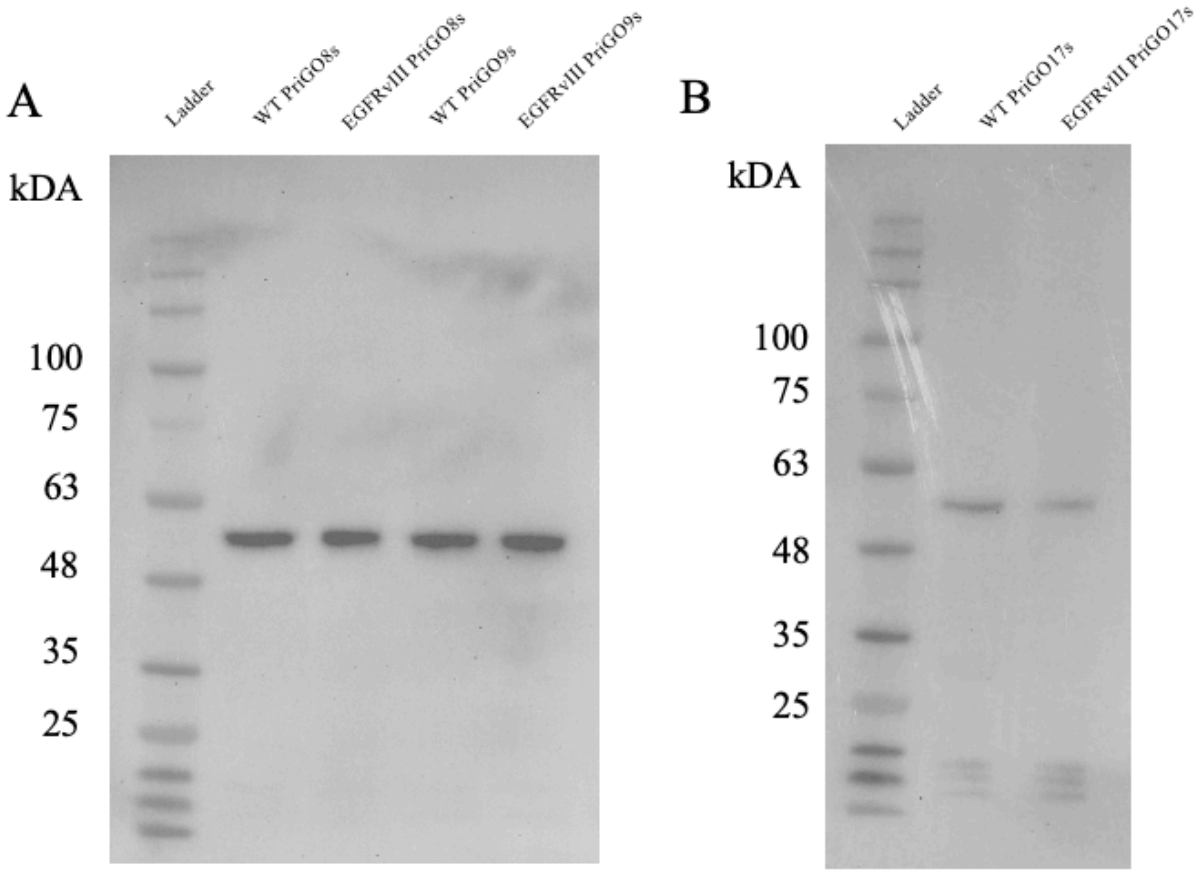

Figure 15: Western blot of EGFRvIII SNIPR inducible lclPTENL onco-neurospheres with PriGO cells. Onco-neurosphere lysates were collected after 72h which were made from PBiNSCs transduced with 500ul of EGFRvIII SNIPR and inducible lclPTENL lentivirus and (A) WT or EGFRvIII expressing PriGO8 and PriGO9 (B) WT or EGFRvIII expressing PriGO17 cells were analyzed by SDS-PAGE and immunoblotting. PTEN was probed using a PTEN monoclonal antibody (clone D4.3, rabbit IgG; 1:1000 dilution). A band at ~65 kDa is consistent with lclPTENL and a band at ~50 kDa is consistent with endogenous PTEN. Molecular weight marker (left) indicates protein size in kDa.

2.2. Engineering PBiNSCs with Glioblastoma-Specific Fc Fusion Protein Targeting CD47

While lclPTENL represents a promising SNIPR-inducible cytotoxic payload by virtue of its ability to restore tumor suppressor signaling in neighboring PTEN-deficient GBM cells, the challenges encountered in detecting EGFRvIII SNIPR-driven lclPTENL expression in primary GBM co-culture models highlight the need to consider complementary cytotoxic strategies. We therefore engineered PBiNSCs to constitutively secrete a bi-specific Fc fusion protein targeting

CD47 alongside GBM-associated antigens, leveraging a distinct but synergistic mechanism of tumor cell elimination through innate immune re-engagement rather than intracellular tumor suppressor restoration.

2.2.1. Structure and Function of IL13/SIRPa Bi-specific Fc-fusion Protein

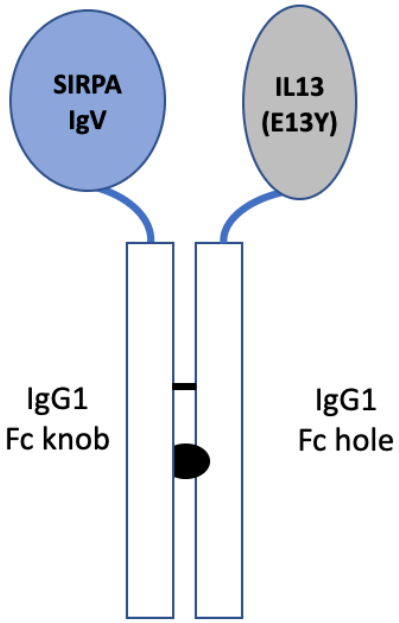

Figure 14: Schematic of the SIRPα/IL13 bispecific Fc-fusion protein. Diagram showing a heterodimeric Fc-fusion construct composed of the IgV domain of SIRPα and an IL13 (E13Y) ligand fused to human IgG1 Fc domains. The two chains are engineered with complementary "knob" and "hole" mutations within the Fc regions to promote heterodimerization, resulting in a single bispecific molecule displaying SIRPα on one arm and IL13 on the other.

The SIRPα/IL13 bi-specific fc-fusion construct was engineered in previous work as a single open reading frame to enable coordinated expression of both targeting moieties while preserving the molecular features originally developed in the separate plasmid system. This single-transcript design encodes an N-terminal signal peptide to direct co-translational entry into the endoplasmic reticulum and ensure efficient secretion, followed by the CD47-binding domain of human SIRPα fused to a human IgG1 Fc domain containing the "knob" mutations (T366W and S354C)[258]. These mutations, originally generated by PCR-based mutagenesis, introduce steric complementarity and an additional disulfide bond to promote heterodimer formation. Downstream of this first Fc region, a furin cleavage site (RRKR) and P2A self-cleaving peptide sequence were incorporated, preserving the strategy used to co-express two proteins from a single transcript.

Ribosomal skipping at the P2A site results in two nascent polypeptides, while furin-mediated cleavage within the Golgi removes residual peptide remnants, yielding two independent secreted proteins with minimal linker sequences. The second half of the transcript encodes the IL13 binding domain fused to a complementary IgG1 Fc "hole" domain containing the mutations T366S, L368A, Y407V, and Y349C. These mutations create a cavity to accommodate the "knob" residue and introduce a paired disulfide bond with S354C, ensuring preferential heterodimerization between the SIRPα–Fc and IL13–Fc chains. In parallel, the IL13 domain contains a E13Y mutation introduced by PCR mutagenesis to confer selective binding to IL13Rα2, enhancing GBM specificity, and incorporates a modified human IgG light-chain leader sequence to improve secretion efficiency. Importantly, both Fc retain canonical structural elements, including the CPPC hinge motif for interchain disulfide bonding and the conserved CH2 N-linked glycosylation site (N297), which is critical for Fcγ receptor engagement and effector function. Within this construct, the two targeting domains serve distinct functional roles: the SIRPα domain drives the cytotoxic mechanism by blocking the CD47 "don't eat me" signal on tumor cells, thereby enabling macrophage-mediated phagocytosis further potentiated by FcγR engagement on myeloid effector cells; however, the SIRPα–CD47 interaction itself is of relatively low intrinsic affinity, with wild-type human SIRPα binding human CD47 with a K^D in the range of ~100–500 nM[259]. Tumor selectivity should therefore be primarily conferred by the IL13(E13Y) domain, which exploits the high and preferential expression of IL13Rα2 on GBM cells. The E13Y substitution confers approximately 50-fold higher affinity for IL13Rα2 compared to wild-type IL-13, while simultaneously reducing affinity for the IL13Rα1/IL-4Rα signaling complex by approximately 5-fold, an important selectivity improvement given that IL13Rα1 is broadly expressed on normal tissues[260]. Wild-type IL-13 binds IL13Rα2 with a K^D in the low nanomolar range (~0.25–2.5 nM), and the E13Y mutein is expected to bind even more tightly, providing the high-affinity tumor-targeting anchor that concentrates SIRPα-mediated CD47 blockade at the GBM cell surface. Following translation and post-translational processing, the system produces two Fc-fusion polypeptides that assemble into a stable, glycosylated heterodimeric bispecific molecule capable of simultaneously targeting CD47 and IL13Rα2[261].

2.2.2. Expression of IL13/SIRPa Fc-Fusion Protein in PBiNSCs

To confirm stable expression of the bi-specific Fc fusion construct, PBiNSCs were transduced and subjected to puromycin selection, enriching for cells that had successfully integrated the expression cassette. This selection step ensures that downstream protein detection reflects true transgene expression rather than transient or heterogeneous expression. Following selection, cells were cultured for 48 hours to allow for transcription, translation, and secretion of the Fc fusion protein. Both whole-cell lysates and cell culture supernatant were collected to assess intracellular production and extracellular release, respectively. Western blot analysis using an anti-human Fc–HRP antibody revealed a distinct band at approximately 90 kDa in both lysate and media samples. Detection of the protein in the lysate can confirm successful intracellular synthesis, along with its presence in conditioned media indicates efficient trafficking through the secretory pathway (Figure 17A). This suggests that the fusion protein is correctly folded and processed within the endoplasmic reticulum and Golgi apparatus, as improper folding or aggregation would typically result in intracellular retention or degradation. The observed molecular weight (~90 kDa) is consistent with the predicted size of the Fc fusion construct, supporting the structural integrity of the expressed protein. Together, these findings demonstrate that engineered PBiNSCs not only express but also secrete a structurally intact Fc fusion protein, supporting their use as a cellular delivery platform for sustained, localized therapeutic protein production.

2.2.3. Assessing the Binding of the IL13/SIRPa Bi-Specific Fc Fusion Protein to Primary Glioblastoma Cells

A key functional feature of this Fc-fusion protein is its ability to bind IL13Rα2-positive GBM cells with high affinity, enabling tumor-specific targeting. Given that IL13Rα2 is frequently overexpressed in GBM and minimally expressed in normal brain tissue, it represents an attractive therapeutic target for selective tumor recognition. Primary GBM cell lines PriGO8, PriGO9, PriGO17 were incubated with pre-cleared cell culture supernatant derived from engineered PBiNSCs for 48 hours and compared to PriGO8 which had been lentivirally modified to express IL13Rα2 confirmed by western blot. Following incubation, cell lysates were analyzed by Western blot using a polyclonal IgG Fc Antibody to detect Fc-fusion protein bound to or internalized by the cells. A band at approximately 90 kDa was detected in all PriGO samples, indicating successful association of the Fc fusion protein with GBM cells (Figure 17B). It can also be seen that there is no visible increase in band intensity corresponding to the PriGO8 cells that are over expressing

IL13Rα2. Mechanistically, the design of the Fc-fusion protein allows for binding mediated through the IL13Rα2 antigen-recognition domain of the bispecific construct, which enables simultaneous interaction with CD47 and IL13Rα2 on the tumor cell surface. The detection of the Fc fusion protein in cell lysates suggests that the construct either remains surface-bound or undergoes receptor-mediated internalization following binding. Importantly, the preservation of the ~90 kDa band following exposure to GBM cells indicates that the protein remains structurally stable in the extracellular environment and retains functional binding capacity after secretion. This supports the hypothesis that PBiNSC-derived Fc fusion proteins can effectively target tumor cells in a biologically relevant context.

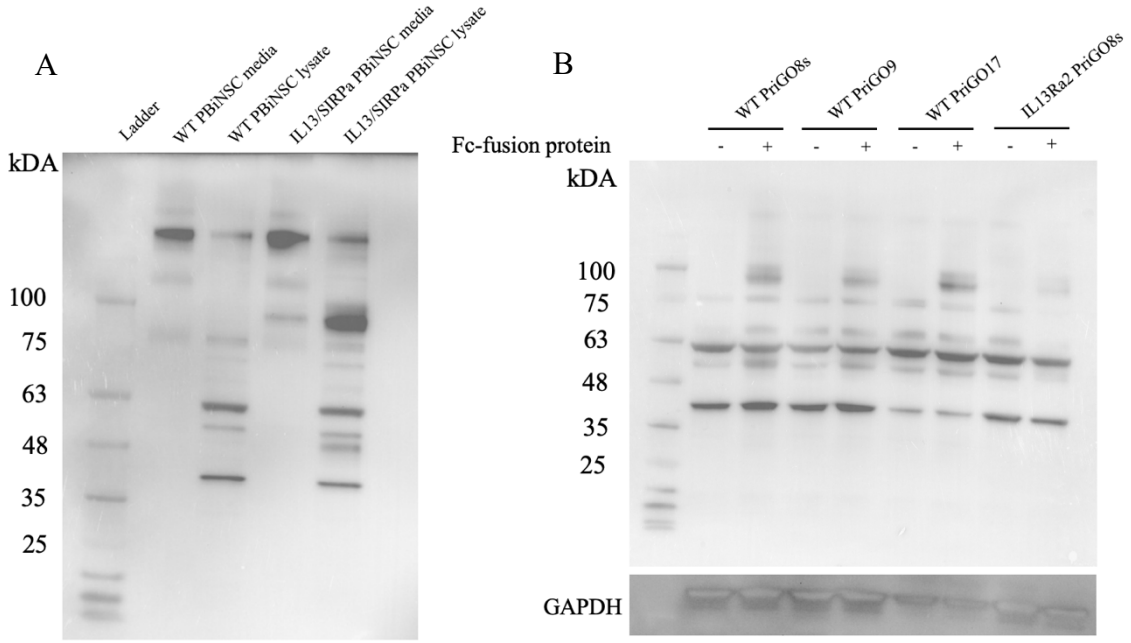

Figure 15: Western blot detection of Expression and Glioblastoma specific binding of IL13/SIRPa bi-specific Fc-fusion protein. (A) Western blot detection of IL13/SIRPa bi-specific Fc fusion protein expressed in PBiNSCs**.** Conditioned media and lysate samples from WT or IL13/SIPRa PBiNSCs were analyzed by SDS-PAGE and immunoblotting. **(B)** Western blot detection of IL13/SIRPa bi-specific Fc fusion protein in PriGO cells lysates cultured in conditioned media**.** Lysates from WT PriGO8s, 9s and 17s and PriGO8s overexpressing IL13Ra2 cultured in either WT-conditioned media or IL13/SIRPa bi-specific-conditioned media were analyzed by SDS-PAGE and immunoblotting. 10ug samples were prepared without BME. Human IgG was probed using an anti-human Fc-HRP-conjugated antibody at a 1:1000 dilution. A band at ~90 kDa is consistent with IL13/SIRPa bi-specific. Molecular weight marker (left) indicates protein size in kDa.

2.2.4. Purification of the IL13/SIRPa Bi-specific Fc Fusion Protein from Cell Culture Supernatant using Affinity Purification

To isolate the IL13/SIRPα bispecific Fc fusion protein from cell culture supernatant for downstream functional and biochemical characterization, affinity purification was performed using Protein G chromatography. Following elution and neutralization, SDS-PAGE and Western blot analysis of the eluted fractions using an anti-human Fc-HRP antibody revealed a band at the expected molecular weight of approximately 90 kDa, consistent with the Fc fusion protein. However, additional higher molecular weight species were also detected, appearing as diffuse bands and smearing above 100 kDa (Figure 18A). Together, these results demonstrate that while Protein G affinity chromatography successfully enriched for the Fc fusion protein from conditioned media, the purified product exhibited heterogeneity consistent with protein aggregation or multimer formation.

2.2.4.1. Elution Optimization using Glycyl-Tyrosine Solution

To mitigate the destabilizing effects associated with conventional pH-based elution, an alternative strategy employing competitive elution at neutral pH was explored using glycine and tyrosine. These amino acids are key contributors to the interaction interface between the Fc domain and Protein G, where binding is mediated through a combination of hydrogen bonding, hydrophobic interactions, and aromatic stacking involving residues within the CH2–CH3 interface of the Fc region. In particular, tyrosine residues within Protein G engage in π–π and hydrophobic interactions with complementary regions on the Fc domain, while glycine contributes to the conformational flexibility required for tight binding[262]. By introducing free glycine and tyrosine in solution at physiological pH (~7.0), these interactions can be competitively disrupted without requiring exposure to extreme acidic or basic conditions. Elution under these mild conditions is expected to better preserve the native conformation of both the Fc region and the fused targeting domains, thereby reducing the risk of aggregation or functional loss. This approach leverages the molecular specificity of the Fc–Protein G interaction to enable gentler recovery of the fusion protein while maintaining structural and functional integrity. Following elution with glycyl-tyrosine, SDS-PAGE and Western blot analysis of the eluted fractions using an anti-human Fc-HRP antibody revealed a faint band comparable to that from the glycine pH 2 elution (Figure 18B) at 90kDa but at a lower band intensity.

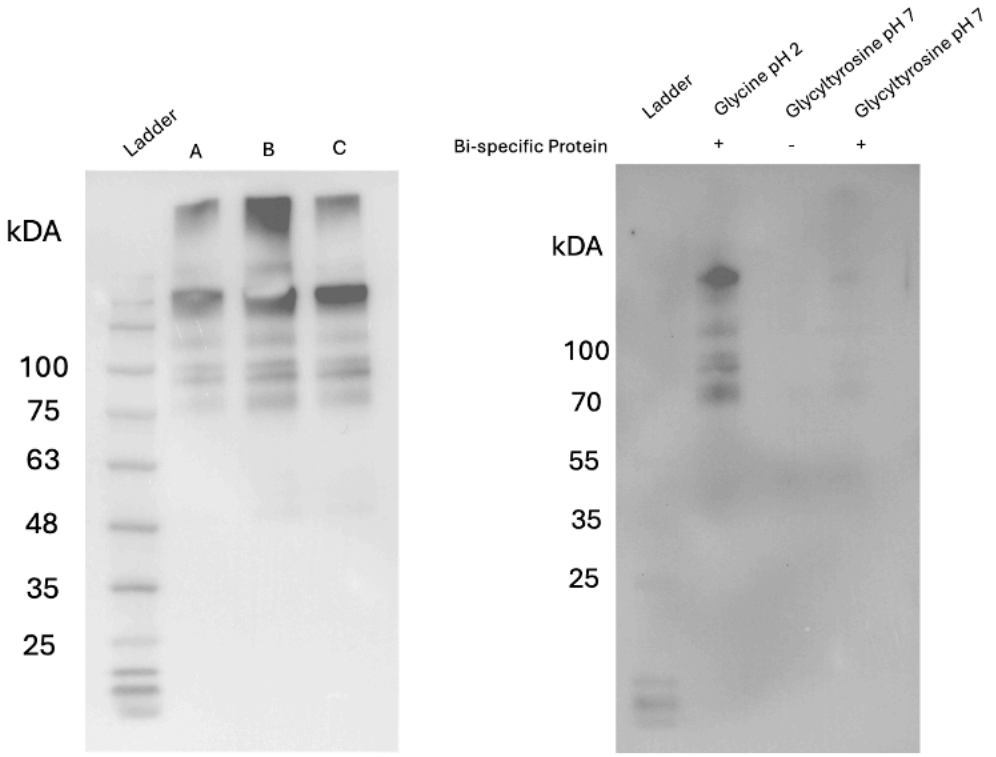

Figure 16: Purification of IL13/SIRPa fc fusion protein from cell culture supernatant. (A) Immunoprecipitation was performed with Protein G Sepharose beads on 1.5mL of bi-specific conditioned media from WT PBiNSCs or PBiNSCs expressing IL13/SIRPa bi-specific. Elution conditions were modified where A. 10 min at 37 C with agitation every 2 minutes B. 10 min at room temperature with agitation every 2 min C. 2min at 37 C with no agitation with Glycine pH 2 as the elution solution. **(B)** Elution optimization of IL13/SIRPa bi-specific Fc fusion protein from Protein G beads**.** Immunoprecipitation was performed with Protein G Sepharose beads on 1.5mL of bi-specific conditioned media from WT PBiNSCs or PBiNSCs expressing IL13/SIRPa bi-specific. Glycine pH 2 and Glycyltyrosine pH 7 were used to optimize elution protocol. Human IgG was probed using an anti-human Fc-HRP-conjugated antibody at a 1:1000 dilution. Molecular weight marker (left) indicates protein size in kDa.

2.2.5. Replacing the Glioblastoma Targeting Domain with MR1 scFv and Evaluating Expression

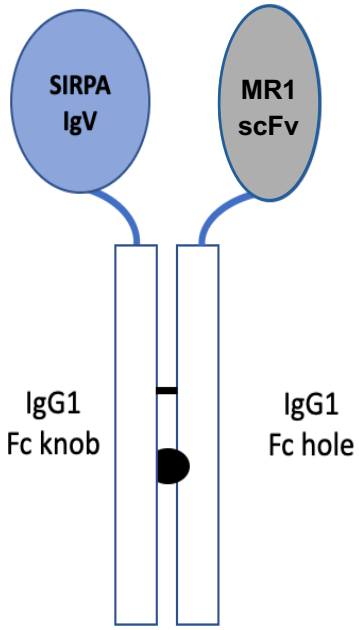

Figure 17: **Schematic of the SIRPα/MR1 bispecific Fc-fusion protein.** Diagram showing a heterodimeric Fc-fusion construct composed of the IgV domain of SIRPα and an MR1-specific scFv fused to human IgG1 Fc domains. The two chains are engineered with complementary "knob" and "hole" mutations within the Fc regions to promote heterodimerization, resulting in a single bispecific molecule displaying SIRPα on one arm and the MR1 scFv on the other.

Due to emerging concerns regarding the affinity of the IL13 (E13Y) interaction with IL13Rα2, a decision was made to redesign the construct as a bispecific protein targeting EGFRvIII using the MR1 scFv, which has been extensively validated for its specificity. This redesign required removal of the IL13-encoding region from the plasmid containing the bispecific Fc-fusion construct and replacement with a DNA fragment encoding the MR1 scFv (Figure 17). The MR1 scFv sequence was amplified by PCR, yielding a ~750 bp product, which was subsequently ligated into the plasmid backbone in place of the IL13 segment, keeping the rest of the sequence as described previously in **Section 3.1.2**. In the MR1/SIRPα construct, tumor selectivity is conferred by the MR1 scFv, which binds the EGFRvIII-specific junction epitope with a K_D of approximately 10–23 nM a moderate to good affinity characteristic of first-generation phage display-derived scFvs and consistent with the therapeutic antibody range[257]. Critically, because MR1 recognizes an epitope present exclusively on EGFRvIII and absent from wild-type EGFR and all normal tissues, this targeting domain provides substantially greater tumor specificity than the IL13(E13Y)/IL13Rα2 interaction, in which residual IL13Rα1/2 cross-reactivity remains a

concern. Following transduction and selection to establish PBiNSCs that express the MR1/SIRPa bi-specific fc fusion protein, cells were cultured for 48 hours and whole-cell lysates and cell culture supernatant were collected to assess intracellular production and extracellular release, respectively. Western blot analysis using an anti-human Fc–HRP antibody revealed a distinct band at approximately 90 kDa in both lysate and conditioned media fractions and not present in the WT PBiNSC lysates. Detection of the protein in the lysate confirms successful intracellular synthesis, while its presence in cell culture supernatant indicates efficient trafficking through the secretory pathway and release (Figure 20A).

2.2.6. Assessing The Binding Specificity of the Bi-specific Fc Fusion protein To Glioblastoma Cells Expressing EGFRvIII

To evaluate whether the newly engineered bispecific Fc-fusion protein can bind GBM cells with specificity toward EGFRvIII, a binding assay was performed. EGFRvIII is a tumor-specific mutant receptor that is frequently expressed in vivo but is often lost during in vitro culture. Therefore, PriGO8 cells were lentivirally engineered to express EGFRvIII, providing a controlled system to assess binding specificity. Pre-cleared conditioned media from wild-type PBiNSCs or expressing the bispecific Fc-fusion protein were collected after 48 hours and incubated with either wild-type or EGFRvIII-expressing PriGO8 cells for 72 hours to allow for protein binding. Following incubation, PriGO8 cell lysates were harvested and analyzed by Western blot to detect the presence of the bispecific Fc-fusion protein. The bispecific Fc-fusion protein was detected in lysates from both wild-type and EGFRvIII-expressing PriGO8 cells, while no signal was observed in wild-type control media lanes (Figure 20B). Notably, the band corresponding to EGFRvIII-expressing cells was more intense, even approaching signal saturation, suggesting enhanced binding relative to wild-type cells. However, given the high concentration of protein present in the conditioned media, it is possible that binding observed in wild-type cells reflects increased non-specific or low-affinity interactions driven by the law of mass action. In this context, the law of mass action dictates that increasing ligand concentration can drive binding even to lower-affinity targets, thereby reducing apparent specificity. To address this, cell culture supernatant sample was diluted (1:2, 1:20, and 1:200) prior to incubation with PriGO8 cells to assess whether reduced protein concentrations would enhance discrimination between EGFRvIII-positive and wild-type cells. The experiment was repeated using these dilutions, followed by Western blot analysis of cell

lysates (Figure 20C). The results demonstrated detectable binding at both undiluted and 1:2 dilution conditions, with the EGFRvIII-expressing PriGO8 cells consistently exhibiting stronger band intensity compared to wild-type cells at the same dilution. This trend supports preferential binding of the bispecific Fc-fusion protein to EGFRvIII, while also indicating that high protein concentrations can partially mask specificity through mass action effects.

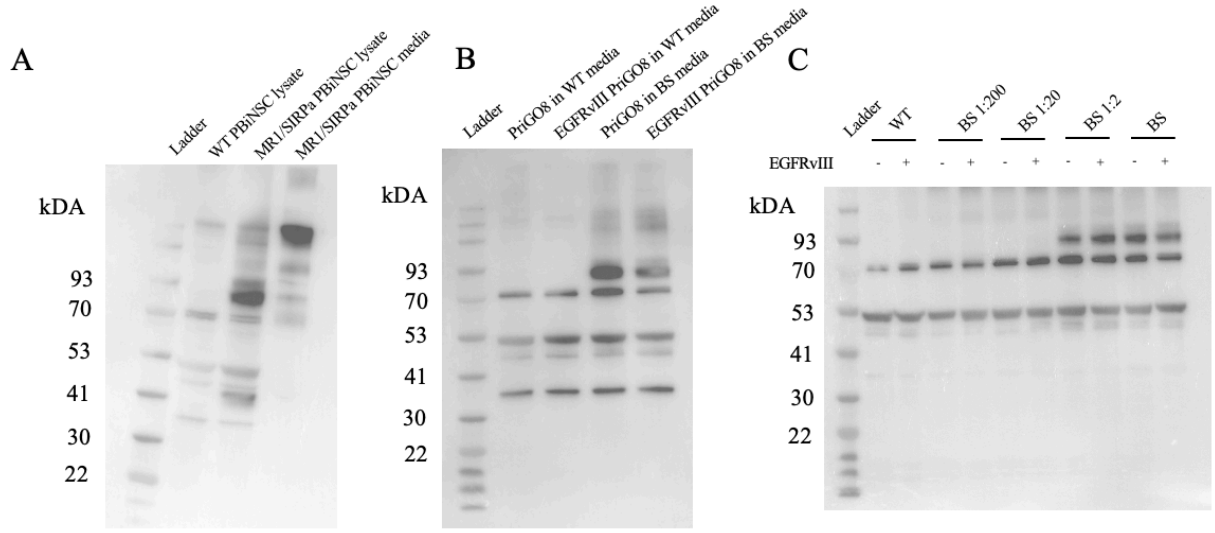

Figure 18: Western blot detection of Expression and Glioblastoma specific binding of MR1/SIRPa bi-specific Fc-fusion protein. (A) Western blot detection of MR1/SIRPa bi-specific Fc fusion protein expressed in PBiNSCs**.** Conditioned media and lysate samples from WT or MR1/SIPRa PBiNSCs were analyzed by SDS-PAGE and immunoblotting. (B) Western blot detection of MR1/SIRPa bi-specific Fc fusion protein in PriGO cells lysates cultured in conditioned media. Lysates from PriGO8s and PriGO8s overexpressing EGFRvIII cultured in either WT-conditioned media or MR1/SIRPa bi-specific-conditioned media were analyzed by SDS-PAGE and immunoblotting. 10ug samples were prepared without BME (C)Western blot detection of MR1/SIRPa bi-specific Fc fusion protein in PriGO cells lysates cultured in conditioned media. Lysates from PriGO8s and PriGO8s overexpressing EGFRvIII cultured in either WT-conditioned media or MR1/SIRPa bi-specific-conditioned media diluted to 1:200, 1:20, 1:2 were analyzed by SDS-PAGE and immunoblotting. 10ug samples were prepared without BME. Human IgG was probed using an anti-human Fc-HRP-conjugated antibody at a 1:1000 dilution. A band at ~90 kDa is consistent with MR1/SIRPa bi-specific. Molecular weight marker (left) indicates protein size in kDa.

2.2.7. Streptavidin Bead-based Affinity Purification Approach Using Biotinylated EGFRvIII Immobilized Ligand

An alternative purification strategy for the bispecific Fc-fusion protein involved affinity capture using streptavidin–agarose in conjunction with a biotinylated target ligand. This method leverages the exceptionally strong non-covalent interaction between biotin and streptavidin,

enabling highly specific immobilization of biotinylated molecules onto a solid support. In this system, streptavidin-coated agarose beads function as the stationary phase, to which a biotinylated form of the target antigen, EGFRvIII, is immobilized. Conditioned media containing the bispecific Fc-fusion protein was subsequently applied to the column under gravity flow, allowing the EGFRvIII-binding arm of the construct to selectively interact with the immobilized ligand. Unbound and non-specifically bound proteins were removed through sequential wash steps, thereby enriching the target protein. Elution was achieved via competitive displacement using soluble EGFRvIII peptide. Given that the reported binding affinity (K_D) of the MR1 scFv for EGFRvIII is approximately 16 nM, the use of a high concentration of free peptide (>1000× K_D) effectively outcompetes the immobilized ligand, resulting in release of the bound bispecific protein from the column. Eluted fractions were analyzed by western blot (Figure 21).

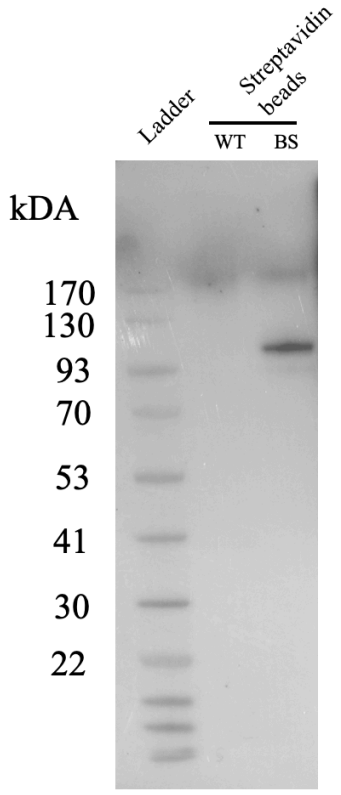

Figure 19: Purification and analysis of MR1/SIRPa bi-specific Fc fusion protein. Streptavidin agarose bound to 5ug biotinylated EGFRvIII with 15mL of pre-cleared conditioned media from WT PBiNSCs or PBiNSCs expressing MR1/SIRPa bi-specific protein and eluted with peptide EGFRvIII. 20ul of eluted samples from WT PBiNSCs or PBiNSCs expressing MR1/SIRPa bi-specific protein were analyzed by SDS-PAGE and immunoblotting. 10ug samples were prepared without BME. Human IgG was probed using an anti-human Fc-HRP-conjugated antibody at

a 1:1000 dilution. A band at ~90 kDa is consistent with MR1/SIRPa bi-specific. Molecular weight marker (left) indicates protein size in kDa.

3. Discussion

Glioblastoma remains one of the most formidable challenges in oncology, defined not merely by its molecular complexity but by the convergence of biological barriers that have confounded decades of therapeutic development. The present study sought to address these barriers through two complementary engineering strategies: a SNIPR-based platform for antigen-inducible therapeutic gene expression in PBiNSCs, and a bispecific Fc fusion protein designed to simultaneously engage CD47 and tumor-associated antigens on GBM cells. Together, these approaches represent an integrated framework that leverages the tumor-tropic properties of neural stem cells, the precision of synthetic receptor biology, and the immune-modulatory potential of engineered biologics. The findings reported here demonstrate meaningful proof-of-concept for each component of this framework, while also identifying clear avenues for further optimization that will be necessary to realize their full therapeutic potential.

3.1. Functional Validation of the SNIPR Platform in PBiNSCs

The successful functional activation of the SNIPR system in PBiNSCs represents an important foundational achievement of this work. Notably, this is the first demonstration of SNIPR functionality in a cell type beyond those used in the original system's characterization, establishing PBiNSCs as a new and clinically relevant vehicle for synthetic receptor platforms. Derived from adult peripheral blood through OCT4-free epigenetic reprogramming, these cells combine the tumor-tropic properties of neural stem cells with a clinically accessible, minimally invasive source material. Their demonstrated genomic stability, long-term self-renewal, and erasure of age-associated epigenetic signatures position them as a translationally viable platform.

The bead-based activation experiments established a clear dose-response relationship between lentiviral input and SNIPR activation, with CD19-conjugated beads eliciting up to 4.7% BFP-positive cells at 500 µL lentiviral input compared to 0.3% in CD19-negative controls. While these absolute activation levels are modest, they likely reflect limitations of artificial bead-based antigen

presentation, which lacks the membrane fluidity, receptor clustering capacity, and endocytic pulling forces of native cell-surface ligand display. This interpretation is strongly supported by the cell-based co-culture experiments, in which BFP activation levels rose dramatically to approximately 53% at the optimal lentiviral input of 400 µL when CD19-positive Raji cells were used as stimulators, representing more than a ten-fold increase compared to bead-based stimulation. This discrepancy between bead-based and cell-based activation is consistent with mechanistic models of Notch and SNIPR signalling. For endogenous Notch, ligand-induced endocytosis in the sending cell generates a mechanical pulling force that exposes the ADAM protease-accessible S2 cleavage site, a process dependent on clathrin-mediated endocytosis, epsin adaptors, and actin dynamics[263]. Streptavidin-coated beads lack the endocytic machinery required to exert such forces, providing a plausible mechanistic basis for the attenuated activation observed in the bead-based system. Emergine evidence also suggests that even SNIPR-based systems may exploit receptor endocytosis and pH-dependent γ-secretase activity in acidified compartments for full activation[138,264]. Adherent ligand-expressing cells are therefore expected to provide superior activation compared to inert beads, consistent with our observations. The finding that optimal activation occurred at 400 µL lentiviral input rather than 500 µL, with a decline in both signal intensity and specificity at the highest viral doses, is consistent with the well-described phenomenon of receptor overexpression reducing signaling fidelity. At very high receptor surface densities, even low-affinity homotypic or heterotypic interactions between adjacent receptor molecules could generate sufficient mechanical strain to trigger baseline NRR relief, contributing to ligand-independent background. This is further supported by published SNIPR design principles, which identify ECD length and exposed protease sites as key determinants of ligand-independent cleavage, with overexpression exacerbating background activity[138]. These observations have direct implications for future optimization, suggesting that careful titration of receptor expression levels will be an important parameter in translating the SNIPR platform into therapeutic settings.

Several technical features of the SNIPR plasmid system merit acknowledgement as factors that may contribute to variability in activation levels across experiments. The lentiviral constructs encoding the SNIPR receptor and response element are large, each exceeding 10,000 bp, which approaches the upper packaging limit of lentiviral vectors and may reduce viral titre, transduction efficiency, and the proportion of full-length integrated proviral copies relative to smaller

constructs. Additionally, the plasmids used in this study lack an antibiotic selection marker linked to the SNIPR receptor construct itself. As a consequence, cells that successfully integrated the response element but not the receptor or vice versa, cannot be reliably distinguished from dual-transduced cells by drug selection alone, potentially diluting the measured activation signal by including non-responsive cells in the quantified population. Finally, lentiviral integration is semi-random, and different integration sites within the host genome are subject to variable chromatin environments and positional silencing effects. This integration-site heterogeneity means that individual cells within a transduced population may express the SNIPR receptor at substantially different levels, contributing to the population-level variability in activation efficiency observed across experiments.

3.2. SNIPR-Driven lclPTENL Expression: Achievements and Optimization Pathways

The construction and validation of the SNIPR-lclPTENL therapeutic plasmid, in which the BFP reporter was replaced with the secretable tumor suppressor isoform lclPTENL, represents an importance advance of the SNIPR component of this project. The incorporation of WPRE posttranscriptional regulatory elements was a rational design choice to enhance transgene expression within the lentiviral context, where transcript stability and translational efficiency are often rate-limiting. The detection of lclPTENL in the conditioned media of CD19 SNIPR-activated PBiNSCs, particularly under cell-based co-culture conditions, demonstrates that the system is functionally capable of coupling antigen recognition to therapeutic protein secretion and confirming the functionality and correct cloning of the inducible plasmid. The finding that the 400 µL CD19-positive co-culture condition produced approximately two-fold higher lclPTENL levels than the constitutive expression control, as assessed by immunoprecipitation, is an encouraging result suggesting that antigen-driven induction can achieve levels comparable to constitutive expression of lclPTENL. This observation can also be contextualized alongside the p16 data described in Section 3.3, where conditioned media from constitutively expressing PBiNSCs was sufficient to induce a detectable biological response in GBM cells.

The observation of some ligand-independent lclPTENL expression in cell lysates, particularly apparent in THP-1 co-culture conditions at higher lentiviral inputs, is best understood as a

calibration challenge rather than a fundamental failure of specificity. One plausible mechanistic contributor is the suspension behavior of THP-1 cells: unlike adherent ligand-expressing cells, suspension cells are not anchored and therefore cannot apply the directed endocytic pulling force that is optimal for SNIPR activation. Paradoxically, the continuous tumbling motion of suspension cells in culture may generate intermittent, non-directional membrane contacts that produce low-level basal cleavage site exposure in a ligand-independent manner. This is consistent with published observations that mechanical perturbations unrelated to cognate antigen engagement can contribute to background synNotch cleavage[265]. The clearer antigen-dependent discrimination observed in immunoprecipitated supernatant samples, where secreted rather than re-uptaken lclPTENL is measured, supports the conclusion that antigen-dependent activation remains the dominant driver of lclPTENL secretion.

The failure to detect lclPTENL in the EGFRvIII SNIPR cell-based model, despite robust activation of the BFP reporter, is a notable and informative observation. The strong BFP signal indicates that antigen recognition and receptor activation via the EGFRvIII–MR1 interaction are intact, suggesting that the defect lies downstream of SNIPR signalling rather than at the level of target engagement. Shifting focus to the inducible construct, lclPTENL appears functional in other contexts: prior CD19 SNIPR experiments show clear expression, and bead-based EGFRvIII SNIPR assays demonstrate at least partial expression. Together, these findings argue against a fundamental issue with construct design or transcriptional activation.

This instead points toward post-transcriptional mechanisms, particularly extracellular protein instability. EGFRvIII expression in GBM is associated with upregulation of extracellular proteases, including matrix metalloproteinases (MMP-2, MMP-9, MMP-13), serine proteases such as uPA, and cysteine proteases like cathepsin B-driven by PI3K/AKT, MAPK, and NF-κB signalling[266]. This protease-rich microenvironment could directly compromise the stability of secreted therapeutic proteins. In the case of lclPTENL, its 173-amino acid N-terminal extension contains a polyarginine stretch that has been reported to be susceptible to cleavage by the proprotein convertase Furin. Cleavage at this site would disrupt the cell-penetrating capability of lclPTEN-L, preventing efficient uptake into target cells and thereby abolishing its functional activity[267]. Within a highly proteolytic environment such as that generated by EGFRvIII-

expressing GBM cells, this cleavage could occur rapidly after secretion, limiting the accumulation of intact, functional protein.

Taken together, the elevated extracellular protease activity in EGFRvIII positive GBM co-cultures may be sufficient to degrade or inactivate lclPTENL before it can be detected or exert its effect. This interpretation is consistent with previous experiments demonstrating successful lclPTENL transfer and activity in other GBM models, such as U87MG and WT PriGOs, where the proteolytic environment may be less pronounced. To address this limitation, a logical next step would be to replace lclPTENL with a more protease-resistant cytotoxic payload could help determine whether extracellular instability is the primary barrier to efficacy in this system.

The 3D onco-neurosphere co-culture model developed in this study represents a particularly useful methodological advance. The physical make up of the onco-neurospheres containing GFP-positive PBiNSCs and mCherry PriGO cells show variability where sometimes the PBiNSCs are predominantly localized to the interior core of the neurosphere while PriGO GBM cells formed the outer surrounding layer which is an architecture that may recapitulate, in simplified form, the spatial relationship between infiltrating stem-like cells and established tumor parenchyma expected in vivo or other times the opposite relationship was seen. Nevertheless, the demonstration that robust BFP-based SNIPR activation was maintained in EGFRvIII-expressing PriGO neurospheres but not in wild-type controls confirms that antigen-dependent activation logic is preserved under conditions of increased physical complexity and constrained diffusion. The structural equivalence of either sphere architectures supports the use of the onco-neurosphere model for downstream assessment of lclPTENL expression in future studies incorporating more sensitive detection strategies.

Several targeted experiments would help disentangle why robust BFP reporter activation in the EGFRvIII SNIPR system did not translate into detectable lclPTENL. Since the HNF1A-responsive promoter functioned well in the CD19 SNIPR co-culture system, the upstream transcriptional machinery is unlikely to be the limiting factor, future investigation should instead focus on the gap between transcriptional activation and protein accumulation.

3.3. Biological Activity of lclPTENL in Glioblastoma Models

Independent of the SNIPR delivery system, the demonstration that conditioned media from PBiNSCs constitutively expressing lclPTENL induces statistically significant upregulation of p16 (CDKN2A) in PriGO9 GBM cells provides meaningful evidence of biological activity. p16 is a critical inhibitor of CDK4/6 that governs G1-S cell cycle progression through the retinoblastoma pathway and is frequently lost in glioblastoma through homozygous deletion of the CDKN2A locus. The finding that extracellular delivery of lclPTENL can upregulate p16 expression is consistent with the established role of PTEN in suppressing PI3K/AKT signaling, which in turn regulates multiple cell cycle checkpoints including CDK inhibitor expression. This aligns with previous studies demonstrating that reintroduction of PTEN into PTEN-deficient glioma cells induces G0/G1 accumulation and suppression of cell cycle progression, effects mediated in part through upregulation of CDK inhibitors as part of a broad growth-suppressive transcriptional response[268]. Increased p16 expression may therefore reflect a shift toward cell cycle arrest or a stress-induced senescence-like program downstream of restored PTEN signaling, rather than oncogenic dysregulation an interpretation consistent with reports demonstrating p16 upregulation as a marker of growth inhibition in response to tumor suppressor pathway restoration in cancer cells. The current data support the interpretation that lclPTENL retains catalytic activity following secretion, uptake into target cells, and intracellular trafficking.

The differential response between PriGO9 and PriGO17 cells likely reflects the molecular heterogeneity that is a hallmark of primary GBM lines differences in baseline PTEN status, PI3K pathway dependency, or p16 promoter methylation between these lines may account for the variation in response magnitude. Future experiments should include systematic characterization of PTEN and p16 status across the PriGO panel, as well as direct measurement of AKT phosphorylation as a proximal readout of PTEN catalytic activity, to better define the molecular prerequisites for lclPTENL responsiveness.

3.4. Retargeting the SNIPR Platform: IL13Rα2 versus EGFRvIII

The comparison between the rIL13-SNIPR and MR1-SNIPR constructs provides important design lessons for the broader field of synthetic receptor engineering. The IL13(E13Y)-based receptor exhibited substantial ligand-independent activation (~40% BFP-positive cells across both IL13Rα2-positive and IL13Rα2-negative conditions in the PriGO9 model). This high background

activation is most likely attributable to the intrinsic biophysical properties of protein-based binding domains, which differ fundamentally from the scFv format for which the SNIPR mechanotransduction architecture was originally optimized.

The dissociation constant of IL13(E13Y) for IL13Rα2 has been reported to be in the low picomolar range, substantially higher affinity than that of the MR1 scFv for EGFRvIII (~16 nM). This extremely tight binding may paradoxically reduce SNIPR specificity: if receptor-ligand engagement cannot be readily reversed, sustained conformational strain on the transmembrane domain may lower the mechanical activation threshold, promoting ligand-independent cleavage events. This is consistent with the SNIPR design principle that ECD affinity must be calibrated to avoid overactivation very high-affinity interactions can constitutively stress the juxtamembrane domain even in the absence of specific antigen, while very low-affinity interactions may fail to generate sufficient receptor clustering for activation[138].

Beyond affinity, IL-13 engages both IL13Rα1 and IL13Rα2, and while the E13Y mutation preferentially enhances IL13Rα2 selectivity, residual IL13Rα1 binding remains a potential source of off-target activation. This limitation is well-established in the IL13-based CAR-T cell literature were early clinical studies with first-generation IL13(E13Y) zetakine CAR T cells demonstrated cross-reactivity with IL13Rα1-positive targets despite the E13Y mutation, leading to concerns about off-target toxicities[192]. More recent IL13-based CAR constructs have incorporated additional mutations (e.g., E12Y in combination with E13Y, or quadruple substitutions such as E13K/R66D/S69D/R109K) that substantially reduce IL13Rα1 binding while preserving IL13Rα2 targeting[269,270]. Incorporation of such refined IL-13 muteins which reduce their affinity for IL13Ra2 could be explored as a route to improving rIL13-SNIPR specificity in future work. Additionally, paracrine interactions with endogenous IL-13 receptors on PBiNSCs themselves cannot be excluded as a contributor to the baseline signaling observed.

In striking contrast, the MR1 scFv-based SNIPR targeting EGFRvIII demonstrated activation levels of 74–81% in EGFRvIII-positive PriGO cells across lentiviral input conditions of 300–500 µL, compared to near-background levels (0–7%) in wild-type PriGO cells a signal-to-noise ratio substantially more favorable for therapeutic applications. This robust discrimination was maintained across two independent primary GBM lines (PriGO8A and PriGO9) and was preserved in the 3D onco-neurosphere co-culture model. The EGFRvIII-specificity of the MR1

scFv is particularly advantageous because EGFRvIII, arising from an in-frame deletion of exons 2–7 generating a novel junction epitope, is genuinely tumor-specific and absent from normal tissues. Collectively, these results establish scFv-based ECDs as the currently preferable format for SNIPR applications in GBM, and the MR1-EGFRvIII axis as the most promising receptor-antigen pair for advancing this platform.

3.5. Engineering PBiNSCs for Bispecific Fc Fusion Protein Delivery

The second major component of this study is engineering PBiNSCs to secrete a bispecific Fc fusion protein targeting CD47 and tumor-associated antigens to address a distinct but complementary dimension of the GBM therapeutic challenge. The successful expression and secretion of the IL13/SIRPα Fc fusion protein by engineered PBiNSCs validates the fundamental feasibility of using PBiNSCs as a platform for sustained local delivery of complex biologic constructs. The molecular architecture of this construct employing knob-into-hole Fc mutations to enforce heterodimer formation, a furin cleavage site and P2A self-cleaving peptide to generate two independent polypeptides from a single transcript, and an IgG light-chain leader to enhance IL13 chain secretion successfully navigates the technical challenges of producing correctly assembled bispecific antibody-like molecules in non-professional antibody-secreting cell types.

For the IL13/SIRPα bispecific, Western blot detection of the ~90 kDa Fc fusion protein in PriGO cell lysates following exposure to bispecific conditioned media indicates that the construct associates with GBM cells. Microarray expression profiling data for the PriGO panel reveals differences in CD47 and IL13Rα2 expression levels across cell lines: CD47 is expressed at log2 values of 8.27, 7.46, and 9.06 in PriGO8, PriGO9, and PriGO17 respectively, while IL13Rα2 expression is log2 values of 6.76, 2.88, and 2.31 in the same lines while RNA sequencing data shows similar levels. It should be noted that microarray data of this type allows comparison of expression levels across cell lines for the same gene, but direct comparison of absolute expression levels between different genes such as directly contrasting CD47 and IL13Rα2 values is not appropriate given differences in probe efficiency and dynamic range between probe sets. To interpret these binding observations in the context of the affinities of each targeting domain, it is important to consider the expected hierarchy of binding interactions within the bispecific construct.

The SIRPα domain binds human CD47 with a KD in the micromolar range under physiological conditions, with the affinity of wild-type SIRPα for CD47 reported to be approximately 1000-fold weaker than that of anti-CD47 antibodies[259]. It is also worth noting that human SIRPα exists as multiple allelic variants, of which SIRPαv1 and SIRPαv2 are the most prevalent, differing by 13 residues in the ligand-binding domain; however, structural and binding studies have demonstrated that these polymorphisms do not significantly alter CD47 binding affinity[259]. Whether post-translational glycosylation of the expressed SIRPα domain which could influence CD47 engagement is occurring as expected in PBiNSCs represents an open question that could be addressed by mass spectrometry-based glycoproteomic analysis of the purified bispecific protein in future work. In contrast, the IL13(E13Y) domain binds IL13Rα2 with a KD of approximately 250 pM, representing an affinity several orders of magnitude greater than that of the SIRPα arm[261]. Based on this affinity hierarchy, the IL13(E13Y) domain would be expected to serve as the primary tumor-anchoring interaction, concentrating SIRPα-mediated CD47 blockade selectively at IL13Rα2-expressing GBM cells. However, the observed uniform detection of the bispecific across all three WT PriGO lines including PriGO9 and PriGO17, which express IL13Rα2 at lower levels than PriGO8 (log2 values of 2.88 and 2.31 compared to 6.76) is inconsistent with IL13Rα2-driven binding as the dominant interaction based on western blot results. Furthermore, the absence of a clearly enhanced signal in PriGO8 cells engineered to overexpress IL13Rα2 relative to WT PriGO8 cells further argues against IL13Rα2 as the primary driver of the observed binding. Instead, this pattern suggests that binding across the WT PriGO panel is predominantly mediated by the SIRPα–CD47 interaction, which is consistent with the uniform CD47 expression observed across all lines tested (log2 values of 8.27, 7.46, and 9.06). The substitution of the MR1 scFv targeting EGFRvIII which binds its target with a KD of approximately 10–23 nM and recognizes an epitope present exclusively on EGFRvIII and absent from all normal tissues represents a more promising solution, as it eliminates the healthy tissue targeting problem entirely while retaining sufficient affinity to serve as the primary tumor-anchoring interaction within the bispecific architecture[257]. Blocking experiments using ligand blocking antibodies, or ideally CRISPR-edited knockouts of each ligand in PriGO cells, would be necessary to formally dissect the relative contributions of each binding arm to the observed Western blot signal. The detection of the Fc fusion protein in cell lysates cannot be used to distinguish surface binding from receptor-mediated internalization following binding to the tumor cell surface. Internalization of CD47

following engagement with targeting constructs has been reported in the context of anti-CD47 antibody binding, whereby antibody-CD47 complexes undergo endocytic uptake, reducing surface CD47 availability and potentially enhancing the phagocytic signal[271]. If the bispecific construct similarly drives CD47 internalization upon binding, this could represent an advantageous additional mechanism of action sequestering CD47 away from the cell surface and thereby achieving more complete and sustained relief of the "don't eat me" signal than surface blockade alone.

The greater discrimination between EGFRvIII-positive and wild-type cells observed with the MR1/SIRPα bispecific at diluted conditioned media concentrations is consistent with a concentration-dependent mass action effect: at high protein concentrations, interactions are driven by the law of mass action, reducing apparent specificity to GBM. Serial dilution experiments restoring preferential EGFRvIII-dependent binding at 1:2 dilution support genuine EGFRvIII targeting by the MR1 arm, while reinforcing the importance of performing specificity assessments across a range of protein concentrations. Taken together, the binding data for both bispecific variants underscore that Western blot detection of Fc fusion protein in cell lysates following co-incubation, while informative as a first-pass expression and association assay, does not distinguish GBM specific binding from surface receptor-mediated binding from non-specific uptake, and cannot resolve the relative contributions of the two targeting arms. Future experiments using surface plasmon resonance and antigen-knockout binding controls will be essential to fully characterize the specificity and functional integrity of the bispecific construct before advancing to phagocytosis assays or in vivo studies.

3.6. Protein Purification Challenges and Engineering Solutions

The aggregation observed following Protein G purification is most likely attributable to the low-pH elution conditions inherent to this chromatography method. Protein G affinity purification relies on acidic elution (typically pH 2.7–3.0) to dissociate the Fc–Protein G interaction. Although effective at releasing bound protein, these conditions can transiently destabilize multidomain fusion proteins, particularly those in which the appended targeting domains in this case the SIRPα and IL13(E13Y) moieties have different conformational stability profiles compared to the Fc region itself. Even with rapid neutralization following elution, transient exposure to low pH may

be sufficient to induce partial unfolding and expose hydrophobic surfaces that promote intermolecular aggregation. The appearance of higher molecular weight smearing exclusively in the purified fractions, rather than in the crude conditioned media, is consistent with this interpretation. These findings underscore a well-recognized limitation of Protein G-based purification for complex Fc fusion constructs and motivated the development of alternative purification strategies, described in **Section 2.2.5**.

The development of the streptavidin bead-based affinity purification approach, using biotinylated EGFRvIII as the capture ligand and competitive elution with soluble EGFRvIII peptide, represents an elegant alternative that simultaneously validates the binding function of the purified protein. The recovery of a detectable amount of purified bispecific Fc fusion protein from 15ml of conditioned media provides a baseline for assessing yield optimization in future preparations. This ligand-based purification strategy has the additional advantage of selecting specifically for correctly folded, functionally active protein, as only constructs with intact EGFRvIII-binding capacity will be captured. Future structural and biochemical characterization of the purified bispecific protein including binding kinetics measurement by surface plasmon resonance to determine K_D values for both EGFRvIII and CD47 arms simultaneously, and mass spectrometry to confirm correct disulfide bond formation, glycosylation at N297 and at other potential sites, and the integrity of the knob-into-hole heterodimer will be important steps in fully characterizing the molecular quality of the purified product before advancing to functional assays. A logical and important next step toward obtaining sufficient quantities of purified bispecific for functional characterization would be to transition this antigen-affinity capture strategy to a Fast Protein Liquid Chromatography (FPLC) platform, in which the biotinylated EGFRvIII ligand is immobilized on a streptavidin-coupled column resin and large volumes of conditioned media are applied under automated, controlled flow-rate conditions. FPLC-based affinity chromatography offers several advantages over the current approach: it enables processing of substantially larger input volumes from hundreds of millilitres to litres of conditioned media with reproducible and programmable wash and elution steps, real-time UV absorbance monitoring to track protein elution, automated fraction collection, and the capacity to be scaled further as production volumes increase[272].

3.7. Clinical Relevance and Translational Perspective

Considered in the broader context of GBM therapeutic development, the work presented here contributes to an emerging paradigm of engineered cell-based delivery systems that seek to overcome the fundamental limitations of systemically administered biologics in brain tumors. The blood-brain barrier restricts approximately 98% of small-molecule drugs and virtually all large biologics from reaching brain tumor tissue at therapeutic concentrations. The use of PBiNSCs as an in-situ production platform circumvents this limitation by generating therapeutic proteins directly within the tumor microenvironment at a high concentration, sustained by cells that have actively migrated to and infiltrated the tumor mass through chemokine-driven tumor tropism.

The SNIPR-based inducible system adds a critical layer of spatial and molecular specificity to this delivery paradigm. Unlike constitutive expression systems that produce therapeutic proteins regardless of cellular location, the SNIPR architecture ensures that therapeutic payload expression is preferentially activated only when the delivery cell has physically engaged tumor antigen. This design philosophy substantially reduces the risk of off-target toxicity a concern of particular relevance for cytotoxic payloads like lclPTENL, whose systemic delivery could theoretically interfere with PTEN signaling in normal tissues. The successful demonstration of EGFRvIII-dependent SNIPR activation in primary GBM co-cultures and 3D neurosphere models suggests that this conditional activation logic is compatible with the biological context of GBM, where EGFRvIII is expressed on approximately 25-33% of tumors.

The bispecific Fc fusion protein strategy addresses a distinct vulnerability in the GBM immune microenvironment: the CD47-mediated suppression of macrophage-mediated phagocytosis. Given that tumor-associated macrophages can comprise 30-50% of the GBM tumor mass, and that these cells are actively recruited to regions of tumor cell turnover, the targeted disruption of CD47 signaling within the tumor microenvironment has the potential to convert an immunosuppressive myeloid infiltrate into a pro-phagocytic effector population. The dual-targeting architecture simultaneously blocking CD47 and engaging a tumor-associated antigen is designed to achieve tumor-selective innate immune activation while avoiding the on-target hematologic toxicities (hemolytic anemia, thrombocytopenia) that have complicated clinical development of systemic CD47-blocking antibodies. The delivery of this construct via engineered PBiNSCs provides sustained local production that should maintain effective concentrations within the tumor microenvironment without requiring systemic dosing.

3.8. Limitations and Future Directions

The work presented here has several limitations that define the roadmap for future investigation. First, the failure to detect high levels of lclPTENL expression under EGFRvIII SNIPR activation in the cell-based model, despite robust BFP reporter expression, reflects a hypothesized protease-mediated degradation mechanism that raises a broader and important challenge for secreted protein therapeutics in the GBM microenvironment. EGFRvIII-expressing GBM cells are known to upregulate a broad spectrum of extracellular proteases through constitutive activation of downstream signalling pathway that may rapidly inactivate secreted proteins before they can exert their intended biological activity. This need to be further explored to confirm the hypothesis and may lead to lclPTENL being replaced with a protease resistant cytotoxic payload. An additional future direction of interest would be to evaluate SNIPR functionality in differentiated neural progeny derived from PBiNSCs to assess whether the synthetic receptor architecture remains operative in post-mitotic cell types, which would expand the potential scope of this delivery platform.

Second, the binding specificity of the bispecific Fc fusion protein requires more rigorous characterization at physiologically relevant protein concentrations. Binding kinetics should be characterized by surface plasmon resonance to determine true affinity constants for both arms of the bispecific simultaneously. Mass spectrometry analysis of the purified protein will be important to confirm correct assembly, glycosylation, and disulfide bond formation, providing structural confidence before advancing to functional studies. In particular, glycosylation at the conserved N297 site within the CH2 domain of the IgG1 Fc region warrants careful characterization, as this modification is critically important for FcγR engagement and downstream effector functions including antibody-dependent cellular phagocytosis (ADCP). Complete removal of the N297 glycan has been shown to abrogate binding to all low-affinity FcγRs and substantially diminish ADCP, with only the high-affinity FcγRI retaining residual binding in the aglycosylated state[273]. Conversely, afucosylation of the core N-glycan has been reported to increase FcγRIIIa affinity by up to 20-fold relative to fucosylated IgG1[274]. For the purposes of this bispecific construct, in which ADCP by macrophage FcγRI and FcγRIIa is on of the primary intended effector mechanisms, it is important to confirm by mass spectrometry that the N297 glycan is correctly installed and that the glycan composition produced in PBiNSCs a non-professional secretory neural stem cell is

compatible with productive FcγR engagement. PBiNSCs are not professional antibody-secreting cells and their glycosylation machinery may differ from that of cells typically used for therapeutic antibody production.

Regarding functional phagocytosis assays, while co-culture of macrophages, GBM cells, and the bispecific construct in vitro is a logical next step, it is important to acknowledge the inherent limitations of such systems. Standard murine or human macrophage lines may not recapitulate the immunosuppressive phenotype of brain-resident tumor-associated macrophages and microglia. The complexity of maintaining three cell types with different culture requirements in the same dish, combined with the difficulty of accurately modeling TAM polarization in two dimensions, means that in vitro phagocytosis assays may underestimate or misrepresent the functional activity of the construct in the GBM microenvironment. For this reason, a more physiologically relevant approach and one that is directly compatible with existing preclinical workflows in our laboratory would be to assess phagocytic activity in an in vivo co-injection model. In this approach, fluorescently labelled PriGO GBM cells engineered to express EGFRvIII, and fluorescently labelled PBiNSCs engineered to secrete the MR1/SIRPα bispecific, are co-injected into the striatum in immunocompetent syngeneic or humanized mice at a defined ratio. This co-injection paradigm is advantageous because it places both the therapeutic cell vehicle and the tumor target within the same brain microenvironment simultaneously, allowing PBiNSC-secreted bispecific protein to engage EGFRvIII and CD47 on adjacent GBM cells in the presence of brain-resident myeloid cells microglia and recruited TAMs that represent the physiologically relevant effector population for the intended mechanism of action. The primary readout of therapeutic efficacy in this model would be a reduction in GBM tumor burden. At experimental endpoint, histological sections of brain tissue would be analyzed by microscopy to provide direct evidence of phagocytic activity by looking for co-localization of mCherry-labelled GBM cell fragments within Iba1-positive microglia or macrophages which would indicate engulfment, while a reduction in the total number of viable mCherry-positive GBM cells relative to control animals receiving PBiNSCs without the bispecific construct would provide a quantitative measure of tumor cell clearance. Comparison between animals receiving the MR1/SIRPα bispecific alongside animals receiving no bispecific, would allow attribution of any observed phagocytic activity specifically to EGFRvIII-targeted CD47 blockade.

Third, while the tumor-homing capacity of unmodified PBiNSCs has been previously demonstrated in our laboratory, consistent with the well-established tumor tropism of induced neural stem cell populations toward GBM lesions the current study did not assess the tumor-homing capacity of the engineered PBiNSCs in the context of these specific constructs, nor the effect of SNIPR or Fc fusion protein expression on cell viability, proliferation, or differentiation potential[275]. These parameters will need to be systematically evaluated to confirm that the engineering modifications do not compromise the biological properties that make PBiNSCs an attractive therapeutic chassis. One specific consideration worth raising is whether PBiNSCs expressing the SIRPα-containing bispecific could engage their own CD47, given that both molecules are present on the same cell. If secreted SIRPα-Fc binds in an autocrine fashion to CD47 on PBiNSC surfaces, it could theoretically promote macrophage-mediated clearance of the therapeutic cells themselves. Strategies to address this have been illuminated by a recent study from Yamada-Hunter et al., which demonstrated that adoptively transferred CAR T cells are rapidly cleared by macrophages when co-administered with anti-CD47 antibodies, due to loss of the endogenous CD47 "don't eat me" signal on the therapeutic cells themselves[276]. To overcome this, the authors engineered a CD47 variant that retains the ability to engage SIRPα and transmit an inhibitory "don't eat me" signal to macrophages, but harbors a point mutation that prevents binding of anti-CD47 antibodies. CAR T cells expressing the variant were resistant to macrophage-mediated clearance even in the presence of CD47-blocking antibodies, while retaining full anti-tumour efficacy[276]. Applied to the PBiNSC context, the SIRPα on the bi-specific protein would be swapped for an anti-CD47 scFv and an analogous strategy could be employed: PBiNSCs could be engineered to overexpress the CD47 variant that is resistant to engagement by the secreted anti-CD47-Fc bispecific thereby protecting the therapeutic cells from autocrine-mediated phagocytic clearance while preserving the intended tumour-selective blockade of CD47 on GBM cells by SIRPα.

Finally, while the 3D onco-neurosphere model represents a meaningful advance toward physiological relevance, future studies should incorporate patient-derived cerebral organoid systems and ultimately in vivo models to validate the spatial and temporal dynamics of SNIPR activation and therapeutic payload delivery in the context of established GBM lesions.

4. Conclusion

In conclusion, this work establishes a multi-component, rationally designed platform for targeted GBM therapy, centered on the tumor-tropic properties of engineered PBiNSCs. The first demonstration of SNIPR functionality in PBiNSCs, and the high selectivity of the MR1-EGFRvIII SNIPR system in clinically relevant primary glioblastoma co-culture and 3D neurosphere models, represents a significant advance in adapting synthetic receptor biology for brain tumor applications. The biological activity of lclPTENL in primary GBM cell lines supports the therapeutic rationale for PTEN restoration, and the successful expression and secretion of a bispecific Fc fusion protein targeting CD47 alongside tumor-associated antigens opens a parallel avenue for innate immune re-engagement within the GBM microenvironment. While technical optimization remains necessary to advance each component toward in vivo validation, the foundational results presented here provide compelling proof-of-concept for a cellular delivery framework that addresses multiple mechanisms of GBM immune evasion and treatment resistance simultaneously.

5. Methods

Antibodies and Reagents: Goat anti-Human HRP-linked IgG Fc Secondary Antibody was purchased from Thermo Fisher Scientific. Anti-PTEN (D4.3) rabbit monoclonal antibody was purchased from Cell Signaling Technology. P16ink4a (1D7D2) mouse monoclonal antibody was from Cell Signaling Technology. ActiveMax® Streptavidin μBeads, Biotinylated Human EGFRvIII Protein and Biotinylated Human CD19 (20-291) were purchased from ACROBiosystems. EGFRvIII peptide (PEPvIII) for purification elution was purchasd from MedChem express. Pierce™ Streptavidin Agarose, Streptavidin Agarose Resin and Pierce™ Centrifuge Columns for Affinity Chromatography were purchased from Thermo Scientific.

Cell culture: Peripheral-blood induced neural stem cells (PBiNSCs) were obtained from the Brüstle laboratory and cultured according to the previously published protocol[121]. Cells were maintained on Matrigel-coated plates in a 1:1 mixture of DMEM/F12 and Neurobasal medium (Thermo Fisher) supplemented with N2, B27, penicillin–streptomycin, L-glutamine, CHIR99021, A83-01, purmorphamine, human LIF (hLIF), and LAAP. For routine maintenance, cultures were passaged twice weekly and used for experiments up to a maximum of 32 passages. Cells were detached using pre-warmed Accutase for 7 minutes at 37 °C to generate a single-cell suspension, which was subsequently diluted and centrifuged at 1200 rpm for 4 minutes to pellet the cells. The cell pellet was resuspended in fresh medium and replated. Cultures were maintained at 37 °C under low-oxygen conditions (5% O_2 and 5% CO_2). Primary glioblastoma cells (PriGOs) were isolated from patients undergoing surgical resection for glioblastoma at The Ottawa Hospital, as previously described. PriGOs were cultured on laminin-coated flasks in Neurobasal-A medium (Thermo Fisher) supplemented with EGF, FGF, and heparin. PriGO cultures were passaged and maintained using the same procedures as those described for PBiNSCs. Raji and THP-1 cells were cultured in RPMI supplemented with 10% FBS and passaged 1 time per week.

Lentiviral and plasmid constructs: Lentiviral and plasmid constructs that were obtained as bacterial stabs from Addgene were streaked onto ampicillin LB agar plates and incubated overnight at 37 °C. Individual colonies were selected and inoculated into LB broth supplemented with ampicillin, followed by incubation at 37 °C with shaking at 220 rpm. Resulting cultures were used to generate glycerol stocks by mixing with an equal volume of 100% glycerol. Large-scale plasmid DNA preparations were performed from glycerol stocks using the BioBasic Maxiprep Plasmid

DNA Extraction Kit according to the manufacturer's instructions. Plasmid concentration and purity were assessed using a NanoDrop spectrophotometer.

Lentiviral particle production and viral transduction: Lentiviral particles were generated by transfecting HEK293T cells with a four-plasmid system consisting of pLP1, pLP2, pLP-VSVG, and the plasmid of interest using Lipofectamine 2000 (Thermo Fisher). Forty-eight hours post-transfection, virus-containing supernatants were collected and concentrated using Lenti-X Concentrator (Takara) at a 3:1 volume ratio. The mixture was incubated overnight at 4 °C with gentle shaking. Viral particles were pelleted the following day by centrifugation at 1500 × g for 40 minutes and resuspended in 1 mL of Neurobasal-A medium. HEK293T cells were maintained in DMEM supplemented with 10% heat-inactivated fetal bovine serum (FBS) and 0.1% penicillin–streptomycin. PBiNSCs were grown to 70–80% confluence prior to transduction. Concentrated viral particles (1 mL) were added directly to the culture medium and removed the following day by complete media replacement. Transduced cells were subsequently subjected to puromycin selection as required for 72 hours at a final concentration of 0.6 µg/mL.

Western blot: In Western blots performed to probe for total protein in cell lysates, cells were lysed in 1XRBC Lysis Buffer (Invitrogen). Lysates were briefly sonicated at 30 kHz and centrifuged at maximum speed for 10 minutes. Protein concentration was determined using the Pierce BCA assay(Thermo Fisher), with samples incubated at 37◦C and absorbance measured at 562 nm using a spectrophotometer. 10ug-35ug of protein was combined with 6ul of Laemmli buffer containing betamercaptoethanol and topped up with lysis buffer. In Western blots performed to probe for protein in immunoprecipitation samples, 15ul of sample was combined with 6ul of Laemmli buffer containing betamercaptoethanol and topped up with lysis buffer. All samples were heated at 95◦C for 5 minutes before loading samples into precast NuPAGE Bis-Tris Mini Protein Gels and run at 150 V for 1 hour. Following electrophoresis, proteins were were transferred from the gel to an Immobilon PVDF membrane (Millipore Sigma) using wet transfer for 1 hour at 100V. Amido Black stain was performed to assess equal protein loading. Membranes were blocked with 5% milk in TBST for 1 hour with shaking, followed by incubation with primary antibody diluted in 5% milk in TBST for 1 hour at room temperature with shaking. The membrane was washed 3 times in TBST for 5 minutes each. HRP-conjugated secondary antibody was applied at a 1:5,000 dilution for 1 hour with shaking. Membrane is washed with TBST (3 times, each for 5 minutes). HRP

substrate (Millipore Sigma) was applied to the membrane, and the membrane was imaged using a ChemiDoc (Bio-rad). A colorimetric image of the ladder was taken at 0.2 sec exposure, followed by a chemiluminescent image. Images were merged to obtain a full blot. Western blot containing cell lysate samples were additionally probed with GAPDH to confirm equal loading and act as normalization.

Immunoprecipitation: Protein Sepharose G beads were washed with 0.1% Tween 20 in PBS solution and incubated with primary antibody for 1 hour at 4C. 1.5ml of cell culture media was then added to beads and incubated with shaking overnight at 4C. The next day beads were washed with 0.1% Tween 20 in PBS and protein was eluted with 40 uL 0.2M glycine pH 2.6 at 37C and neutralized with 45ul of 0.2M Tris pH 8.

SNIPR activation co-culture assays: SNIPR PBiNSCs were plated on Matrigel-coated 6-wells plated at a density of $0.75x10^6$ cells per well. For co-cultures with streptavidin beads, beads were coated with 40ug/mg of beads of biotinylated protein and subsequently added to SNIPR cells. For cultures with target cells, cells were subsequently added at a 1:1 target-to-effect ratio in each well. Co-culture with a BFP readout were fixed to coverslips after 72h for 10 minutes using 1% PFA and mounted to coverslips. Samples were imaged using the Carl Ziess M2 Fluorescent microscope. For co-culture with lclPTENL read out, 1.5ml of cell culture media was collected after 72h and immunoprecipitation was performed. All experiments were cultured in a 1:1 mixture of DMEM/F12 and Neurobasal medium (Thermo Fisher) supplemented with N2, B27, penicillin–streptomycin, L-glutamine, CHIR99021, A83-01, purmorphamine, human LIF (hLIF), and LAAP.

SNIPR fluorescent imaging quantification: Fluorescence imaging was performed using a Zeiss Axio Imager M2 microscope for fixed cell samples or using the BioTek Cytation 5 for live cell imaging. Constitutive mCitrine expression was used to identify transduced cells, while inducible BFP expression served as a readout of SNIPR activation. Quantification was performed in Fiji (ImageJ) by normalizing total BFP-positive signal to total mCitrine-positive signal to account for differences in transduction efficiency.

Bi-specific binding assay: PBiNSCs expressing the bispecific Fc fusion protein were cultured in pre-cleared media for 48 hours to allow secretion and accumulation of the recombinant protein. Following this conditioning period, 2 ml of the resulting culture supernatant was harvested and transferred onto PriGO8A cells that had been seeded at a density of 0.75×10^6 cells per well in a

standard 6-well plate format. Treated cells were then incubated for a further 72 hours, after which cell lysates were collected and analysed by western blot to assess downstream protein expression.

Bi-specific purification using streptavidin agarose columns: PBiNSCs expressing the bispecific Fc fusion protein were cultured in pre-cleared media for 48 hours to allow secretion and accumulation of the bi-specific protein. Following this conditioning period, 2 ml of the resulting culture supernatant was harvested and spun down at 1200xg for 4 minutes to remove any cell debris and then filtered through a 0.45um filter. 5ug of biotinylated EGFRvIII was added to the column and allowed to flow by gravity followed by 2x washes with PBS. Total conditioned media volume was run through the column in 5ml volumes twice and washed x2 with PBS. Column was centrifuged at 1000xg for 1 minute to remove remaining PBS and bi-specific protein was eluted with 100ul of a 25uM solution of peptide EGFRvIII.

Statistical analysis: All graphs were generated using Microsoft excel. Error bars represent standard error of the mean. Statistical significance was assessed using a two-tailed unpaired Welch's t-test performed in Microsoft Excel.

DNA constructs:

SNIPR ind. lclPTENL - lclPTENL coding sequence was cloned into a SNIPR reporter plasmid (pHR_HNF1A-RE_tBFP_PGK_mCitrine, #188387) digested with BamHI and XhoI. For the lclPTENL-WPRE construct, the insert was amplified by PCR from an lclPTENL template using primers PHRP10LFOR(5'-CCAGAGCTCATCGCTAGCGCTACCGGATCCACCATGAGGGTGCCCGCC-3') and WPREFULL (5'-CCGAGCTCGAATTAATTCCCTCGAGCAGGCGGGGAGGCGGCCCAAAGG-3'). For the lclPTENL-WPRE3 construct, primers PHRP10LFOR (5'-CCAGAGCTCATCGCTAGCGCTACCGGATCCACCATGAGGGTGCCCGCC-3') and PHRP10LINT2 were used to obtain lclPTENL sequence, while the WPRE3 element was amplified separately from a gBlock template using primers PHRP10LINT1 (5'-GCATACAGAAATTACAAAAGTCTGAGTCGACAATCAACCTCTGGATTA-3') and PHRP10LREV (5'-CCGAGCTCGAATTAATTCCCTCGAGAACACCACGGAATTGTCAGTGCCC-3').

Assembly of inserts into the digested backbone was performed using HiFi DNA assembly at a 2:1 insert-to-backbone molar ratio to generate the final SNIPR-responsive constructs. Plasmid was sent for sequencing using SNIPRFOR: 3'- GGGTTTATTACAGGGACAGC - 5' SNIPRREV: 3'- GCAGATCTTGTCTTCGTTGG - 5' SNIPRINT: 3'- GTCAAATCCAGAGGCTAGC - 5'.

Constitutive IL13Ra2: Digestion of pLenti CMV GFP Puro Plasmid #17448 from Addgene with BamHI and SalI and ligating it with a gblock containing the coding sequence for IL13Ra2.

IL13 SNIPR: rIL13 coding sequence was cloned into a SNIPR receptor (pHR_PGK_SNIPR_humanized Hinge Notch SNIPR (HNF1A)) digested with EcoRI and NotI. The rIL13 sequence was obtained from another construct using SNPR13FOR (5'-CTCATCTCCGGGCCTTTCGAATTCACCATGAGAGTCCCCGTCCAATTGC-3') and SNPR13INTREV (5'-GCTGGCGTCGTGGTTGAGGAATTAAACTGTCCTTCTCGAAAGAGC-3') and was assembled with PCR product of SNPR13INTFOR (5'-GCTCTTTCGAGAAGGACAGTTTAATTCCTCAACCACGACGCCAGC-3') and SNPRREV (5'-GCATGTTGCAGGTGGGAGTTGCGGCCGCAAGTCAAGGATCTTAGGAGC-3') at a 2:1 insert to backbone ratio using Hifi assembly. Plasmid was sequenced using HV1FOR (5'-CATTCTGCACGCTTCAAAAG-3') and HV3REV (5'-CATAGCGTAAAAGGAGCAACA-3').

Constitutive EGFRvIII: Digestion of pLenti CMV GFP Puro Plasmid #17448 from Addgene with BamHI and SalI and ligating it with a PCR product of EGFRFOR2 (5'-CCATAGAAGACACCGACTCTAGAGGATCCACCATGCGACCCTCCGGGACGGC -3') and EGFRREV2 (3'-CACAAATTTTGTAATCCAGAGGTTGATTGTCGACTCATGCTCCAATAAATTCACTGC - 5') containing the coding sequence for EGFRvIII. Plasmid was sequenced with EGFRINT1 (5' - CCTCAAGGAGATAAGTGATGG - 3'), EGFRINT2 (5' - CGAATGGGCCTAAGATCC - 3') and EGFRINT3 (5' - CGTACTGGTGAAAACACCG - 3').

MR1 SNIPR: MR1 coding sequence was cloned into a SNIPR receptor (pHR_PGK_SNIPR_humanized Hinge Notch SNIPR (HNF1A)) digested with EcoRI and NotI. The MR1 sequence was obtained from another construct using SNIPRMR1FOR (3'-

CTCATCTCCGGGCCTTTCGAATCCCAGGTGAAACTGCAGCAGTCTGGGG-5') and SNIPRMR1INTREV (3'-GCTGGCGTCGTGGTTGAGGATTTGATTTCCAGCTTGGTGCCATCACC-5') and was assembled with PCR product of SNIPRMR1INTFOR (5'-GGTGATGGCACCAAGCTGGAAATCAAATCCTCAACCACGACGCCAGC-3') and SNPRREV (5'-GCATGTTGCAGGTGGGAGTTGCGGCCGCAAGTCAAGGATCTTAGGAGC-3') at a 7:3 insert to backbone ratio using Hifi assembly.

MR1/SIRPa bi-specific:

Cloning PCR product of VSIRPAFOR (5'-GAAGACACCGACTCTAGAGGATCCACCATGGAGCCAGCTGGTCCTGC3') and LSIRPAREV (5'-CTGGCACCGAGCGCCAGGAAGC-3') to obtain the IgG domains of the bi-specific protein, PCR product of LMR1FOR (5'-GCTTCCTGGCGCTCGGTGCCAGGTGAAGCTGCAGCAGTC -3') and FCMR1REV (5'-GCATGTGTGAGTTTTGTCGCCTCCGCTACCTTTGATTTCCAGCTTGGRGCC -3') to obtain the MR1 sequence and PCR product of MR1FCFOR (5'-GGCACCAAGCTGGAAATCAAAGGTAGCGGAGGCGACAAAACTCACACATGA-3') + VFCREV (5'-GTAATCCAGAGGTTGATTGTCCGACTCATTTACCCGGAGACAGGGAGAG-3') to obtain the IL13 sequence pieced together at a 7:3 insert to backbone ratio using Hifi assembly.

6. References

1. Sipos D, Raposa BL, Freihat O, et al. Glioblastoma: Clinical Presentation, Multidisciplinary Management, and Long-Term Outcomes. *Cancers (Basel)*. *Multidisciplinary Digital Publishing Institute (MDPI)*. 2025;17(1). doi:10.3390/cancers17010146

2. Mehta M, Wen P, Nishikawa R, Reardon D, Peters K. Critical review of the addition of tumor treating fields (TTFields) to the existing standard of care for newly diagnosed glioblastoma patients. *Crit Rev Oncol Hematol*. 2017;111:60-65. doi:10.1016/J.CRITREVONC.2017.01.005

3. Osborn AG, Louis DN, Poussaint TY, Linscott LL, Salzman KL. The 2021 World Health Organization Classification of Tumors of the Central Nervous System: What Neuroradiologists Need to Know. *American Journal of Neuroradiology*. *American Society of Neuroradiology*. 2022;43(7):928-937. doi:10.3174/ajnr.A7462

4. Lakomy R, Kazda T, Selingerova I, et al. Real-World Evidence in Glioblastoma: Stupp's Regimen After a Decade. *Front Oncol*. 2020;10:840. doi:10.3389/FONC.2020.00840

5. Stupp R, Mason WP, van den Bent MJ, et al. Radiotherapy plus Concomitant and Adjuvant Temozolomide for Glioblastoma. *New England Journal of Medicine*. 2005;352(10):987-996. doi:10.1056/NEJMOA043330/SUPPL_FILE/987SA1.PDF

6. Strobel H, Baisch T, Fitzel R, et al. Temozolomide and Other Alkylating Agents in Glioblastoma Therapy. *Biomedicines*. 2019;7(3):69. doi:10.3390/BIOMEDICINES7030069

7. Gilbert MR, Wang M, Aldape KD, et al. Dose-dense temozolomide for newly diagnosed glioblastoma: A randomized phase III clinical trial. *Journal of Clinical Oncology*. 2013;31(32):4085-4091. doi:10.1200/JCO.2013.49.6968/SUPPL_FILE/PROTOCOL_JCO.2013.49.6968.PDF

8. Couturier CP, Ayyadhury S, Le PU, et al. Single-cell RNA-seq reveals that glioblastoma recapitulates a normal neurodevelopmental hierarchy. *Nat Commun*. 2020;11(1). doi:10.1038/s41467-020-17186-5

9. Gousias K, Theocharous T, Simon M. Mechanisms of Cell Cycle Arrest and Apoptosis in Glioblastoma. *Biomedicines*. *MDPI*. 2022;10(3). doi:10.3390/biomedicines10030564

10. Santosh V, Arivazhagan A, Sreekanthreddy P, et al. Grade-specific expression of insulin-like growth factor-binding proteins-2, -3, and -5 in astrocytomas: IGFBP-3 emerges as a strong predictor of survival in patients with newly diagnosed glioblastoma. *Cancer Epidemiology Biomarkers and Prevention*. 2010;19(6):1399-1408. doi:10.1158/1055-9965.EPI-09-1213

11. Comincini S, Paolillo M, Barbieri G, et al. Gene expression analysis of an EGFR indirectly related pathway identified PTEN and MMP9 as reliable diagnostic markers for human glial tumor specimens. *J Biomed Biotechnol*. 2009;2009. doi:10.1155/2009/924565

12. Huang PH, Mukasa A, Bonavia R, et al. Quantitative analysis of EGFRvIII cellular signaling networks reveals a combinatorial therapeutic strategy for glioblastoma. *Proc Natl Acad Sci U S A*. 2007;104(31):12867-12872. doi:10.1073/PNAS.0705158104

13. Nagarajan RP, Costello JF. Epigenetic mechanisms in glioblastoma multiforme. *Semin Cancer Biol*. 2009;19(3):188-197. doi:10.1016/J.SEMCANCER.2009.02.005

14. Ohgaki H, Kleihues P. Genetic pathways to primary and secondary glioblastoma. *American Journal of Pathology*. 2007;170(5):1445-1453. doi:10.2353/AJPATH.2007.070011

15. Montana V, Sontheimer H. Bradykinin promotes the Chemotactic invasion of primary brain tumors. *Journal of Neuroscience*. 2011;31(13):4858-4867. doi:10.1523/JNEUROSCI.3825-10.2011

16. Cuddapah VA, Robel S, Watkins S, Sontheimer H. A neurocentric perspective on glioma invasion. *Nat Rev Neurosci*. 2014;15(7):455-465. doi:10.1038/NRN3765

17. de Gooijer MC, Guillén Navarro M, Bernards R, Wurdinger T, van Tellingen O. An Experimenter's Guide to Glioblastoma Invasion Pathways. *Trends Mol Med*. 2018;24(9):763-780. doi:10.1016/J.MOLMED.2018.07.003

18. Rammeloo E, Young JS, Schouten JW, et al. Preoperative assessment of tumor eloquence and resectability: an international survey. *J Neurooncol*. 2025;175(1):47. doi:10.1007/S11060-025-05067-0

19. Ahmed SU, Carruthers R, Gilmour L, Yildirim S, Watts C, Chalmers AJ. Selective inhibition of parallel DNA damage response pathways optimizes radiosensitization of glioblastoma stem-like cells. *Cancer Res*. 2015;75(20):4416-4428. doi:10.1158/0008-5472.CAN-14-3790

20. Carruthers R, Ahmed SU, Strathdee K, et al. Abrogation of radioresistance in glioblastoma stem-like cells by inhibition of ATM kinase. *Mol Oncol*. 2015;9(1):192-203. doi:10.1016/J.MOLONC.2014.08.003

21. Moeller BJ, Cao Y, Li CY, Dewhirst MW. Radiation activates HIF-1 to regulate vascular radiosensitivity in tumors: Role of reoxygenation, free radicals, and stress granules. *Cancer Cell*. 2004;5(5):429-441. doi:10.1016/S1535-6108(04)00115-1

22. Monteiro AR, Hill R, Pilkington GJ, Madureira PA. The role of hypoxia in glioblastoma invasion. *Cells*. 2017;6(4). doi:10.3390/CELLS6040045

23. Chédeville AL, Madureira PA. The role of hypoxia in glioblastoma radiotherapy resistance. *Cancers (Basel)*. 2021;13(3):1-16. doi:10.3390/CANCERS13030542

24. Kreisl TN, Kim L, Moore K, et al. Phase II trial of single-agent bevacizumab followed by bevacizumab plus irinotecan at tumor progression in recurrent glioblastoma. *Journal of Clinical Oncology*. 2009;27(5):740-745. doi:10.1200/JCO.2008.16.3055

25. Thon N, Kreth S, Kreth FW. Personalized treatment strategies in glioblastoma: MGMT promoter methylation status. *Onco Targets Ther*. 2013;6:1363-1372. doi:10.2147/OTT.S50208

26. Weller M. Assessing the MGMT status in glioblastoma: One step forward, two steps back? *Neuro Oncol*. 2013;15(3):253-254. doi:10.1093/NEUONC/NOT014

27. Pandith AA, Qasim I, Zahoor W, et al. Concordant association validates MGMT methylation and protein expression as favorable prognostic factors in glioma patients on alkylating chemotherapy (Temozolomide). *Sci Rep*. 2018;8(1). doi:10.1038/S41598-018-25169-2

28. Levin V, Edwards M, Dc W, et al. Modified procarbazine, CCNU, and vincristine (PCV 3) combination chemotherapy in the treatment of malignant brain tumors. *Cancer Treat Rep*. Published online 1980.

29. Cornetta K, Croop J, Dropcho E, et al. A pilot study of dose-intensified procarbazine, CCNU, vincristine for poor prognosis brain tumors utilizing fibronectin-assisted, retroviral-mediated modification of CD34+ peripheral blood cells with O6-methylguanine DNA methyltransferase. *Cancer Gene Ther*. 2006;13(9):886-895. doi:10.1038/SJ.CGT.7700963

30. D'Amico RS, Aghi MK, Vogelbaum MA, Bruce JN. Convection-enhanced drug delivery for glioblastoma: a review. *J Neurooncol*. 2021;151(3):415-427. doi:10.1007/S11060-020-03408-9

31. Pardridge WM. Drug transport across the blood–brain barrier. *Journal of Cerebral Blood Flow & Metabolism*. 2012;32(11):1959. doi:10.1038/JCBFM.2012.126

32. Pardridge WM. The Blood-Brain Barrier: Bottleneck in Brain Drug Development. *NeuroRx*. 2005;2(1):3. doi:10.1602/NEURORX.2.1.3

33. Dréan A, Goldwirt L, Verreault M, et al. Blood-brain barrier, cytotoxic chemotherapies and glioblastoma. *Expert Rev Neurother*. 2016;16(11):1285-1300. doi:10.1080/14737175.2016.1202761

34. Oberoi RK, Parrish KE, Sio TT, Mittapalli RK, Elmquist WF, Sarkaria JN. Strategies to improve delivery of anticancer drugs across the blood-brain barrier to treat glioblastoma. *Neuro Oncol*. 2016;18(1):27-36. doi:10.1093/NEUONC/NOV164

35. Dobrynina LA, Shamtieva K V., Kremneva EI, et al. Daily blood pressure profile and blood–brain barrier permeability in patients with cerebral small vessel disease. *Sci Rep*. 2022;12(1). doi:10.1038/S41598-022-11172-1

36. AMMAYA AK. SUBCUTANEOUS RESERVOIR AND PUMP FOR STERILE ACCESS TO VENTRICULAR CEREBROSPINAL FLUID. *The Lancet*. 1963;282(7315):983-984. doi:10.1016/S0140-6736(63)90681-0

37. Bleyer WA, Poplack DG. Intraventricular versus intralumbar methotrexate for central-nervous-system leukemia: Prolonged remission with the ommaya reservoir. *Med Pediatr Oncol*. 1979;6(3):207-213. doi:10.1002/MPO.2950060304

38. Glantz MJ, LaFollette S, Jaeckle KA, et al. Randomized Trial of a Slow-Release Versus a Standard Formulation of Cytarabine for the Intrathecal Treatment of Lymphomatous Meningitis. *Journal of Clinical Oncology*. 1999;17(10):3110-3116. doi:10.1200/JCO.1999.17.10.3110

39. Grossman SA, Finkelstein DM, Ruckdeschel JC, Trump DL, Moynihan T, Ettinger DS. Randomized prospective comparison of intraventricular methotrexate and thiotepa in patients with previously untreated neoplastic meningitis. Eastern Cooperative Oncology Group. *Journal of Clinical Oncology*. 1993;11(3):561-569. doi:10.1200/JCO.1993.11.3.561

40. Shapiro WR, Young DF, Mehta BM. Methotrexate: Distribution in Cerebrospinal Fluid after Intravenous, Ventricular and Lumbar Injections. *New England Journal of Medicine*. 1975;293(4):161-166. doi:10.1056/NEJM197507242930402/ASSET/95428F02-30E6-4DAC-8149-72388BEC2D31/ASSETS/IMAGES/LARGE/NEJM197507242930402_F4.JPG

41. Sandberg DI, Bilsky MH, Souweidane MM, Bzdil J, Gutin PH, Greenberg HS. Ommaya reservoirs for the treatment of leptomeningeal metastases. *Neurosurgery*. 2000;47(1):49-55. doi:10.1097/00006123-200007000-00011

42. Blasberg RG, Patlak C, Fenstermacher JD. Intrathecal chemotherapy: brain tissue profiles after ventriculo cisternal perfusion. *Journal of Pharmacology and Experimental Therapeutics*. 1975;195(1):73-83. doi:10.1016/s0022-3565(25)30311-3

43. Lei Y, Tang R, Xu J, et al. Applications of single-cell sequencing in cancer research: progress and perspectives. *J Hematol Oncol*. 2021;14(1). doi:10.1186/S13045-021-01105-2

44. Xin S, Liu X, Li Z, et al. ScRNA-seq revealed an immunosuppression state and tumor microenvironment heterogeneity related to lymph node metastasis in prostate cancer. *Exp Hematol Oncol*. 2023;12(1). doi:10.1186/S40164-023-00407-0

45. Haley MJ, Bere L, Minshull J, et al. Hypoxia coordinates the spatial landscape of myeloid cells within glioblastoma to affect survival. *Sci Adv*. 2024;10(20):eadj3301. doi:10.1126/SCIADV.ADJ3301

46. Lam KHB, Valkanas K, Djuric U, Diamandis P. Unifying models of glioblastoma's intratumoral heterogeneity. *Neurooncol Adv*. 2020;2(1). doi:10.1093/NOAJNL/VDAA096

47. Charles NA, Holland EC, Gilbertson R, Glass R, Kettenmann H. The brain tumor microenvironment. *Glia*. 2012;60(3):502-514. doi:10.1002/GLIA.21264

48. Ginhoux F, Prinz M. Origin of microglia: Current concepts and past controversies. *Cold Spring Harb Perspect Biol*. 2015;7(8). doi:10.1101/CSHPERSPECT.A020537

49. Hansen LJ, Jackson CM. The glioma microenvironment and its impact on antitumor immunity. *Neurooncol Adv*. 2025;7(Supplement_4):iv19-iv31. doi:10.1093/NOAJNL/VDAE204

50. Ravichandran KS. Beginnings of a good apoptotic meal: the find-me and eat-me signaling pathways. *Immunity*. 2011;35(4):445-455. doi:10.1016/J.IMMUNI.2011.09.004

51. Ravichandran KS. Find-me and eat-me signals in apoptotic cell clearance: progress and conundrums. *J Exp Med*. 2010;207(9):1807. doi:10.1084/JEM.20101157

52. Park SY, Kim IS. Engulfment signals and the phagocytic machinery for apoptotic cell clearance. *Experimental & Molecular Medicine 2017 49:5*. 2017;49(5):e331-e331. doi:10.1038/emm.2017.52

53. Huynh MLN, Fadok VA, Henson PM. Phosphatidylserine-dependent ingestion of apoptotic cells promotes TGF-β1 secretion and the resolution of inflammation. *J Clin Invest*. 2002;109(1):41-50. doi:10.1172/JCI11638

54. Szondy Z, Sarang Z, Kiss B, Garabuczi É, Köröskényi K. Anti-inflammatory Mechanisms Triggered by Apoptotic Cells during Their Clearance. *Front Immunol*. 2017;8(AUG):909. doi:10.3389/FIMMU.2017.00909

55. Fadok VA, Bratton DL, Konowal A, Freed PW, Westcott JY, Henson PM. Macrophages that have ingested apoptotic cells in vitro inhibit proinflammatory cytokine production through autocrine/paracrine mechanisms involving TGF-beta, PGE2, and PAF. *Journal of Clinical Investigation*. 1998;101(4):890. doi:10.1172/JCI1112

56. Xu J, Ding L, Mei J, et al. Dual roles and therapeutic targeting of tumor-associated macrophages in tumor microenvironments. *Signal Transduction and Targeted Therapy 2025 10:1*. 2025;10(1):268-. doi:10.1038/s41392-025-02325-5

57. Zhao W, Zhang Z, Xie M, et al. Exploring tumor-associated macrophages in glioblastoma: from diversity to therapy. *npj Precision Oncology 2025 9:1*. 2025;9(1):126-. doi:10.1038/s41698-025-00920-x

58. Khan F, Pang L, Dunterman M, Lesniak MS, Heimberger AB, Chen P. Macrophages and microglia in glioblastoma: heterogeneity, plasticity, and therapy. *J Clin Invest*. 2023;133(1):e163446. doi:10.1172/JCI163446

59. Yeo AT, Rawal S, Delcuze B, et al. Single-cell RNA sequencing reveals evolution of immune landscape during glioblastoma progression. *Nat Immunol*. 2022;23(6):971-984. doi:10.1038/S41590-022-01215-0

60. Gabrusiewicz K, Rodriguez B, Wei J, et al. Glioblastoma-infiltrated innate immune cells resemble M0 macrophage phenotype. *JCI Insight*. 2016;1(2):85841. doi:10.1172/JCI.INSIGHT.85841

61. Pinton L, Masetto E, Vettore M, et al. The immune suppressive microenvironment of human gliomas depends on the accumulation of bone marrow-derived macrophages in the center of the lesion. doi:10.1186/s40425-019-0536-x

62. Ismailov A, Spallone A, Belogurov A, Herbert A, Poptsova M. Molecular biology of the deadliest cancer – glioblastoma: what do we know? *Front Immunol*. 2025;16:1530305. doi:10.3389/FIMMU.2025.1530305/FULL

63. Kalos M, Levine BL, Porter DL, et al. T cells with chimeric antigen receptors have potent antitumor effects and can establish memory in patients with advanced leukemia. *Sci Transl Med*. 2011;3(95). doi:10.1126/SCITRANSLMED.3002842

64. Eshhar Z, Waks T, Gkoss G, Schindler DG. Specific activation and targeting of cytotoxic lymphocytes through chimeric single chains consisting of antibody-binding domains and the γ or ζ subunits of the immunoglobulin and T-cell receptors. *Proc Natl Acad Sci U S A*. 1993;90(2):720-724. doi:10.1073/PNAS.90.2.720

65. Guedan S, Ruella M, June CH. Emerging Cellular Therapies for Cancer. *Annu Rev Immunol*. 2019;37:145-171. doi:10.1146/ANNUREV-IMMUNOL-042718-041407

66. Maude SL, Laetsch TW, Buechner J, et al. Tisagenlecleucel in Children and Young Adults with B-Cell Lymphoblastic Leukemia. *New England Journal of Medicine*. 2018;378(5):439-448. doi:10.1056/NEJMOA1709866

67. Rosenberg SA, Spiess P, Lafreniere R. A New Approach to the Adoptive Immunotherapy of Cancer with Tumor-Infiltrating Lymphocytes. *Science (1979)*. 1986;233(4770):1318-1321. doi:10.1126/SCIENCE.3489291

68. Maggs L, Cattaneo G, Dal AE, Moghaddam AS, Ferrone S. CAR T Cell-Based Immunotherapy for the Treatment of Glioblastoma. *Front Neurosci*. 2021;15. doi:10.3389/FNINS.2021.662064

69. Brown CE, Alizadeh D, Starr R, et al. Regression of Glioblastoma after Chimeric Antigen Receptor T-Cell Therapy. *New England Journal of Medicine*. 2016;375(26):2561-2569. doi:10.1056/NEJMOA1610497

70. O'Rourke DM, Nasrallah MP, Desai A, et al. A single dose of peripherally infused EGFRvIII-directed CAR T cells mediates antigen loss and induces adaptive resistance in patients with recurrent glioblastoma. *Sci Transl Med*. 2017;9(399). doi:10.1126/SCITRANSLMED.AAA0984

71. Ahmed N, Brawley V, Hegde M, et al. HER2-specific chimeric antigen receptor–modified virus-specific T cells for progressive glioblastoma: A phase 1 dose-escalation trial. *JAMA Oncol*. 2017;3(8):1094-1101. doi:10.1001/JAMAONCOL.2017.0184

72. Majzner RG, Theruvath JL, Nellan A, et al. CAR T cells targeting B7-H3, a pan-cancer antigen, demonstrate potent preclinical activity against pediatric solid tumors and brain tumors. *Clinical Cancer Research*. 2019;25(8):2560-2574. doi:10.1158/1078-0432.CCR-18-0432

73. Woroniecka KI, Rhodin KE, Chongsathidkiet P, Keith KA, Fecci PE. T-Cell dysfunction in glioblastoma: Applying a new framework. *Clinical Cancer Research*. 2018;24(16):3792-3802. doi:10.1158/1078-0432.CCR-18-0047

74. Majzner RG, Mackall CL. Tumor antigen escape from car t-cell therapy. *Cancer Discov*. 2018;8(10):1219-1226. doi:10.1158/2159-8290.CD-18-0442

75. Genßler S, Burger MC, Zhang C, et al. Dual targeting of glioblastoma with chimeric antigen receptor-engineered natural killer cells overcomes heterogeneity of target antigen expression and enhances antitumor activity and survival. *Oncoimmunology*. 2016;5(4). doi:10.1080/2162402X.2015.1119354

76. Hegde M, Mukherjee M, Grada Z, et al. Tandem CAR T cells targeting HER2 and IL13Rα2 mitigate tumor antigen escape. *Journal of Clinical Investigation*. 2016;126(8):3036-3052. doi:10.1172/JCI83416

77. Brown CE, Rodriguez A, Palmer J, et al. Off-the-shelf, steroid-resistant, IL13Rα2-specific CAR T cells for treatment of glioblastoma. *Neuro Oncol*. 2022;24(8):1318-1330. doi:10.1093/NEUONC/NOAC024

78. Neelapu SS, Locke FL, Bartlett NL, et al. Axicabtagene Ciloleucel CAR T-Cell Therapy in Refractory Large B-Cell Lymphoma. *N Engl J Med*. 2017;377(26):2531-2544. doi:10.1056/NEJMOA1707447

79. June CH, Sadelain M. Chimeric Antigen Receptor Therapy. *N Engl J Med*. 2018;379(1):64-73. doi:10.1056/NEJMRA1706169

80. Turtle CJ, Hanafi LA, Berger C, et al. Immunotherapy of non-Hodgkin's lymphoma with a defined ratio of CD8+ and CD4+ CD19-specific chimeric antigen receptor-modified T cells. *Sci Transl Med*. 2016;8(355). doi:10.1126/SCITRANSLMED.AAF8621

81. Roybal KT, Williams JZ, Morsut L, et al. Engineering T Cells with Customized Therapeutic Response Programs Using Synthetic Notch Receptors. *Cell*. 2016;167(2):419-432.e16. doi:10.1016/J.CELL.2016.09.011/ATTACHMENT/23387FA6-D4FD-491C-9E5D-F6EAB7C7A432/MMC1.PDF

82. Eyquem J, Mansilla-Soto J, Giavridis T, et al. Targeting a CAR to the TRAC locus with CRISPR/Cas9 enhances tumour rejection. *Nature*. 2017;543(7643):113. doi:10.1038/NATURE21405

83. Newick K, O'Brien S, Moon E, Albelda SM. CAR T Cell Therapy for Solid Tumors. *Annu Rev Med*. 2017;68:139-152. doi:10.1146/ANNUREV-MED-062315-120245

84. Brown CE, Aguilar B, Starr R, et al. Optimization of IL13Rα2-Targeted Chimeric Antigen Receptor T Cells for Improved Anti-tumor Efficacy against Glioblastoma. *Molecular Therapy*. 2017;26(1):31. doi:10.1016/J.YMTHE.2017.10.002

85. Buccarelli M, Beninati S, Tabolacci C. Cancer stem cell differentiation: A realistic potential therapeutic option? *Front Oncol*. 2023;13:1188765. doi:10.3389/fonc.2023.1188765

86. Calinescu AA, Kauss MC, Sultan Z, Al-Holou WN, O'Shea SK. Stem cells for the treatment of glioblastoma: a 20-year perspective. *CNS Oncol*. 2021;10(2):CNS73. doi:10.2217/cns-2020-0026

87. Bryukhovetskiy I. Cell-based immunotherapy of glioblastoma multiforme. *Oncol Lett*. 2022;23(4):133. doi:10.3892/ol.2022.13253

88. Egea V, Von Baumgarten L, Schichor C, et al. TNF-α respecifies human mesenchymal stem cells to a neural fate and promotes migration toward experimental glioma. *Cell Death Differ*. 2011;18(5):853-863. doi:10.1038/cdd.2010.154

89. Kim DS, Kim JH, Kwon Lee J, et al. Overexpression of CXC chemokine receptors is required for the superior glioma-tracking property of umbilical cord blood-derived mesenchymal stem cells. *Stem Cells Dev*. 2009;18(3):511-519. doi:10.1089/scd.2008.0050

90. Menon LG, Picinich S, Koneru R, et al. Differential Gene Expression Associated with Migration of Mesenchymal Stem Cells to Conditioned Medium from Tumor Cells or Bone Marrow Cells. *Stem Cells*. 2007;25(2):520-528. doi:10.1634/stemcells.2006-0257

91. Ahmed AU, Tyler MA, Thaci B, et al. A comparative study of neural and mesenchymal stem cell-based carriers for oncolytic adenovirus in a model of malignant glioma. *Mol Pharm*. 2011;8(5):1559-1572. doi:10.1021/MP200161F/SUPPL_FILE/MP200161F_SI_001.TIF

92. Thin ZS, Ng NCS, Ming LC, Wong RSY, Goh BH. Stem Cell-Based Cancer Therapies: A Commentary on Therapeutic Promise, Health Impacts and Translational Barriers. *Cancer Innovation*. 2025;4(5):e70025. doi:10.1002/CAI2.70025

93. Ahmed AU, Thaci B, Tobias AL, et al. A preclinical evaluation of neural stem cell-based cell carrier for targeted antiglioma oncolytic virotherapy. *J Natl Cancer Inst*. 2013;105(13):968-977. doi:10.1093/JNCI/DJT141

94. Frank RT, Najbauer J, Aboody KS. Concise Review: Stem Cells As an Emerging Platform for Antibody Therapy of Cancer. *Stem Cells*. 2010;28(11):2084. doi:10.1002/STEM.513

95. Sonabend AM, Ulasov I V., Tyler MA, Rivera AA, Mathis JM, Lesniak MS. Mesenchymal stem cells effectively deliver an oncolytic adenovirus to intracranial glioma. *Stem Cells*. 2008;26(3):831-841. doi:10.1634/STEMCELLS.2007-0758

96. Oh MC, Lim DA. Novel Treatment Strategies for Malignant Gliomas Using Neural Stem Cells. *Neurotherapeutics*. 2009;6(3):458-464. doi:10.1016/J.NURT.2009.05.003

97. Portnow J, Synold TW, Badie B, et al. Neural Stem Cell-Based Anticancer Gene Therapy: A First-in-Human Study in Recurrent High-Grade Glioma Patients. *Clin Cancer Res*. 2017;23(12):2951-2960. doi:10.1158/1078-0432.CCR-16-1518

98. Aboody KS, Najbauer J, Metz MZ, et al. Neural stem cell-mediated enzyme/prodrug therapy for glioma: Preclinical studies. *Sci Transl Med*. 2013;5(184). doi:10.1126/SCITRANSLMED.3005365

99. Li S, Tokuyama T, Yamamoto J, Koide M, Yokota N, Namba H. Bystander effect-mediated gene therapy of gliomas using genetically engineered neural stem cells. *Cancer Gene Ther*. 2005;12(7):600-607. doi:10.1038/SJ.CGT.7700826

100. Zhang J, Huang X, Wang H, et al. The challenges and promises of allogeneic mesenchymal stem cells for use as a cell-based therapy. *Stem Cell Res Ther*. 2015;6(1):234. doi:10.1186/S13287-015-0240-9

101. Uwishema O, Shariff S, Wojtara M, et al. Stem cell therapies and glioma stem cells in glioblastoma: a systematic review of current challenges and research directions. *Int J Emerg Med*. 2025;18(1):144. doi:10.1186/S12245-025-00921-4

102. Leonov GE, Grinchevskaya LR, Makhnach O V., Samburova M V., Goldshtein D V., Salikhova DI. Safety Assessment of Stem Cell-Based Therapies: Current Standards and Advancing Frameworks. *Cells*. 2025;14(21):1660. doi:10.3390/CELLS14211660

103. Stuckey DW, Shah K. Stem cell-based therapies for cancer treatment: separating hope from hype. *Nat Rev Cancer*. 2014;14(10):683. doi:10.1038/NRC3798

104. Studer L, Vera E, Cornacchia D. Programming and Reprogramming Cellular Age in the Era of Induced Pluripotency. *Cell Stem Cell*. *Cell Press*. 2015;16(6):591-600. doi:10.1016/j.stem.2015.05.004

105. Li Y, Zhang Q, Yin X, et al. Generation of iPSCs from mouse fibroblasts with a single gene, Oct4, and small molecules. *Cell Res*. 2011;21(1):196-204. doi:10.1038/cr.2010.142

106. Takahashi K, Tanabe K, Ohnuki M, et al. Induction of Pluripotent Stem Cells from Adult Human Fibroblasts by Defined Factors. *Cell*. 2007;131(5):861-872. doi:10.1016/j.cell.2007.11.019

107. Takahashi K, Yamanaka S. Induction of Pluripotent Stem Cells from Mouse Embryonic and Adult Fibroblast Cultures by Defined Factors. *Cell*. 2006;126(4):663-676. doi:10.1016/j.cell.2006.07.024

108. Hu BY, Weick JP, Yu J, et al. Neural differentiation of human induced pluripotent stem cells follows developmental principles but with variable potency. *Proc Natl Acad Sci U S A*. 2010;107(9):4335-4340. doi:10.1073/pnas.0910012107

109. Vierbuchen T, Ostermeier A, Pang ZP, Kokubu Y, Südhof TC, Wernig M. Direct conversion of fibroblasts to functional neurons by defined factors. *Nature*. 2010;463(7284):1035-1041. doi:10.1038/nature08797

110. Ladewig J, Mertens J, Kesavan J, et al. Small molecules enable highly efficient neuronal conversion of human fibroblasts. *Nat Methods*. 2012;9(6):575-578. doi:10.1038/nmeth.1972

111. Pang ZP, Yang N, Vierbuchen T, et al. Induction of human neuronal cells by defined transcription factors. *Nature*. 2011;476(7359):220-223. doi:10.1038/nature10202

112. Mertens J, Paquola ACM, Ku M, et al. Directly reprogrammed human neurons retain aging-associated transcriptomic signatures and reveal age-related nucleocytoplasmic defects. *Cell Stem Cell*. 2015;17(6):705-718. doi:10.1016/j.stem.2015.09.001

113. Ring KL, Tong LM, Balestra ME, et al. Direct reprogramming of mouse and human fibroblasts into multipotent neural stem cells with a single factor. *Cell Stem Cell*. 2012;11(1):100-109. doi:10.1016/j.stem.2012.05.018

114. Zou Q, Yan Q, Zhong J, et al. Direct conversion of human fibroblasts into neuronal restricted progenitors. *J Biol Chem*. 2014;289(8):5250-5260. doi:10.1074/jbc.m113.516112

115. Weissbein U, Ben-David U, Benvenisty N. Virtual karyotyping reveals greater chromosomal stability in neural cells derived by transdifferentiation than those from stem cells. *Cell Stem Cell*. 2014;15(6):687-691. doi:10.1016/j.stem.2014.10.018

116. Lee JH, Mitchell RR, McNicol JD, et al. Single transcription factor conversion of human blood fate to NPCs with CNS and PNS developmental capacity. *Cell Rep*. 2015;11(9):1367-1376. doi:10.1016/j.celrep.2015.04.056

117. Bar-Nur O, Verheul C, Sommer AG, et al. Lineage conversion induced by pluripotency factors involves transient passage through an iPSC stage. *Nat Biotechnol*. 2015;33(7):1-11. doi:10.1038/nbt.3247

118. Shahbazi E, Moradi S, Nemati S, et al. Generation of stably self-renewing multipotent neural stem cells by direct conversion of human fibroblasts with a novel single transcription factor. *Stem Cell Rep*. 2016;6(4):1-13. doi:10.1016/j.stemcr.2016.02.013

119. Maza I, Caspi I, Zviran A, et al. Transient acquisition of pluripotency during somatic cell transdifferentiation with iPSC reprogramming factors. *Nat Biotechnol*. 2015;33(7):769-774. doi:10.1038/nbt.3270

120. Castaño J, Menendez P, Bruzos-Cidon C, et al. Fast and efficient neural conversion of human hematopoietic cells. *Stem Cell Rep*. 2014;3(6):1118-1131. doi:10.1016/j.stemcr.2014.10.008

121. Sheng C, Jungverdorben J, Wiethoff H, et al. A stably self-renewing adult blood-derived induced neural stem cell exhibiting patternability and epigenetic rejuvenation. *Nat Commun*. 2018;9(1). doi:10.1038/s41467-018-06398-5

122. Choi VW, McCarty DM, Samulski RJ. Host Cell DNA Repair Pathways in Adeno-Associated Viral Genome Processing. *J Virol*. 2006;80(21):10346. doi:10.1128/JVI.00841-06

123. Basner-Tschakarjan E, Mingozzi F. Cell-Mediated Immunity to AAV Vectors, Evolving Concepts and Potential Solutions. *Front Immunol*. 2014;5(JUL). doi:10.3389/FIMMU.2014.00350

124. Mays LE, Wang L, Lin J, et al. AAV8 Induces Tolerance in Murine Muscle as a Result of Poor APC Transduction, T Cell Exhaustion, and Minimal MHCI Upregulation on Target Cells. *Molecular Therapy*. 2013;22(1):28. doi:10.1038/MT.2013.134

125. Wu Z, Yang H, Colosi P. Effect of Genome Size on AAV Vector Packaging. *Molecular Therapy*. 2009;18(1):80. doi:10.1038/MT.2009.255

126. Dong B, Nakai H, Xiao W. Characterization of Genome Integrity for Oversized Recombinant AAV Vector. *Molecular Therapy*. 2009;18(1):87. doi:10.1038/MT.2009.258

127. Mann R, Mulligan RC, Baltimore D. Construction of a retrovirus packaging mutant and its use to produce helper-free defective retrovirus. *Cell*. 1983;33(1):153-159. doi:10.1016/0092-8674(83)90344-6

128. Ginn SL, Fleming J, Rowe PB, Alexander IE. Promoter interference mediated by the U3 region in early-generation HIV-1-derived lentivirus vectors can influence detection of transgene expression in a cell-type and species-specific manner. *Hum Gene Ther*. 2003;14(12):1127-1137. doi:10.1089/104303403322167975

129. Zufferey R, Dull T, Mandel RJ, et al. Self-Inactivating Lentivirus Vector for Safe and Efficient In Vivo Gene Delivery. *J Virol*. 1998;72(12):9873. doi:10.1128/JVI.72.12.9873-9880.1998

130. Miyoshi H, Blömer U, Takahashi M, Gage FH, Verma IM. Development of a Self-Inactivating Lentivirus Vector. *J Virol*. 1998;72(10):8150. doi:10.1128/JVI.72.10.8150-8157.1998

131. Barnea G, Strapps W, Herrada G, et al. The genetic design of signaling cascades to record receptor activation. *Proc Natl Acad Sci U S A*. 2007;105(1):64. doi:10.1073/PNAS.0710487105

132. Daringer NM, Dudek RM, Schwarz KA, Leonard JN. Modular extracellular sensor architecture for engineering mammalian cell-based devices. *ACS Synth Biol*. 2014;3(12):892-902. doi:10.1021/SB400128G

133. Kopan R, Ilagan MXG. The Canonical Notch Signaling Pathway: Unfolding the Activation Mechanism. *Cell*. 2009;137(2):216. doi:10.1016/J.CELL.2009.03.045

134. Artavanis-Tsakonas S, Rand MD, Lake RJ. Notch signaling: cell fate control and signal integration in development. *Science*. 1999;284(5415):770-776. doi:10.1126/SCIENCE.284.5415.770

135. Gordon WR, Zimmerman B, He L, et al. Mechanical Allostery: Evidence for a Force Requirement in the Proteolytic Activation of Notch. *Dev Cell*. 2015;33(6):729. doi:10.1016/J.DEVCEL.2015.05.004

136. Morsut L, Roybal KT, Xiong X, et al. Engineering Customized Cell Sensing and Response Behaviors Using Synthetic Notch Receptors. *Cell*. 2016;164(4):780-791. doi:10.1016/J.CELL.2016.01.012

137. Gordon WR, Roy M, Vardar-Ulu D, et al. Structure of the Notch1-negative regulatory region: implications for normal activation and pathogenic signaling in T-ALL. *Blood*. 2008;113(18):4381. doi:10.1182/BLOOD-2008-08-174748

138. Zhu I, Liu R, Garcia JM, et al. Modular design of synthetic receptors for programmed gene regulation in cell therapies. *Cell*. 2022;185(8):1431-1443.e16. doi:10.1016/J.CELL.2022.03.023

139. Israni D V., Li HS, Gagnon KA, et al. Clinically-driven design of synthetic gene regulatory programs in human cells. *bioRxiv*. Published online February 23, 2021:2021.02.22.432371. doi:10.1101/2021.02.22.432371

140. Choe JH, Watchmaker PB, Simic MS, et al. SynNotch-CAR T cells overcome challenges of specificity, heterogeneity, and persistence in treating glioblastoma. *Sci Transl Med*. 2021;13(591):eabe7378. doi:10.1126/SCITRANSLMED.ABE7378

141. Köhler G, Milstein C. Continuous cultures of fused cells secreting antibody of predefined specificity. *Nature*. 1975;256(5517):495-497. doi:10.1038/256495A0

142. Mitra S, Tomar PC. Hybridoma technology; advancements, clinical significance, and future aspects. *Journal of Genetic Engineering & Biotechnology*. 2021;19(1):159. doi:10.1186/S43141-021-00264-6

143. Verhoeyen M, Milstein C, Winter G. Reshaping human antibodies: grafting an antilysozyme activity. *Science (1979)*. 1988;239(4847):1534-1536. doi:10.1126/science.2451287

144. Boulianne GL, Hozumi N, Shulman MJ. Production of functional chimaeric mouse/human antibody. *Nature*. 1984;312(5995):643-646. doi:10.1038/312643a0

145. Jones PT, Dear PH, Foote J, Neuberger MS, Winter G. Replacing the complementarity-determining regions in a human antibody with those from a mouse. *Nature*. 1986;321(6069):522-525. doi:10.1038/321522a0

146. Riechmann L, Clark M, Waldmann H, Winter G. Reshaping human antibodies for therapy. *Nature*. 1988;332(6162):323-327. doi:10.1038/332323a0

147. Morrison SL, Johnson MJ, Herzenberg LA, Oi VT. Chimeric human antibody molecules: mouse antigen-binding domains with human constant region domains. *Proc Natl Acad Sci USA*. 1984;81(21 I):6851-6855. doi:10.1073/pnas.81.21.6851

148. Paul S, Konig MF, Pardoll DM, et al. Cancer therapy with antibodies. *Nature Reviews Cancer 2024 24:6*. 2024;24(6):399-426. doi:10.1038/S41568-024-00690-X

149. Yu J, Song Y, Tian W. How to select IgG subclasses in developing anti-tumor therapeutic antibodies. *J Hematol Oncol*. 2020;13(1):45. doi:10.1186/s13045-020-00876-4

150. Vidarsson G, Dekkers G, Rispens T. IgG subclasses and allotypes: from structure to effector functions. *Front Immunol*. 2014;5(OCT):520. doi:10.3389/fimmu.2014.00520

151. Salfeld JG. Isotype selection in antibody engineering. *Nat Biotechnol*. 2007;25(12):1369-1372. doi:10.1038/nbt1207-1369

152. Porebski BT, Balmforth M, Browne G, et al. Rapid discovery of high-affinity antibodies via massively parallel sequencing, ribosome display and affinity screening. *Nat Biomed Eng*. 2024;8(3):214-232. doi:10.1038/S41551-023-01093-3

153. Saleh MN, LoBuglio AF, Wheeler RH, et al. A phase II trial of murine monoclonal antibody 17-1A and interferon-gamma: clinical and immunological data. *Cancer Immunol Immunother*. 1990;32(3):185-190. doi:10.1007/BF01771455

154. Redman JM, Hill EM, AlDeghaither D, Weiner LM. Mechanisms of action of therapeutic antibodies for cancer. *Mol Immunol*. 2015;67(2 Pt A):28-45. doi:10.1016/J.MOLIMM.2015.04.002

155. Golay J, Taylor RP. The Role of Complement in the Mechanism of Action of Therapeutic Anti-Cancer mAbs. *Antibodies (Basel)*. 2020;9(4). doi:10.3390/ANTIB9040058

156. Wang C, Thudium KB, Han M, et al. In vitro characterization of the anti-PD-1 antibody nivolumab, BMS-936558, and in vivo toxicology in non-human primates. *Cancer Immunol Res*. 2014;2(9):846-856. doi:10.1158/2326-6066.CIR-14-0040

157. McDermott DF, Sosman JA, Sznol M, et al. Atezolizumab, an Anti-Programmed Death-Ligand 1 Antibody, in Metastatic Renal Cell Carcinoma: Long-Term Safety, Clinical Activity, and Immune Correlates From a Phase Ia Study. *J Clin Oncol*. 2016;34(8):833-842. doi:10.1200/JCO.2015.63.7421

158. Tyagi P, Chu E, Jain VK. Recent results and ongoing trials with panitumumab (ABX-EGF), a fully human anti-epidermal growth factor receptor antibody, in metastatic colorectal cancer. *Clin Colorectal Cancer*. 2005;5(1):21-23. doi:10.1016/S1533-0028(11)70161-X

159. Cobleigh MA, Vogel CL, Tripathy D, et al. Multinational study of the efficacy and safety of humanized anti-HER2 monoclonal antibody in women who have HER2-overexpressing metastatic breast cancer that has progressed after chemotherapy for metastatic disease. *J Clin Oncol*. 1999;17(9):2639-2648. doi:10.1200/JCO.1999.17.9.2639

160. Pillay V, Gan HK, Scott AM. Antibodies in oncology. *N Biotechnol*. 2011;28(5):518-529. doi:10.1016/J.NBT.2011.03.021

161. Ravetch J. In vivo veritas: the surprising roles of Fc receptors in immunity. *Nature Immunology 2010 11:3*. 2010;11(3):183-185. doi:10.1038/ni0310-183

162. Weiner LM, Surana R, Wang S. Monoclonal antibodies: versatile platforms for cancer immunotherapy. *Nature Reviews Immunology 2010 10:5*. 2010;10(5):317-327. doi:10.1038/nri2744

163. Wang B, Han Y, Zhang Y, et al. Overcoming acquired resistance to cancer immune checkpoint therapy: potential strategies based on molecular mechanisms. *Cell Biosci*. 2023;13(1):120. doi:10.1186/S13578-023-01073-9

164. Wang B, Han Y, Zhang Y, et al. Overcoming acquired resistance to cancer immune checkpoint therapy: potential strategies based on molecular mechanisms. *Cell Biosci*. 2023;13(1):120. doi:10.1186/S13578-023-01073-9

165. Konishi T, Ochi T, Maruta M, et al. Reinforced antimyeloma therapy via dual-lymphoid activation mediated by a panel of antibodies armed with bridging-BiTE. *Blood*. 2023;142(21):1789-1805. doi:10.1182/BLOOD.2022019082

166. Zhou S, Liu M, Ren F, Meng X, Yu J. The landscape of bispecific T cell engager in cancer treatment. *Biomark Res*. 2021;9(1):38. doi:10.1186/S40364-021-00294-9

167. Zhu H, Zhang W, Guo Q, Fan R, Luo G, Liu Y. Engineered oncolytic virus expressing B7H3-targeting BiTE enhances antitumor T-cell immune response. *J Immunother Cancer*. 2024;12(11):e009901. doi:10.1136/JITC-2024-009901

168. Shim H. Bispecific Antibodies and Antibody–Drug Conjugates for Cancer Therapy: Technological Considerations. *Biomolecules*. 2020;10(3):360. doi:10.3390/BIOM10030360

169. Hutchings M, Morschhauser F, Iacoboni G, et al. Glofitamab, a Novel, Bivalent CD20-Targeting T-Cell–Engaging Bispecific Antibody, Induces Durable Complete Remissions in Relapsed or Refractory B-Cell Lymphoma: A Phase I Trial. *Journal of Clinical Oncology*. 2021;39(18):1959. doi:10.1200/JCO.20.03175

170. Topp MS, Gökbuget N, Stein AS, et al. Safety and activity of blinatumomab for adult patients with relapsed or refractory B-precursor acute lymphoblastic leukaemia: a multicentre, single-arm, phase 2 study. *Lancet Oncol*. 2015;16(1):57-66. doi:10.1016/S1470-2045(14)71170-2

171. Zhou S, Li F, Niu M, Wu K, Li T, Yi M. Advances in the clinical application of bispecific antibodies in cancer therapy. *iScience*. 2025;28(12):114203. doi:10.1016/J.ISCI.2025.114203

172. Czajkowsky DM, Hu J, Shao Z, Pleass RJ. Fc-fusion proteins: new developments and future perspectives. *EMBO Mol Med*. 2012;4(10):1015. doi:10.1002/EMMM.201201379

173. Congy-Jolivet N, Probst A, Watier H, Thibault G. Recombinant therapeutic monoclonal antibodies: Mechanisms of action in relation to structural and functional duality. *Crit Rev Oncol Hematol*. 2007;64(3):226-233. doi:10.1016/J.CRITREVONC.2007.06.013

174. Mekhaiel DNA, Czajkowsky DM, Andersen JT, et al. Polymeric human Fc-fusion proteins with modified effector functions. *Sci Rep*. 2011;1:124. doi:10.1038/SREP00124

175. Kontermann RE. Strategies for extended serum half-life of protein therapeutics. *Curr Opin Biotechnol*. 2011;22(6):868-876. doi:10.1016/J.COPBIO.2011.06.012

176. Roopenian DC, Akilesh S. FcRn: the neonatal Fc receptor comes of age. *Nat Rev Immunol*. 2007;7(9):715-725. doi:10.1038/NRI2155

177. Strohl WR. Optimization of Fc-mediated effector functions of monoclonal antibodies. *Curr Opin Biotechnol*. 2009;20(6):685-691. doi:10.1016/J.COPBIO.2009.10.011

178. Galvez-Cancino F, Simpson AP, Costoya C, et al. Fcγ receptors and immunomodulatory antibodies in cancer. *Nature Reviews Cancer 2023 24:1*. 2023;24(1):51-71. doi:10.1038/S41568-023-00637-8

179. Liu R, Oldham RJ, Teal E, Beers SA, Cragg MS. Fc-Engineering for Modulated Effector Functions—Improving Antibodies for Cancer Treatment. *Antibodies*. 2020;9(4):64. doi:10.3390/ANTIB9040064

180. Peppel K, Crawford D, Beutler B. A tumor necrosis factor (TNF) receptor-IgG heavy chain chimeric protein as a bivalent antagonist of TNF activity. *J Exp Med*. 1991;174(6):1483-1489. doi:10.1084/JEM.174.6.1483

181. Al-Laith M, Jasenecova M, Abraham S, et al. Arthritis prevention in the pre-clinical phase of RA with abatacept (the APIPPRA study): a multi-centre, randomised, double-blind, parallel-group, placebo-controlled clinical trial protocol. *Trials*. 2019;20(1):429. doi:10.1186/S13063-019-3403-7

182. Holash J, Davis S, Papadopoulos N, et al. VEGF-Trap: A VEGF blocker with potent antitumor effects. *Proc Natl Acad Sci U S A*. 2002;99(17):11393. doi:10.1073/PNAS.172398299

183. Debinski W, Gibo DM. Molecular expression analysis of restrictive receptor for interleukin 13, a brain tumor-associated cancer/testis antigen. *Molecular Medicine*. 2000;6(5):440. doi:10.1007/BF03401786

184. Receptor for Interleukin 13 Is a Marker and Therapeutic Target for Human High-Grade Gliomas1 | Clinical Cancer Research | American Association for Cancer Research. Accessed March 24, 2026. https://aacrjournals.org/clincancerres/article/5/5/985/287499/Receptor-for-Interleukin-13-Is-a-Marker-and

185. Zeng J, Zhang J, Yang YZ, et al. IL13RA2 is overexpressed in malignant gliomas and related to clinical outcome of patients. *Am J Transl Res*. 2020;12(8):4702. Accessed March 24, 2026. https://pmc.ncbi.nlm.nih.gov/articles/PMC7476143/

186. Wood N, Whitters MJ, Jacobson BA, et al. Enhanced Interleukin (IL)-13 Responses in Mice Lacking IL-13 Receptor α 2. *J Exp Med*. 2003;197(6):703. doi:10.1084/JEM.20020906

187. IL-13Rα2, a Decoy Receptor for IL-13 Acts As an Inhibitor of IL-4-dependent Signal Transduction in Glioblastoma Cells1 | Cancer Research | American Association for Cancer Research. Accessed March 24, 2026. https://aacrjournals.org/cancerres/article/62/4/1103/509578/IL-13R-2-a-Decoy-Receptor-for-IL-13-Acts-As-an

188. Fichtner-Feigl S, Terabe M, Kitani A, et al. Restoration of Tumor Immune Surveillance via Targeting of IL-13Receptor-α2. *Cancer Res*. 2008;68(9):3467. doi:10.1158/0008-5472.CAN-07-5301

189. Brown CE, Warden CD, Starr R, et al. Glioma IL13Rα2 Is Associated with Mesenchymal Signature Gene Expression and Poor Patient Prognosis. *PLoS One*. 2013;8(10):e77769. doi:10.1371/JOURNAL.PONE.0077769

190. Brown CE, Starr R, Aguilar B, et al. Stem-like tumor initiating cells isolated from IL13Rα2-expressing gliomas are targeted and killed by IL13-zetakine redirected T cells. *Clin Cancer Res*. 2012;18(8):2199. doi:10.1158/1078-0432.CCR-11-1669

191. Eyler CE, Rich JN. Survival of the Fittest: Cancer Stem Cells in Therapeutic Resistance and Angiogenesis. *J Clin Oncol*. 2008;26(17):2839. doi:10.1200/JCO.2007.15.1829

192. Knudson KM, Hwang SJ, McCann MS, Joshi BH, Husain SR, Puri RK. Recent Advances in IL-13Rα2-Directed Cancer Immunotherapy. *Front Immunol*. 2022;13:878365. doi:10.3389/FIMMU.2022.878365

193. Brown CE, Alizadeh D, Starr R, et al. Regression of Glioblastoma after Chimeric Antigen Receptor T-Cell Therapy. *New England Journal of Medicine*. 2016;375(26):2561-2569. doi:10.1056/NEJMOA1610497/SUPPL_FILE/NEJMOA1610497_DISCLOSURES.PDF

194. Ekstrand AJ, Sugawa N, James CD, Collins VP. Amplified and rearranged epidermal growth factor receptor genes in human glioblastomas reveal deletions of sequences encoding portions of the N- and/or C-terminal tails. *Proc Natl Acad Sci U S A*. 1992;89(10):4309-4313. doi:10.1073/PNAS.89.10.4309

195. Sugawa N, Ekstrand AJ, James CD, Collins VP. Identical splicing of aberrant epidermal growth factor receptor transcripts from amplified rearranged genes in human glioblastomas. *Proc Natl Acad Sci U S A*. 1990;87(21):8602-8606. doi:10.1073/PNAS.87.21.8602

196. Maiden LT, Novak U, Kaye AH, Burgess AW. Selective Amplification of the Cytoplasmic Domain of the Epidermal Growth Factor Receptor Gene in Glioblastoma Multiforme.

Cancer Res. 1988;48:2711-2714. Accessed March 24, 2026. http://aacrjournals.org/cancerres/article-pdf/48/10/2711/2431248/cr0480102711.pdf

197. (PDF) Analysis of EGFR Overexpression, EGFR gene amplification and the EGFRvIII Mutation in portuguese high-grade gliomas. Accessed March 24, 2026. https://www.researchgate.net/publication/5343985_Analysis_of_EGFR_Overexpression_EGFR_gene_amplification_and_the_EGFRvIII_Mutation_in_portuguese_high-grade_gliomas

198. Olapade-Olaopa EO, Moscatello DK, MacKay EH, et al. Evidence for the differential expression of a variant EGF receptor protein in human prostate cancer. *British Journal of Cancer 2000 82:1*. 1999;82(1):186-194. doi:10.1054/bjoc.1999.0898

199. Frequent Expression of a Mutant Epidermal Growth Factor Receptor in Multiple Human Tumors1 | Cancer Research | American Association for Cancer Research. Accessed March 24, 2026. https://aacrjournals.org/cancerres/article/55/23/5536/501676/Frequent-Expression-of-a-Mutant-Epidermal-Growth

200. A Common Mutant Epidermal Growth Factor Receptor Confers Enhanced Tumorigenicity on Human Glioblastoma Cells by Increasing Proliferation and Reducing Apoptosis1 | Cancer Research | American Association for Cancer Research. Accessed March 24, 2026. https://aacrjournals.org/cancerres/article/56/21/5079/502777/A-Common-Mutant-Epidermal-Growth-Factor-Receptor

201. Monoclonal Antibodies against EGFRvIII Are Tumor Specific and React with Breast and Lung Carcinomas and Malignant Gliomas1 | Cancer Research | American Association for Cancer Research. Accessed March 24, 2026. https://aacrjournals.org/cancerres/article/55/14/3140/501182/Monoclonal-Antibodies-against-EGFRvIII-Are-Tumor

202. Humphrey PA, Wong AJ, Vogelstein B, et al. Amplification and expression of the epidermal growth factor receptor gene in human glioma xenografts. *Cancer Res*. 1988;48(8):2231-2238. Accessed March 24, 2026. https://pure.johnshopkins.edu/en/publications/amplification-and-expression-of-the-epidermal-growth-factor-recep-4/

203. Thorne AH, Zanca C, Furnari F. Epidermal growth factor receptor targeting and challenges in glioblastoma. *Neuro Oncol*. 2016;18(7):914-918. doi:10.1093/NEUONC/NOV319

204. Nishikawa R, Ji XD, Harmon RC, et al. A mutant epidermal growth factor receptor common in human glioma confers enhanced tumorigenicity. *Proceedings of the National Academy of Sciences*. 1994;91(16):7727-7731. doi:10.1073/PNAS.91.16.7727

205. Gan HK, Cvrljevic AN, Johns TG. The epidermal growth factor receptor variant III (EGFRvIII): Where wild things are altered. *FEBS Journal*. 2013;280(21):5350-5370. doi:10.1111/FEBS.12393

206. Batra SK, Castelino-Prabhu S, Wikstrand CJ, et al. Epidermal growth factor ligand-independent, unregulated, cell-transforming potential of a naturally occurring human mutant EGFRvIII gene. *Cell Growth Differ*. 1995;6(10):1251-1259. Accessed March 24, 2026. https://europepmc.org/article/MED/8845302

207. Mutant Epidermal Growth Factor Receptor Signaling Down-Regulates p27 through Activation of the Phosphatidylinositol 3-Kinase/Akt Pathway in Glioblastomas1 | Cancer Research | American Association for Cancer Research. Accessed March 24, 2026. https://aacrjournals.org/cancerres/article/62/22/6764/509368/Mutant-Epidermal-Growth-Factor-Receptor-Signaling?guestAccessKey=

208. Aldape KD, Ballman K, Furth A, et al. Immunohistochemical Detection of EGFRvIII in High Malignancy Grade Astrocytomas and Evaluation of Prognostic Significance. *J Neuropathol Exp Neurol*. 2004;63(7):700-707. doi:10.1093/JNEN/63.7.700

209. Li B, Yuan M, Kim IA, Chang CM, Bernhard EJ, Shu HKG. Mutant epidermal growth factor receptor displays increased signaling through the phosphatidylinositol-3 kinase/AKT pathway and promotes radioresistance in cells of astrocytic origin. *Oncogene 2004 23:26*. 2004;23(26):4594-4602. doi:10.1038/sj.onc.1207602

210. Cell surface localization and density of the tumor-associated variant of the epidermal growth factor receptor, EGFRvIII - Fingerprint - Icahn School of Medicine at Mount Sinai. Accessed March 24, 2026. https://scholars.mssm.edu/en/publications/cell-surface-localization-and-density-of-the-tumor-associated-var-2/fingerprints/?sortBy=alphabetically

211. Patel D, Lahiji A, Patel S, et al. Monoclonal Antibody Cetuximab Binds to and Down-regulates Constitutively Activated Epidermal Growth Factor Receptor vIII on the Cell Surface. *Anticancer Res*. 2007;27(5A):3355-3366. Accessed March 24, 2026. https://ar.iiarjournals.org/content/27/5A/3355

212. Bode U, Massimino M, Bach F, et al. Nimotuzumab treatment of malignant gliomas. *Expert Opin Biol Ther*. 2012;12(12):1649-1659. doi:10.1517/14712598.2012.733367

213. Capietto AH, Keirallah S, Gross E, et al. Emerging Concepts for the Treatment of Hematological Malignancies with Therapeutic Monoclonal Antibodies. *Curr Drug Targets*. 2010;11(7):790-800. doi:10.2174/138945010791320845

214. Mutant Epidermal Growth Factor Receptor Up-Regulates Molecular Effectors of Tumor Invasion1 | Cancer Research | American Association for Cancer Research. Accessed

March 24, 2026. https://aacrjournals.org/cancerres/article/62/12/3335/508899/Mutant-Epidermal-Growth-Factor-Receptor-Up

215. Ohno M, Natsume A, Ichiro Iwami K, et al. Retrovirally engineered T-cell-based immunotherapy targeting type III variant epidermal growth factor receptor, a glioma-associated antigen. *Cancer Sci*. 2010;101(12):2518-2524. doi:10.1111/J.1349-7006.2010.01734.X

216. Bullain SS, Sahin A, Szentirmai O, et al. Genetically engineered T cells to target EGFRvIII expressing glioblastoma. *J Neurooncol*. 2009;94(3):373-382. doi:10.1007/S11060-009-9889-1/METRICS

217. O'Rourke DM, Nasrallah MP, Desai A, et al. A single dose of peripherally infused EGFRvIII-directed CAR T cells mediates antigen loss and induces adaptive resistance in patients with recurrent glioblastoma. *Sci Transl Med*. 2017;9(399). doi:10.1126/SCITRANSLMED.AAA0984

218. Chalhoub N, Baker SJ. PTEN and the PI3-kinase pathway in cancer. *Annual Review of Pathology: Mechanisms of Disease*. 2009;4:127-150. doi:10.1146/ANNUREV.PATHOL.4.110807.092311

219. Verhaak RGW, Hoadley KA, Purdom E, et al. An integrated genomic analysis identifies clinically relevant subtypes of glioblastoma characterized by abnormalities in PDGFRA, IDH1, EGFR and NF1. *Cancer Cell*. 2010;17(1):98. doi:10.1016/J.CCR.2009.12.020

220. Brennan CW, Verhaak RGW, McKenna A, et al. The somatic genomic landscape of glioblastoma. *Cell*. 2013;155(2):462. doi:10.1016/J.CELL.2013.09.034

221. YANG Y, SHAO N, LUO G, et al. Mutations of PTEN Gene in Gliomas Correlate to Tumor Differentiation and Short-term Survival Rate. *Anticancer Res*. 2010;30(3):981. http://ar.iiarjournals.org/content/30/3/981.abstract

222. Saito Y, Swanson X, Mhashilkar AM, et al. Adenovirus-mediated transfer of the PTEN gene inhibits human colorectal cancer growth in vitro and in vivo. *Gene Ther*. 2003;10(23):1961-1969. doi:10.1038/SJ.GT.3302100

223. Sakurada A, Hamada H, Fukushige S, et al. Adenovirus-mediated delivery of the PTEN gene inhibits cell growth by induction of apoptosis in endometrial cancer. *Int J Oncol*. 1999;15(6):1069-1074. doi:10.3892/IJO.15.6.1069

224. Han L, Zhang AL, Xu P, et al. Combination gene therapy with PTEN and EGFR siRNA suppresses U251 malignant glioma cell growth in vitro and in vivo. *Med Oncol*. 2010;27(3):843-852. doi:10.1007/S12032-009-9295-8

225. Rosser CJ, Tanaka M, Pisters LL, et al. Adenoviral-mediated PTEN transgene expression sensitizes Bcl-2-expressing prostate cancer cells to radiation. *Cancer Gene Ther*. 2004;11(4):273-279. doi:10.1038/SJ.CGT.7700673

226. Russell L, Swanner J, Jaime-Ramirez AC, et al. PTEN expression by an oncolytic herpesvirus directs T-cell mediated tumor clearance. *Nat Commun*. 2018;9(1):5006. doi:10.1038/S41467-018-07344-1

227. Kim S, Jung BK, Kim J, et al. Anticancer effect of the oncolytic Newcastle disease virus harboring the PTEN gene on glioblastoma. *Oncol Lett*. 2024;29(1):6. doi:10.3892/OL.2024.14752

228. Lavictoire SJ, Gont A, Julian LM, et al. Engineering PTEN-L for Cell-Mediated Delivery. *Mol Ther Methods Clin Dev*. 2018;9:12-22. doi:10.1016/J.OMTM.2017.11.006

229. Hopkins BD, Fine B, Steinbach N, et al. A secreted PTEN phosphatase that enters cells to alter signaling and survival. *Science*. 2013;341(6144):399-402. doi:10.1126/SCIENCE.1234907

230. Blazar BR, Lindberg FP, Ingulli E, et al. CD47 (integrin-associated protein) engagement of dendritic cell and macrophage counterreceptors is required to prevent the clearance of donor lymphohematopoietic cells. *J Exp Med*. 2001;194(4):541-549. doi:10.1084/JEM.194.4.541

231. Oldenborg PA. Role of CD47 in erythroid cells and in autoimmunity. *Leuk Lymphoma*. 2004;45(7):1319-1327. doi:10.1080/1042819042000201989

232. Oldenborg PA, Gresham HD, Lindberg FP. CD47-signal regulatory protein alpha (SIRPalpha) regulates Fcgamma and complement receptor-mediated phagocytosis. *J Exp Med*. 2001;193(7):855-861. doi:10.1084/JEM.193.7.855

233. Jaiswal S, Chao MP, Majeti R, Weissman IL. Macrophages as mediators of tumor immunosurveillance. *Trends Immunol*. 2010;31(6):212-219. doi:10.1016/J.IT.2010.04.001

234. Jiang P, Lagenaur CF, Narayanan V. Integrin-associated protein is a ligand for the P84 neural adhesion molecule. *J Biol Chem*. 1999;274(2):559-562. doi:10.1074/JBC.274.2.559

235. Brown EJ, Frazier WA. Integrin-associated protein (CD47) and its ligands. *Trends Cell Biol*. 2001;11(3):130-135. doi:10.1016/S0962-8924(00)01906-1

236. Oldenborg PA, Zheleznyak A, Fang YF, Lagenaur CF, Gresham HD, Lindberg FP. Role of CD47 as a marker of self on red blood cells. *Science*. 2000;288(5473):2051-2054. doi:10.1126/SCIENCE.288.5473.2051

237. Timms JF, Carlberg K, Gu H, et al. Identification of major binding proteins and substrates for the SH2-containing protein tyrosine phosphatase SHP-1 in macrophages. *Mol Cell Biol*. 1998;18(7):3838-3850. doi:10.1128/MCB.18.7.3838

238. Fujioka Y, Matozaki T, Noguchi T, et al. A novel membrane glycoprotein, SHPS-1, that binds the SH2-domain-containing protein tyrosine phosphatase SHP-2 in response to mitogens and cell adhesion. *Mol Cell Biol*. 1996;16(12):6887-6899. doi:10.1128/MCB.16.12.6887

239. Kharitonenkov A, Chen Z, Sures I, Wang H, Schilling J, Ullrich A. A family of proteins that inhibit signalling through tyrosine kinase receptors. *Nature*. 1997;386(6621):181-186. doi:10.1038/386181A0

240. Tsai RK, Discher DE. Inhibition of "self" engulfment through deactivation of myosin-II at the phagocytic synapse between human cells. *J Cell Biol*. 2008;180(5):989-1003. doi:10.1083/JCB.200708043

241. Willingham SB, Volkmer JP, Gentles AJ, et al. The CD47-signal regulatory protein alpha (SIRPa) interaction is a therapeutic target for human solid tumors. *Proc Natl Acad Sci U S A*. 2012;109(17):6662-6667. doi:10.1073/PNAS.1121623109/SUPPL_FILE/SM02.AVI

242. Li F, Lv B, Liu Y, et al. Blocking the CD47-SIRPα axis by delivery of anti-CD47 antibody induces antitumor effects in glioma and glioma stem cells. *Oncoimmunology*. 2018;7(2). doi:10.1080/2162402X.2017.1391973

243. Matlung HL, Szilagyi K, Barclay NA, van den Berg TK. The CD47-SIRPα signaling axis as an innate immune checkpoint in cancer. *Immunol Rev*. 2017;276(1):145-164. doi:10.1111/IMR.12527

244. Huang Y, Ma Y, Gao P, Yao Z. Targeting CD47: the achievements and concerns of current studies on cancer immunotherapy. *J Thorac Dis*. 2017;9(2):E168-E174. doi:10.21037/JTD.2017.02.30

245. Zhang M, Hutter G, Kahn SA, et al. Anti-CD47 Treatment Stimulates Phagocytosis of Glioblastoma by M1 and M2 Polarized Macrophages and Promotes M1 Polarized Macrophages In Vivo. *PLoS One*. 2016;11(4):e0153550. doi:10.1371/JOURNAL.PONE.0153550

246. Petrova PS, Viller NN, Wong M, et al. TTI-621 (SIRPαFc): A CD47-blocking innate immune checkpoint inhibitor with broad antitumor activity and minimal erythrocyte binding. *Clinical Cancer Research*. 2017;23(4):1068-1079. doi:10.1158/1078-0432.CCR-16-1700/128960/AM/TTI-621-SIRP-FC-A-CD47-BLOCKING-INNATE-IMMUNE

247. Ring NG, Herndler-Brandstetter D, Weiskopf K, et al. Anti-SIRPα antibody immunotherapy enhances neutrophil and macrophage antitumor activity. *Proc Natl Acad*

Sci U S A. 2017;114(49):E10578-E10585. doi:10.1073/PNAS.1710877114/SUPPL_FILE/PNAS.201710877SI.PDF

248. Advani R, Flinn I, Popplewell L, et al. CD47 Blockade by Hu5F9-G4 and Rituximab in Non-Hodgkin's Lymphoma. *New England Journal of Medicine*. 2018;379(18):1711-1721. doi:10.1056/NEJMOA1807315/SUPPL_FILE/NEJMOA1807315_DISCLOSURES.PDF

249. Whipple N, Molinaro A, Reddy A, et al. CTP-18. PNOC025: A phase 1 study assessing the safety and tolerability of magrolimab in children and adults with recurrent or progressive malignant brain tumors. *Neuro Oncol*. 2025;27(Supplement_5):v149-v150. doi:10.1093/NEUONC/NOAF201.0590

250. Zhang W, Huang Q, Xiao W, et al. Advances in Anti-Tumor Treatments Targeting the CD47/SIRPα Axis. *Front Immunol*. 2020;11:502552. doi:10.3389/FIMMU.2020.00018/XML

251. Oldenborg PA, Zheleznyak A, Fang YF, Lagenaur CF, Gresham HD, Lindberg FP. Role of CD47 as a Marker of Self on Red Blood Cells. *Science (1979)*. 2000;288(5473):2051-2054. doi:10.1126/SCIENCE.288.5473.2051

252. Catani L, Sollazzo D, Ricci F, et al. The CD47 pathway is deregulated in human immune thrombocytopenia. *Exp Hematol*. 2011;39(4):486-494. doi:10.1016/j.exphem.2010.12.011

253. Maute R, Xu J, Weissman IL. CD47–SIRPα-targeted therapeutics: status and prospects. *Immuno-Oncology and Technology*. 2022;13:100070. doi:10.1016/J.IOTECH.2022.100070/ASSET/5AE165E8-2E0A-495B-92DE-1027338F2980/MAIN.ASSETS/GR3.JPG

254. Sheybani ND, Breza VR, Paul S, et al. ImmunoPET-informed sequence for focused ultrasound-targeted mCD47 blockade controls glioma. *Journal of Controlled Release*. 2021;331:19-29. doi:10.1016/J.JCONREL.2021.01.023

255. Seek Rhee G, hyun Seok J, Sun Kim S, et al. 828. Optimizing the Woodchuck Hepatitis Virus Post-Transcriptional Regulatory Element (WPRE) for Safety and Function in Lentiviral Vectors. *Molecular Therapy*. 2005;11:S322. doi:10.1016/j.ymthe.2005.07.371

256. Ueki K, Ono Y, Henson J, Efird J, Deimling A, Louis D. CDKN2/p16 or RB alterations occur in the majority of glioblastomas and are inversely correlated. *Cancer Res*. Published online 1996.

257. KUAN CT, REIST CJ, FOULON CF, et al. 125I-labeled anti-epidermal growth factor receptor-vIII single-chain Fv exhibits specific and high-level targeting of glioma xenografts. *Clinical cancer research*. 1999;5(6):1539-1549.

258. Merchant AM, Zhu Z, Yuan JQ, et al. An efficient route to human bispecific IgG. *Nature Biotechnology 1998 16:7*. 1998;16(7):677-681. doi:10.1038/nbt0798-677

259. Hatherley D, Lea SM, Johnson S, Barclay AN. Polymorphisms in the human inhibitory signal-regulatory protein α do not affect binding to its ligand CD47. *J Biol Chem*. 2014;289(14):10024-10028. doi:10.1074/JBC.M114.550558

260. Debinski W, Gibo DM, Obiri NI, Kealiher A, Puri RK. Novel anti-brain tumor cytotoxins specific for cancer cells. *Nat Biotechnol*. 1998;16(5):449-453. doi:10.1038/NBT0598-449

261. Donaldson DD, Whitters MJ, Fitz LJ, et al. The Murine IL-13 Receptor α2: Molecular Cloning, Characterization, and Comparison with Murine IL-13 Receptor α1. *The Journal of Immunology*. 1998;161(5):2317-2324. doi:10.4049/JIMMUNOL.161.5.2317

262. Stone GC, Sjöbring U, Björck L, Sjöquist J, Barber C V, Nardella FA. The Fc binding site for streptococcal protein G is in the C gamma 2-C gamma 3 interface region of IgG and is related to the sites that bind staphylococcal protein A and human rheumatoid factors. *The Journal of Immunology*. 1989;143(2):565-570. doi:10.4049/JIMMUNOL.143.2.565

263. Meloty-Kapella L, Shergill B, Kuon J, Botvinick E, Weinmaster G. Notch Ligand Endocytosis Generates Mechanical Pulling Force Dependent on Dynamin, Epsins and Actin. *Dev Cell*. 2012;22(6):1299. doi:10.1016/J.DEVCEL.2012.04.005

264. Piraner DI, Abedi MH, Duran Gonzalez MJ, et al. Engineered receptors for soluble cellular communication and disease sensing. *Nature 2024 638:8051*. 2024;638(8051):805-813. doi:10.1038/s41586-024-08366-0

265. Khamaisi B, Luca VC, Blacklow SC, Sprinzak D. Functional Comparison between Endogenous and Synthetic Notch Systems. *ACS Synth Biol*. 2022;11(10):3343-3353. doi:10.1021/ACSSYNBIO.2C00247/SUPPL_FILE/SB2C00247_SI_002.XLSX

266. Keller S, Schmidt MHH. EGFR and EGFRvIII Promote Angiogenesis and Cell Invasion in Glioblastoma: Combination Therapies for an Effective Treatment. *Int J Mol Sci*. 2017;18(6):1295. doi:10.3390/IJMS18061295

267. Zhang C, Ma HM, Dong SS, et al. Furin extracellularly cleaves secreted PTENα/β to generate C-terminal fragment with a tumor-suppressive role. *Cell Death Dis*. 2022;13(6):532. doi:10.1038/S41419-022-04988-2

268. Li DM, Sun H. PTEN/MMAC1/TEP1 suppresses the tumorigenicity and induces G1 cell cycle arrest in human glioblastoma cells. *Proc Natl Acad Sci U S A*. 1998;95(26):15406. doi:10.1073/PNAS.95.26.15406

269. Stern LA, Gholamin S, Moraga I, et al. Engineered IL13 variants direct specificity of IL13Rα2-targeted CAR T cell therapy. *Proc Natl Acad Sci U S A*. 2022;119(33):e2112006119. doi:10.1073/PNAS.2112006119/SUPPL_FILE/PNAS.2112006119.SAPP.PDF

270. Kim K, Gwak HS, Han N, et al. Chimeric Antigen Receptor T Cells With Modified Interleukin-13 Preferentially Recognize IL13Rα2 and Suppress Malignant Glioma: A Preclinical Study. *Front Immunol*. 2021;12:715000. doi:10.3389/FIMMU.2021.715000/TEXT

271. Métayer LE, Vilalta A, Amos Burke GA, Brown GC. Anti-CD47 antibodies induce phagocytosis of live, malignant B cells by macrophages via the Fc domain, resulting in cell death by phagoptosis. *Oncotarget*. 2017;8(37):60892-60903. doi:10.18632/ONCOTARGET.18492

272. Buss NAPS, Henderson SJ, McFarlane M, Shenton JM, De Haan L. Monoclonal antibody therapeutics: history and future. *Curr Opin Pharmacol*. 2012;12(5):615-622. doi:10.1016/J.COPH.2012.08.001

273. Chung S, Quarmby V, Gao X, et al. Quantitative evaluation of fucose reducing effects in a humanized antibody on Fcγ receptor binding and antibody-dependent cell-mediated cytotoxicity activities. *MAbs*. 2012;4(3):326-340. doi:10.4161/MABS.19941

274. Ferrara C, Grau S, Jağer C, et al. Unique carbohydrate-carbohydrate interactions are required for high affinity binding between FcgammaRIII and antibodies lacking core fucose. *Proc Natl Acad Sci U S A*. 2011;108(31):12669-12674. doi:10.1073/PNAS.1108455108

275. Aboody KS, Brown A, Rainov NG, et al. Neural stem cells display extensive tropism for pathology in adult brain: evidence from intracranial gliomas. *Proc Natl Acad Sci U S A*. 2000;97(23):12846-12851. doi:10.1073/PNAS.97.23.12846

276. Yamada-Hunter SA, Theruvath J, McIntosh BJ, et al. Engineered CD47 protects T cells for enhanced antitumour immunity. *Nature 2024 630:8016*. 2024;630(8016):457-465. doi:10.1038/s41586-024-07443-8